2013

Experimental Laboratory Procedures for the Construction and Testing of Seismic Resistant Unbonded Post-Tensioned Special Reinforced Concrete Walls

Moises Rivera
Lehigh University

EXPERIMENTAL LABORATORY PROCEDURES FOR THE CONSTRUCTION AND TESTING OF SEISMIC RESISTANT UNBONDED POST-TENSIONED SPECIAL REINFORCED CONCRETE WALLS

by

Moises Rivera

A Thesis

Presented to the Graduate and Research Committee

of Lehigh University

in Candidacy for the Degree of

Masters of Science

in

Structural Engineering

Department of Civil and Environmental Engineering

Lehigh University

Bethlehem, Pennsylvania

December 6, 2013

This thesis is accepted an approved in partial fulfillment of the requirement for the Master of Science.

_____

Date:

_____

Dr. Stephen Pessiki

Thesis Co-Advisor

_____

Dr. Richard Sause

Thesis Co-Advisor

_____

Dr. Panayiotis Diplas

Chairperson of Department

ACKNOWLEDGEMENTS

The work presented in this thesis was supported by the Charles Pankow Foundation and conducted at the Center for Advanced Technology for Large Structural Systems (ATLSS) at Lehigh University, Bethlehem, Pennsylvania.

Special acknowledgements are presented to DSI America from donating the prestressing system utilized in this research project, to NUCOR Steel Connecticut for donating the necessary rebar to complete the project, and to A.H. Harris Construction Supplies for the formwork panels for the duration of the project. Additional thanks are expressed to VSL for the technical expertise that they provided.

The author gratefully acknowledges the guidance, encouragement, and support provided by his research advisors Dr. Stephen Pessiki and Dr. Richard Sause. They both provided the author with the necessary tools to apply and further develop his structural engineering skills.

Above all, the author would like to dedicate this thesis to his loving wife, Nadia Rivera, whose endless support and continuous love became a cornerstone stimulus which allowed for the realization of this and all future work. The author acknowledges that there is no greater love than the one shared by the author and his wife. The love for his wife is what makes the author a better person, a better husband, and a better engineer. May this thesis serve as a tenth wedding anniversary present to her.

El autor excepcionalmente agradece a sus siempre amados padres, Jose Antonio y Bertha Rivera. Ellos siempre han sido la fuente de inspiración del autor. El autor agradece infinitamente a sus padres por proporcionar al autor con orientación ética y espiritual en todas las etapas de su vida. El autor también les dedica esta tesis en agradecimiento por el infinito amor que le han tenido al autor desde su nacimiento, gracias Apa y Ama.

The author would also like to thank his brothers Jesus Antonio and Marco Aurelio and sister Alma Leticia for their unconditional support, friendship and encouragement towards all of the author's endeavors. The author thanks his brothers and sister for all the memories and experiences shared with the author. The author knows there are no closer friends than his brothers and sister.

The opinions, findings, and conclusions expressed in this report are those of the author's and do not necessarily reflect the views of the individuals acknowledged above.

TABLE OF CONTENTS

LIST OF FIGURES

LIST OF TABLES

ABSTRACT

This research investigates the experimental lateral load response of an unbonded post-tensioned cast-in-place concrete special structural wall with bonded longitudinal mild steel reinforcement under the action of quasi-static lateral load. The objective of this report is to describe the procedures for the construction and testing of the wall and to present a summary of testing results.

The unbonded post-tensioned cast-in-place concrete special structural wall with bonded longitudinal mild steel reinforcement provides energy dissipation through the yielding of the boundary and web longitudinal steel reinforcement. This steel reinforcement extends from the wall into the foundation block. Additionally, self-centering capabilities are provided by the unbonded post-tensioning strands that extend from the foundation block to the top of the wall.

It was found that the limit states that characterize the lateral load response of an unbonded post-tensioned cast-in-place structural wall with longitudinal mild bonded steel reinforcement occurred as presented by Srivastava (2013). Also, yielding of the longitudinal mild steel reinforcement was effective as an energy dissipator. However, self-centering capabilities were greatly diminished after the yielding of the longitudinal bars at a drift of approximately 0.5%. Therefore, self-centering capabilities were greatly limited by the insufficiency of the restoring force provided by post-tensioning. Finally, results showed that initial residual drift of 0.2% occurred as early as the longitudinal bars started to yield which occurred at 0.6%.

CHAPTER 1

INTRODUCTION

Past and recent earthquakes have revealed the importance of utilizing adequate lateral force resisting systems in regions of high seismicity. In the design of such systems, the design goal is often to provide life safety through ductility and energy dissipation. In some cases, the goal is to control lateral residual drift and to allow for immediate occupancy after the seismic event. Nonetheless, there are inherent limitations with current types of structural walls. As explained by Srivastava (2013), there exist two major limitations with commonly used types of structural walls: (1) damage is required to provide the required nonlinearity or softening of the wall; and (2) the wall has residual lateral drift after a seismic event. Wall damage can be caused by the yielding of the steel reinforcement, softening of concrete in compression, and concrete cracking. Residual lateral drift is due to the lack of a restoring force that would bring the wall to the original upright position. Fortunately, these limitations can be controlled by the use of post-tensioning.

Figure 1-1 shows a graphic representation of a typical cast-in-place ACI-complaint wall, an unbonded post-tensioned precast concrete wall, and an unbonded post-tensioned hybrid cast-in-place concrete wall. Included in this figure is an illustration of the base moment-lateral drift response of each wall. The unbonded post-tensioned precast concrete wall (Figure 1-1(b)) represents construction similar to the precast wall with post-tensioning for self-centering studied by Kurama et al. (1996), Kurama (1997), Perez (2004), and Perez et al. (2007). The unbonded post-tensioned hybrid cast-in-place concrete wall (Figure 1-1(c))

represents construction similar the cast-in-place wall with post-tensioning for self-centering presented in work studied by Srivastava (2013), Pakiding (2014), and this report.

The structural wall in Figure 1-1(a) is a cast-in-place concrete wall with longitudinal mild steel reinforcement extending into the foundation (as per ACI 318), but without post-tensioning. As lateral force is applied, the wall softens due to the yielding of the steel reinforcement, concrete cracking, and non-linear stress-strain concrete response in compression. After the seismic event, is likely to have some residual lateral drift due to the absence of a restoring force. However, it can be seen in the expected base moment-lateral drift curve that the yielding of the longitudinal steel reinforcement provided energy dissipation, which could translate into the reduction of overall drift, but ultimately extensive damage to the wall is expected.

Figure 1-1(b) is an unbonded post-tensioned precast wall with post-tensioning for self-centering that extends from the top of the wall to the foundation, but without longitudinal mild steel reinforcement extending into the foundation. Under earthquake loading, larger drifts are expected, compared to a cast-in-place wall (refer to Kurama). After the seismic event, restoring forces are provided by the post-tensioning and therefore residual lateral drift is virtually zero. However, the expected moment-lateral drift curve shows no energy dissipation. This is due to the lack of longitudinal mild steel reinforcement crossing the horizontal joint between the stacked precast panels and the foundation. Nonetheless, with adequate concrete confinement, minimum damage of the wall is expected.

Figure 1-1(c) is an unbonded post-tensioned hybrid cast-in-place concrete wall with post-tensioning that extends from the top of the wall to the foundation with longitudinal mild steel reinforcement extending into the foundation (as per ACI 318). As the lateral force is applied, drifts are reduced by the energy dissipation provided by the longitudinal mild steel reinforcement and residual lateral drift is reduced by the post-tensioning. After a seismic event, residual drift is virtually zero and damage to the wall is minimal. As shown in the expected moment-lateral drift curve, this hybrid system provides for life safety through ductility, and energy dissipation, and the reduction of residual drift allows for immediate occupancy after the seismic event.

1.1 OBJECTIVE

In a current research program at Lehigh University, three structural walls are going to be tested at ATLSS laboratory. The major differences between each test wall are the longitudinal reinforcement ratio and the amount of post-tensioning. The objective of this report is to describe the procedures for the construction and testing of the first structural wall. Experimental testing results and an explanation of the response are also presented for this wall.

1.2 NOTATION

The following notation is used in this report:

E_c = concrete modulus of elasticity

E_d = normalized cumulative hysteretic energy dissipation

F = lateral force acting on wall

f'_c	=	compressive strength of unconfined concrete
f'_{cce}	=	compressive strength of confined concrete
f_{pi}	=	initial stress in the post-tensioning steel after elastic shortening
f_{pu}	=	ultimate strength of the post-tensioning steel
f_{py}	=	yield strength of the post-tensioning steel
f'_r	=	concrete modulus of rupture
f_{ue}	=	actual ultimate strength of the steel reinforcement ($1.5f_{ye}$)
f_y	=	yield strength of the steel reinforcement
f_{ye}	=	yield strength of the steel reinforcement ($1.1f_y$)
H_f	=	height of the applied lateral force from the base of the wall
H_w	=	total height of wall
L_w	=	length of the wall cross-section
P_p	=	post-tensioning tension force
P_{py_n}	=	nominal yielding force of post-tensioning steel
t_w	=	thickness of the wall cross-section
Δ	=	displacement due to lateral force acting on wall
Δ_r	=	residual displacement after a seismic event
ε_c	=	measured concrete strain
ε_{sy_n}	=	nominal yield strains of longitudinal mild steel
ε_{r_n}	=	nominal modulus of rupture of concrete strain at f'_c
Θ_{bms_o}	=	drift of the wall at observed buckling of longitudinal mild steel
Θ_{ccr_o}	=	drift of the wall at observed flexural concrete cracking

Θ_{fms_o} = drift of the wall at observed fracture of longitudinal mild steel reinforcement

Θ_{llp_n} = drift of the wall at nominal yielding of post-tensioning steel

Θ_{spl_o} = drift of the wall at observed concrete spalling

Θ_{yms_n} = drift of the wall at nominal yielding of longitudinal mild steel reinforcement

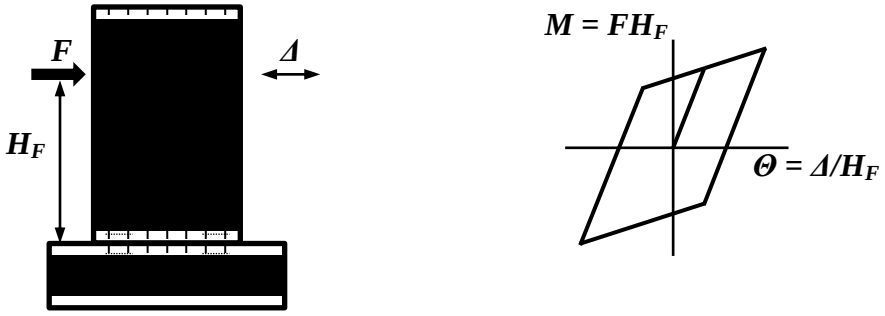

(a) ACI compliant cast-in-place wall and base and base moment-lateral drift response

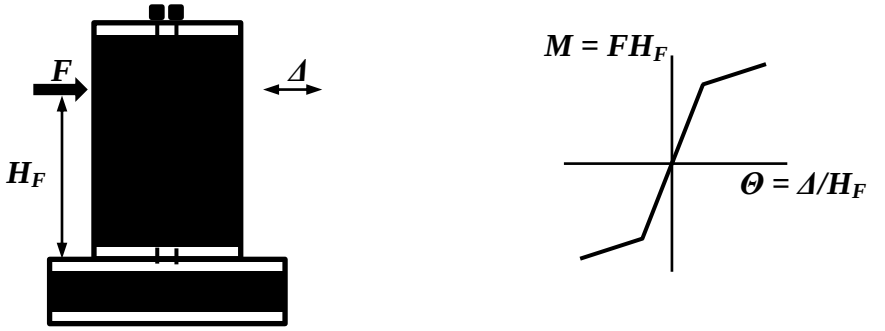

(b) Unbonded post-tensioned precast concrete wall and base moment-lateral drift response

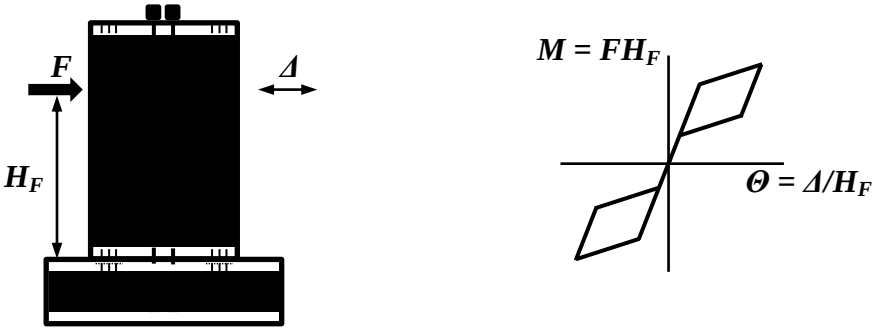

(c) Unbonded post-tensioned hybrid precast concrete wall and base moment-lateral drift response

Figure 1-1 Walls under lateral load and moment-lateral drift curve

CHAPTER 2

BACKGROUND

2.1 UNBONDED POST-TENSIONED PRECAST CONCRETE WALLS

In comparison to cast-in-place walls, unbonded post-tensioned precast walls reach larger overall deformations. This is because the post-tensioning steel is unbonded and its assumed deformation is uniformly distributed over the entire length (Kurama 1997). Unbonded post-tensioned construction is achieved by placing the post-tensioning steel in ducts, which remains ungrouted. This eliminates strain compatibility between post-tensioning steel and the surrounding concrete.

There have been other investigations of the flexural behavior of unbonded post-tensioned precast concrete walls including work at Lehigh University and University of Notre Dame as presented by Kurama et al. (1996, 1997) and Perez (2004, 2007, 2013). These analytical and experimental studies included vertically stacked precast panels with horizontal joints between panels. However, in order to increase the energy dissipation of these walls while retaining the self-centering behavior such as in a hybrid wall, bonded mild steel is placed across the horizontal joint between the wall and the foundation. To dissipate energy, this bonded mild steel is designed to yield in tension and compression.

This addition of longitudinal mild steel reinforcement for energy dissipation was studied by Restrepo and Rahman (2007), Smith and Kurama (2009) and Smith et al. (2011).

2.2 UNBONDED POST-TENSIONED CAST-IN-PLACE SPECIAL STRUCTURAL WALLS WITH LONGITUDINAL MILD STEEL REINFORCEMENT

As with the precast panels, the post-tensioning steel is placed in ducts and left ungrouted to prevent strain-compatibility with the surrounding concrete. The test wall is cast-in-place monolithically with the foundation. As Figure 2-1 shows, the longitudinal steel reinforcement is extended into the foundation and the post-tensioning steel extends from the top of the wall to the foundation. This figure also shows two groups of PT steel as well as the boundary elements, anchor heads, and foundation block.

The details of experimental program, construction and testing of the first test wall are presented in the following chapters.

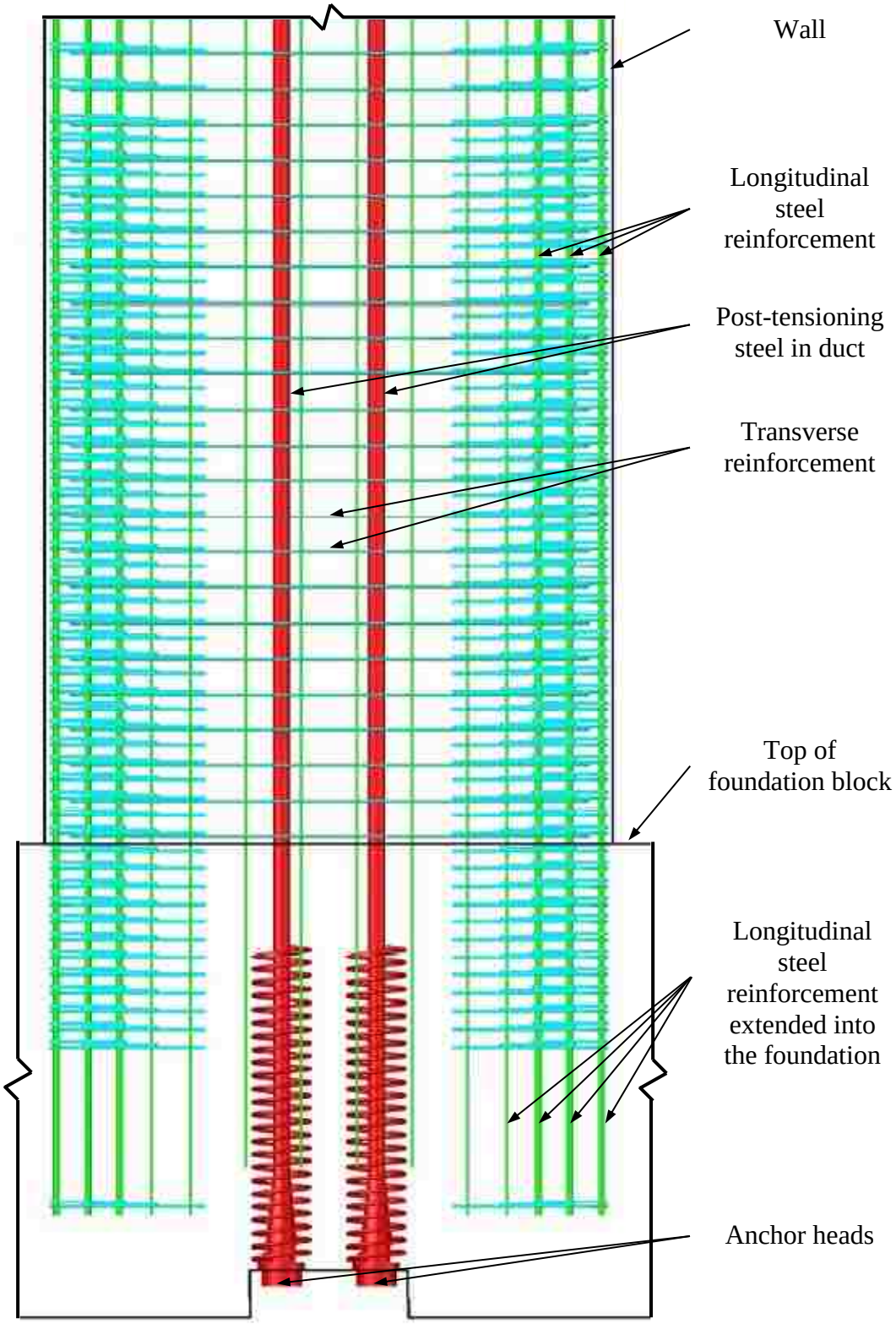

Figure 2-1 Typical structural elements in an unbonded PT structural wall

CHAPTER 3

DESCRIPTION OF EXPERIMENTAL PROGRAM

As explained in Chapter 1, the current overall research program includes test of three walls. Due to structural similarities between wall one and wall two, these two walls will be described in this chapter. Only results from wall one are presented in this report. The description of the first two test walls is presented in Section 3.1 and their overall wall geometry is described in Section 3.2. Section 3.3 describes the mild steel reinforcement layout and the fabrication sequence. Section 3.4 describes the prestressing system as well as the prestressing of the foundation block. Section 3.5 describes the wall fabrication. Section 3.6 describes the loading apparatus and load cells. Section 3.7 describes the lateral bracing system, while Section 3.8 describes the material properties and Section 3.9 describes the overall construction sequence of the test wall.

3.1 DESCRIPTION OF TEST WALL

Figure 3-1 shows the cross-sectional geometry of the test wall and the elements conforming to this section. As mentioned in work done by Srivastava (2013), the unbonded post-tensioned hybrid structural walls provide energy dissipation through the yielding of the boundary and web longitudinal reinforcement continued into the foundation. Self-centering capabilities are provided by the unbonded post-tensioning system.

Table 3-1 and Figure 3-2 show the tabulated and geometrical differences between the two walls. It is anticipated that Wall 1 (W01.10) will provide higher energy dissipation through the use of larger size longitudinal bars on the boundary elements that extend into

the foundation. On the other hand, it is expected that Wall 2 (W03.12) will exhibit better self-centering capabilities due to the additional post-tensioning strands and the size reduction of boundary elements that extend into the foundation. Since construction procedures are similar for both walls, construction details in this report are presented only for Wall 1.

The design of the special structural walls was done by Pakiding (2014). Requirements set by ACI 318-11 were followed.

3.2 OVERALL WALL GEOMETRY

Figure 3-3 shows the overall geometry, which includes the test wall, foundation block, and a thickened upper portion of the wall to accommodate the load cells that measure post-tension forces.

Once the cross-section design was finalized and following a 0.40 scale factor, the overall wall dimensions were completed. The foundation block dimensions were desiged as explained in the following chapter. Figure 3-4 shows the overall dimensions of these structural components. As mentioned before, overall dimensions for both Wall 1 and Wall 2 are similar. Other details such as the top anchor head encasement, bearing plates and load cells are explained in a later section.

3.3 MILD STEEL REINFORCEMENT LAYOUT

The test wall is represented by three different sections throughout the height of the wall, with each section characterized by a different steel reinforcement arrangement. Particular details pertaining to the design of these three sections are presented in Pakiding (2014). Figure 3-5 shows the elevation and the cross-section of these sections, namely the special boundary section, ordinary boundary section and minimum design requirement section.

The longitudinal mild steel, which provides both energy dissipation and flexural strength, was extended into the foundation as shown in Figure 3-6. The transverse confinement steel was also extended into the foundation a length equal to the development length of the boundary longitudinal bars. These bars however, were extended at least two times their development length as well as the web longitudinal bars. To increase space around the lower anchor heads, the web longitudinal bars were extended six inches less than the special boundary longitudinal bars. In the section inside the foundation and according to ACI 318, web transverse reinforcement was not required, and was therefore omitted.

3.3.1 Special Boundary Section

The special boundary element is the section of the wall where the maximum axial forces, due to and overturning moment, are expected. This section extends from the top of the foundation to an elevation of 90 inches above the foundation. In this critical section for flexure, adequate longitudinal and transverse reinforcement is required and concrete cover spalling is expected due to the formation of plastic hinges. Figure 3-7 is a photograph describing the steel layout and spacing in this section of the wall.

3.3.2 Ordinary Boundary Section

This section experiences smaller bending moment and accompanying internal axial forces as compared to the special boundary section. Accordingly, less concrete confinement is required as compared to the special boundary, and therefore transverse reinforcement spacing is doubled. However, longitudinal cross-section steel layout remains the same. Figure 3-5 and Figure 3-6 describe the spacing and the steel layout. This section extends from the end of the special boundary element (90 inches from the base of the wall) to an elevation of 150 inches from the base of the wall. This section, 60 inches long, ends at the elevation where the loading apparatus is located.

3.3.3 Minimum Design Requirement Section

This section, which extends from the end of the ordinary boundary section to an elevation of 235 inches from the base of the wall, was designed using ACI 318 minimum steel requirements. This section, 85 inches in height, is also shown in Figure 3-5 and Figure 3-6. The longitudinal bars are spliced at this location.

Also shown in these figures, transverse confinement reinforcement was not required and the boundary longitudinal bars were replaced by #3 size bars. This longitudinal cross-section configuration was continued through the thickened portion of the wall. In the thickened portion of the wall, only minimum steel for temperature and shrinkage was used.

3.4 PRESTRESSING SYSTEM

The prestressing system is divided into components used in the prestressing of the wall and components used in the prestressing of the foundation block. As shown in Figure 3-8, the complete wall prestressing system is formed by top and bottom anchor heads, top anchor head encasement, steel reinforcement spirals, horizontal foundation post-tensioning and foundation block tie-downs.

3.4.1 Test Wall Prestressing System

The anchor head assembly, shown in Figure 3-9(a), is a two-part anchor head consisting of a wedge plate (Figure 3-9(c)) and a compact conical anchor body. The wedges (Figure 3-9(b)) fit inside the wedge plate. Figure 3-9(d) shows a photograph of the strands already seated in the wedges (procedure explained in Section 3.5.4). This anchor system also offered the flexibility of having space for five or seven strands. As described earlier, Wall 1 consists of two bundles of five strands, while Wall 2 consists of two bundles of seven strands and one bundle of five strands.

In most engineering projects, these anchor heads are embedded in concrete. However, in order to obtain the tendon forces during the test, the anchor heads at the top of the wall were anchored outside the test wall so load cell could be placed between the top anchor head and the wall as shown in Figure 3-4 and Figure 3-8. Figure 3-10 shows the details of the external anchorage. This top anchor head encasement section housed the anchor head and trumpet as shown in Figure 3-10. The encasement is a hollow structural section (HSS) rectangular tube half inch thick filled with grout between the tube and the trumpet.

The HSS tube replaces the steel reinforcement spiral and keeps the concrete confined. Additionally, to reduce the stress between the strands and the wedges in the wedge plate, a portion of the strand was unsheathed and bonded to grout. Figure 3-11 shows a total bonded length of 27.5 inches that starts from the middle of the load cell and extends to the top of the anchor head. Using expansive insulation foam, a plug was made to keep the grout from extending beyond the intended bonded length that is shown in Figure 3-11. Figure 3-12 shows construction photographs of the top anchor head encasement.

At the bottom end of the tendons, the bottom anchor heads were embedded in concrete in the foundation block, as shown in Figure 3-13. Originally, the anchor head system comes with a 24 inch long, 0.5 inch in diameter #4 bar spiral reinforcement. In order to increase confinement in the anchor heads, since the foundation block is only 24 inches wide, a 40 inch long #4 bar spiral was used. Figure 3-13 also shows the different prestressing components of this system.

As with the upper anchor head, a portion of the strand before the bottom anchor head was bonded. However, the unsheathed bonded length for the lower anchor head was 36 inches. Expansive insulation foam was also used to create a plug to prevent the grout to extend beyond the intended bonded length. Figure 3-14 shows a pocket at the bottom of the foundation block was used to access the bottom anchor head and to monitor the strands while prestressing the walls and during testing.

The post-tension strands, as shown in Figure 3-15, were delivered greased and sheathed, and a PVC conduit was also used to ensure they remained debonded. Bonded lengths at the end of each strand had the plastic sheath and grease removed and were cleaned prior to grouting.

3.4.2 Foundation Block Prestressing System

Longitudinal prestress was used to eliminate cracking in the foundation block during testing. This is discussed further in the following chapter. In addition to these longitudinal prestressing forces, the foundation block was prestressed down to the laboratory strong floor. Figure 3-16 shows both the vertical and horizontal prestressing systems used in the foundation block, as well as the equipment required to prestress the bars. As shown in the figure, both the vertical rods and horizontal high strength bars are placed inside PVC conduit to keep them from bonding to surrounding concrete. Figure 3-17 shows the equipment involved in prestressing the longitudinal bars.

3.5 FABRICATION OF TEST WALLS

Fabrication of the test wall began as soon as the material from different sources arrived to the laboratory. This included steel reinforcement rebar, tendons and high strength prestressing system, formwork panels and lifting inserts.

3.5.1 Site Preparation

The first step in the fabrication sequence was preparing the site. A plastic cover was placed on the floor to protect it. Shear keys on the floor were wrapped in duct tape and PVC conduits were used to protect the steel rods used to tie-down the foundation block.

3.5.2 Steel Reinforcement Cage Fabrication

Once the site preparation was complete, the foundation block, as shown in Figure 3-18, was the first cage to be built. The fabrication of the wall steel reinforcement cage was formed by three individual cages. Figure 3-19 shows the sequence in which the wall cage was fabricated. The web section was constructed first, followed by the boundary cages. Once these three sections were complete, the boundary cages were inserted into the web section and tied together. Finally, the fish hook was inserted on the edges of the cage. Once the wall cage was completed, the bottom anchor heads, already seated (see Section 3.5.3), were set at the bottom of the cage and the strands were passed through the center of the wall cage.

The wall cage, along with the lower anchor heads and strands, were inserted into the foundation block (Figure 3-19). The lower anchor heads were placed in their final position and set on the pocket previously mentioned. The wall cage was supported by hooks mounted on support columns to keep the cage plumb during concrete placement.

3.5.3 Formwork and Concrete Placement

With the insertion of the wall cage into the foundation cage, the next step was to form the foundation block to place the concrete. Figure 3-20, Figure 3-21 and Figure 3-22 show the formwork arrangement using prefabricated formwork panels.

A complete concrete placing schedule is presented in Figure 3-23. Cold joints were prepared by roughing the concrete surface with an amplitude of quarter to half inch at each joint. Figure 3-24 shows additional construction photographs.

3.5.4 Seating of Strands in Anchors Heads

Since access to the lower anchor head was limited, strands for the lower anchor heads were seated before casting the foundation block. In order to seat the strands in the wedges, a special fixture was constructed as shown in Figure 3-25. On one end was a short W12x190 column with a hole matching the wedge plate, and on this side the strands were seated into the wedge plate. On the other end, another short column with only one hole through which a strand was tensioned to 20 kips using a standard jack. The prestressing was done to 38% of yielding. The strands were seated one by one. The strands were tensioned by gripping at 396 inches (33 feet) to avoid damage to the strand within the 300 inch unbonded length.

3.6 LOADING APPARATUS

Lateral forces were applied to the test wall using a horizontal actuator. The actuator has a 38 inch stroke, and has a tension force capacity of 348 kips and a compressive force

capacity of 462 kips. Figure 3-26 shows a photograph of the actuator and the actuator support framing.

The clear distance between the reaction wall and the test wall is 204 inches. The actuator is 140-7/8 inches in length at midstroke. To bridge the gap, an actuator support fixture shown in Figure 3-26 was fabricated to support a stud column that extended the reach of the actuator and extend its reach to 204 inch target at mid-stroke. The actuator support fixture positions the actuator so it can attach to the test wall while extended at midstroke. Figure 3-27 also shows the location of the B7 (A325) rods and the bearing plate. Eight B7 rods were used to attach the wall to the actuator.

The actuator was placed at 17.5 feet from the floor, or at 12.5 feet from the base of the wall, as shown in Figure 3-27. Prior to placement, proper movement of the actuator was verified by laboratory technicians, and the actuator load cell was calibrated to ensure proper functioning during the test. Details of the loading sequence, shown in Figure 3-28, were developed by Pakiding (2014).

3.7 LATERAL BRACING

In order to prevent out-of-plane movement of the test wall during testing, bracing as shown in Figure 3-29 was provided. The columns and beams used to assemble the bracing were readily available in the laboratory. The W12-190 columns were bolted to floor anchors. These columns were placed 10 feet apart in the N-S direction, as well as in the E-W direction. The beams in the N-S direction were bolted to the columns while the

beams in the E-W direction were attached to the N-S beams using structural clamps. Using structural clamps provided versatility in location and allowed the beam to be as close as desired to the test wall.

The lower set of E-W beams were placed 16 inches below the actuator, while the upper set of E-W beams were placed 16 inches below thickened portion of the wall. These E-W beams were rotated 90 degrees so that their flanges would bear against the test wall. Polytetrafluoroethylene (PTFE) pads shown in Figure 3-30 were placed between the E-W beam flanges and the wall. These pads helped to reduce any friction forces that would develop between the wall and the bracing.

3.8 INSTRUMENTATION AND DATA ACQUISITION

A variety of gauges and other types of instrumentation were used to gather data during the experimental testing. Figure 3-31 shows a #3 steel reinforcement rebar 16.5 inches long embedded in each confined region. These strain gauges, located at 8.25 inches from the base of the wall, measure the compressive and tensile strains in this rebar. Using strain compatibility, concrete strains can be obtained until the point that this bar becomes debonded from its surrounding concrete. This bars where placed on the centroid of the confined boundary section.

Figure 3-32 shows the location of the strain gauges on the transverse shear reinforcement #4 steel bars. These strains gauges are located at five locations throughout this transverse bar on the North side, and on five different locations on the South side. These bars are

located at 9.90 inches from the base of the wall. These strain gauges are used to estimate the portion of the transverse shear carried by the shear reinforcement.

Figure 3-33 shows the location of the strain gauges on the stirrups at various elevations. These strain gauges measure the deformation in the confined region due to compressive forces and can be used to estimate confining stress. On the West end of the wall, strain gauges were located on the West and North face of the stirrup and on the East end of the wall, strain gauges were located on the North, South, East, and West side of the stirrup.

Figure 3-34 shows the location of the strain gauges located on the longitudinal steel reinforcement. These gauges measure the steel bar strain under compressive and tensile forces at various elevations. On the West end of the wall, these gauges were located on the middle bar of the far end. On this bar, strain gauges were placed on each side (North and South) of the bar. On the East end of the wall, strain gauges were placed on two bars. Gauges on the middle bar of the far end were also place on each side (North and South). The second bar was located on the South-East corner. Gauges on the bar were only placed on the East face of the rebar.

Figure 3-35 shows the location of the linear variable differential transformers (LVDT) located on the north face of the wall. These LVDTs measure displacement which is can help estimate shear deformations during the application of lateral loads. Three rods were cast inside the concrete at each end of the wall on the North side. These rods were cast at 30 and 60 inches from the base of the foundation block and at 3-3/4 inches from the end

of the wall. LVDTs were attached to these rods in a diagonal manner as shown in Figure 3-35.

Figure 3-35 also shows the location of the rotation meters located on the North side of the wall. These rotation meters are located on the longitudinal center line of wall and are located at 30 and 60 inches from the base of the wall. These rotation meters are used to estimate the lateral displacement that corresponds to rotation and the portion of the lateral displacement that corresponds to shear displacement.

Figure 3-36 shows the location of potentiometers at the base of the wall. These potentiometers measure displacement and are essential to obtain gap opening measurements. In total, five potentiometers were placed on the North face of the wall. These potentiometers can help determine the gap opening at each cycle during testing and any possible residual gap after the testing.

Figure 3-37 shows an overall view of additional instrumentation for in-plane measurements. A string potentiometers is located at the top of the wall to measure lateral displacement at the top of the wall (a). A LVDT is located at the actuator level connected to an independent column to measure displacement at the actuator level (b). Two additional string potentiometers are located at this level to measure vertical displacement due to flexure (c). A final LVDT is located at the end of the foundation block (d). This LVDT measures lateral foundation block displacement. This figure also shows a load cell attached to the actuator, which measures applied forces, and two load cells located at the

top of the wall. These last two load cells measure prestressing forces applied by the PT strands.

Figure 3-38 shows a photograph of the instrumentation placed on the North side of the wall. This photograph shows the location of LVDTs for shear deformation, the potentiometers for gap opening measurement, and the rotation meters.

Figure 3-39 shows a photograph of the load cells used to obtain the prestressing forces applied to the wall. The load cells were fabricated from steel tubing and placed between the top anchor head encasement and the top of the wall. These load cells have a maximum load capacity of 450 kips, which is 43% higher than the maximum expected compressive force.

Figure 3-40 shows a photograph of actuator load cell, which has a maximum capacity of 340 kips. This load cell is attached to the actuator as shown in Figure 3-37.

3.9 MATERIAL PROPERTIES

Design material properties are presented in Table 3-2. This table includes concrete, steel reinforcement, and post-tension strands. Design material properties were used to design the structural wall and foundation block. Available actual material properties are presented in Table 3-3. Steel reinforcement properties were obtained from tensile testing according to ASTM standards. Bars used for this test were cut-off of the same bars used to fabricate the wall.

3.10 OVERALL CONSTRUCTION SEQUENCE

Construction of the first test wall was performed in the following sequence and is also the recommended sequence for construction of the second test wall:

1. Place columns and bracing beams.
2. Prepare floor surface.
3. Build foundation block reinforcement cage.
4. Build wall reinforcement cages up to actuator elevation.
5. Install strain gauges on this lower portion of the wall reinforcing cage.
6. Insert the previously seated lower anchor heads through the wall cage. At this point the tendons are already inside the conduits.
7. Foam/seal a portion of the conduit and insert plastic hose to bleed out the air while grouting.
8. Insert wall cage (with anchor heads) into the foundation block and secure the wall reinforcement cage at the final elevation.
9. Set anchor heads at final position.
10. On the floor, build upper portion of the wall reinforcing cage.
11. Form and cast foundation block.
12. Form and cast wall.
13. Install LVDT transformers.
14. At the top of the wall, place the lower bearing plate on hydro-stone.
15. On top of the lower bearing plate, place the load cells, top bearing plate and top anchor head encasement.

16. Post-tension the horizontal high strength bars in the foundation block starting with the center bars. Apply half the final stress, and then on the second round apply final stress.
17. Post-tension the foundation block tie-downs.
18. Post-tension the wall strands. Apply half the initial prestressing force, and then on the second round apply final stress.
19. Grout trumpets.
20. Install actuator support bracing, actuator, hydraulic hoses and control systems.
21. Test and calibrate actuator for load control.
22. Set cameras and video recording devices.
23. Perform test.
24. Demolish/remove test wall.

Table 3-1 Description of test walls

Property			Wall 1	Wall 2
Dimensions (in)	H_w		300	300
	H_f		150	150
	L_w		72	72
	t_w		10	10
Aspect Ratio	H_w/L_w		4.2	4.2
	L_w/t_w		7.2	7.2
Reinforcement	Boundary	Long.	8 #7 and 2 #3 (A706)	8 #5 and 2 #3 (A706)
		Trans.	#3 @ 2.25 in (A706)	#3 @ 2.25 in (A706)
	Web	Long.	12 #3 (A615)	12 #3 (A615)
		Trans.	#4 @ 4.5 in (A615)	#4 @ 4.5 in (A615)
Number of PT Strands (0.6 in dia.)			10	19
Unbonded Length (in)			300	300

Table 3-2 Design material properties

Property		Wall 1	Wall 2
Concrete (ksi)	f'_c	6.0	6.0
	f'_{cce}	9.9	9.9
Steel Reinforcement (ksi)	f_y	60	60
	f_{ye}	66	66
	f_{ue}	99	99
PT Strands (ksi)	f_{py}	243	243
	f_{pu}	270	270
	$f_{pi} = 0.61 f_{pu}$	164.7	164.6

Table 3-3 Actual material properties

Wall ID		Wall 1	Wall 2
Steel Reinforcement (ksi)	f_y	68.6	68.6
	f_{ye}	68.6	68.6
	f_{ue}	110.1	110.1

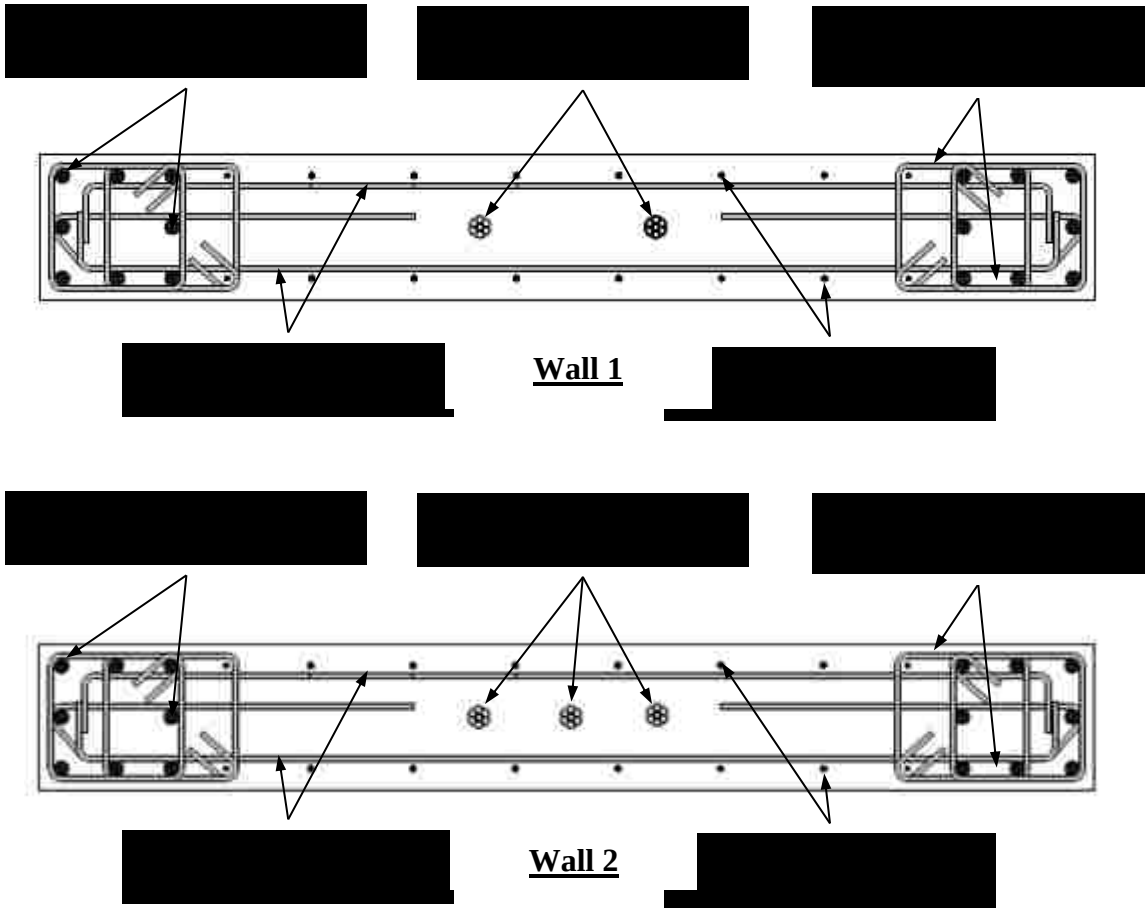

Figure 3-1 Wall cross-sectional elements included for Wall 1 and 2

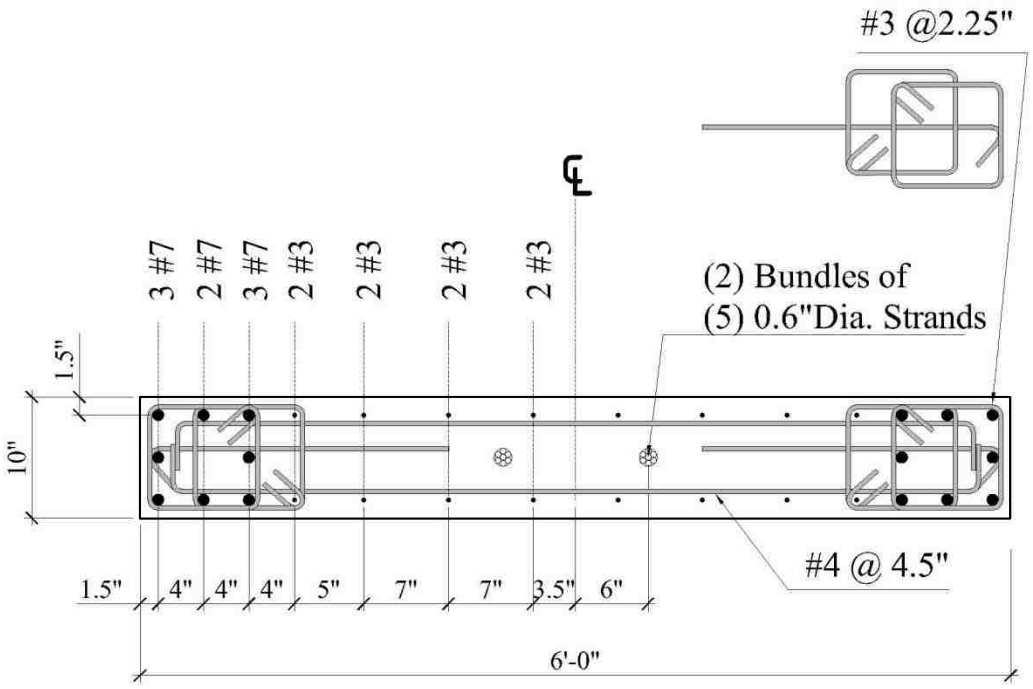

Wall 1

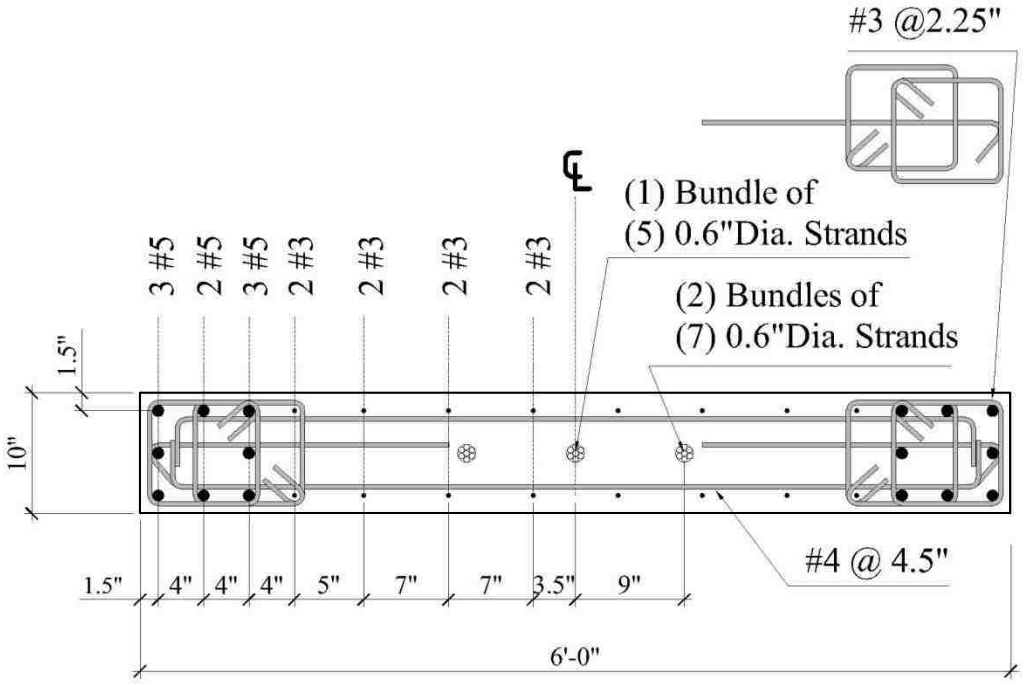

Wall 2

Figure 3-2: Cross-section geometry of Wall 1 and Wall 2

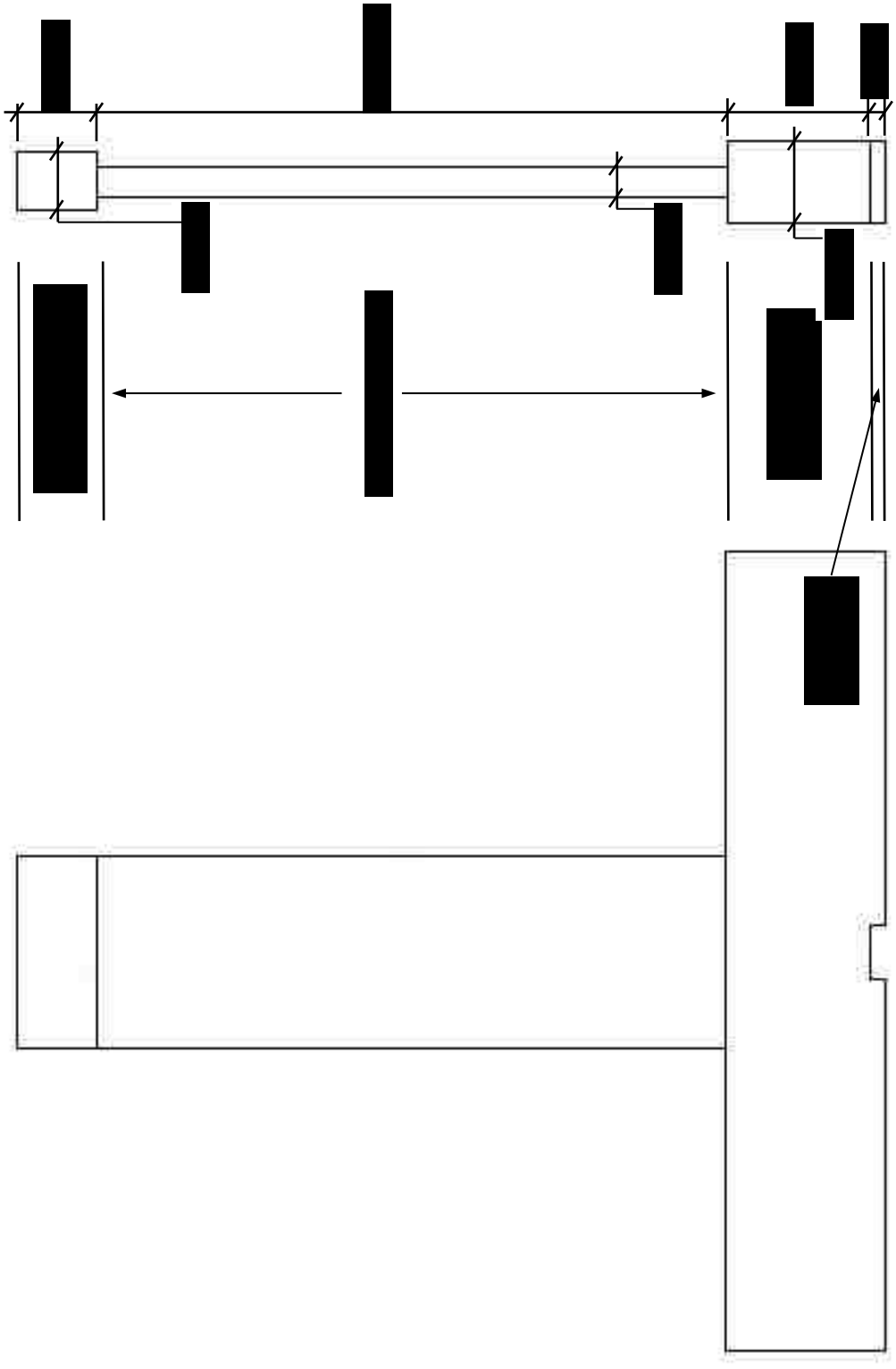

Figure 3-3 Overall geometry of the test wall

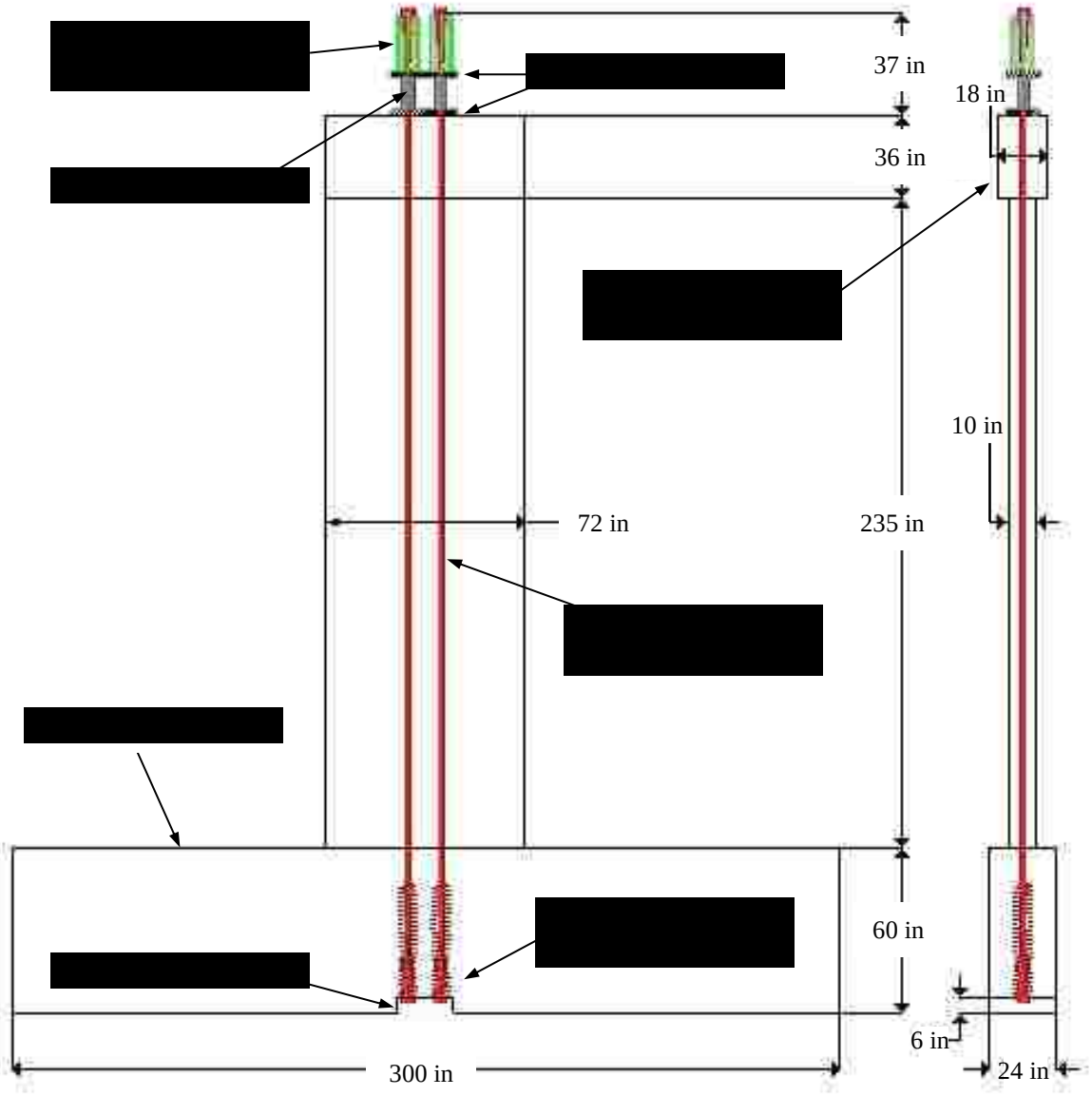

Figure 3-4 Overall test wall dimensions including major components

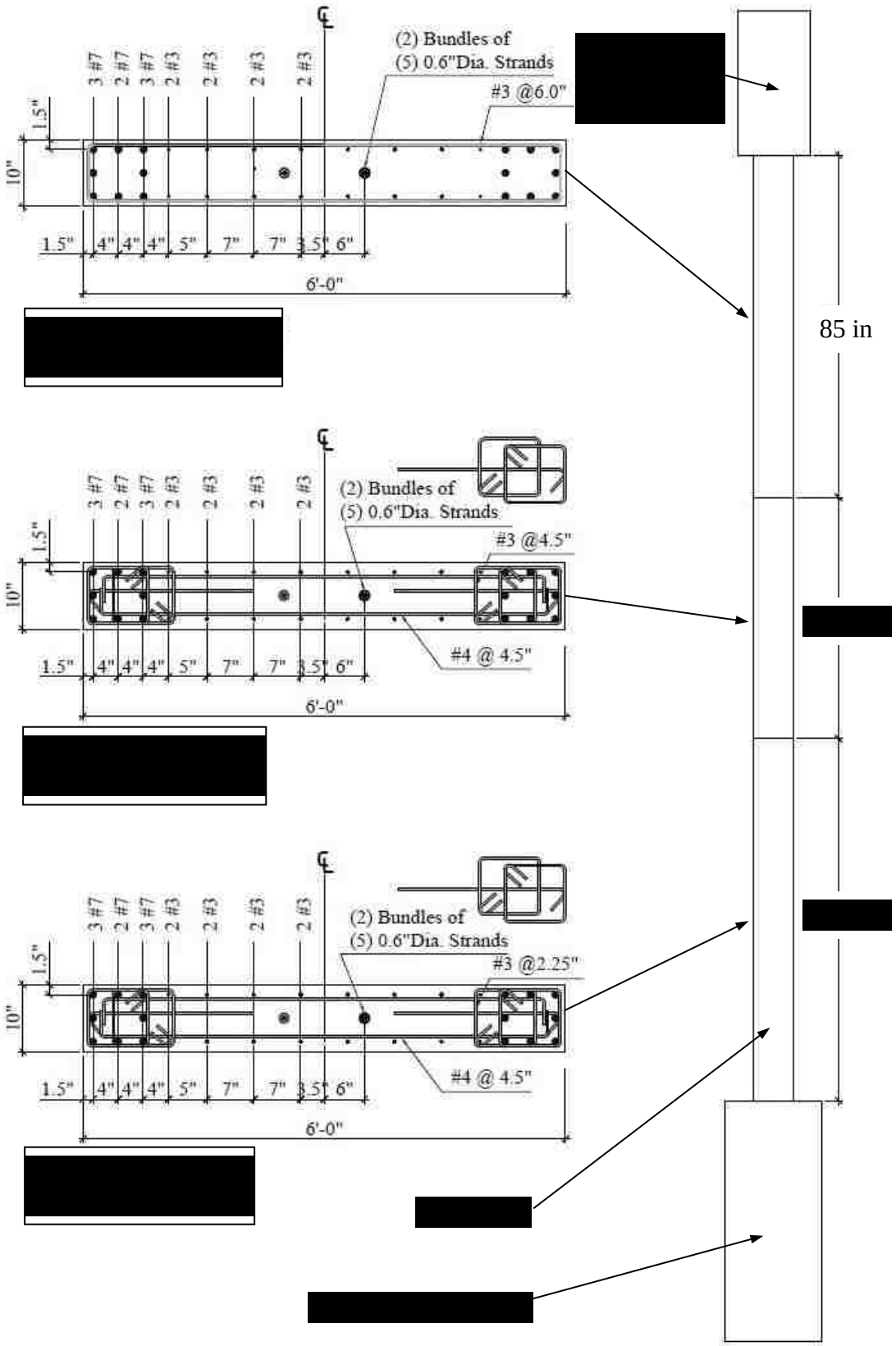

Figure 3-5 Wall cross-sections at different elevations of test wall for Wall 1

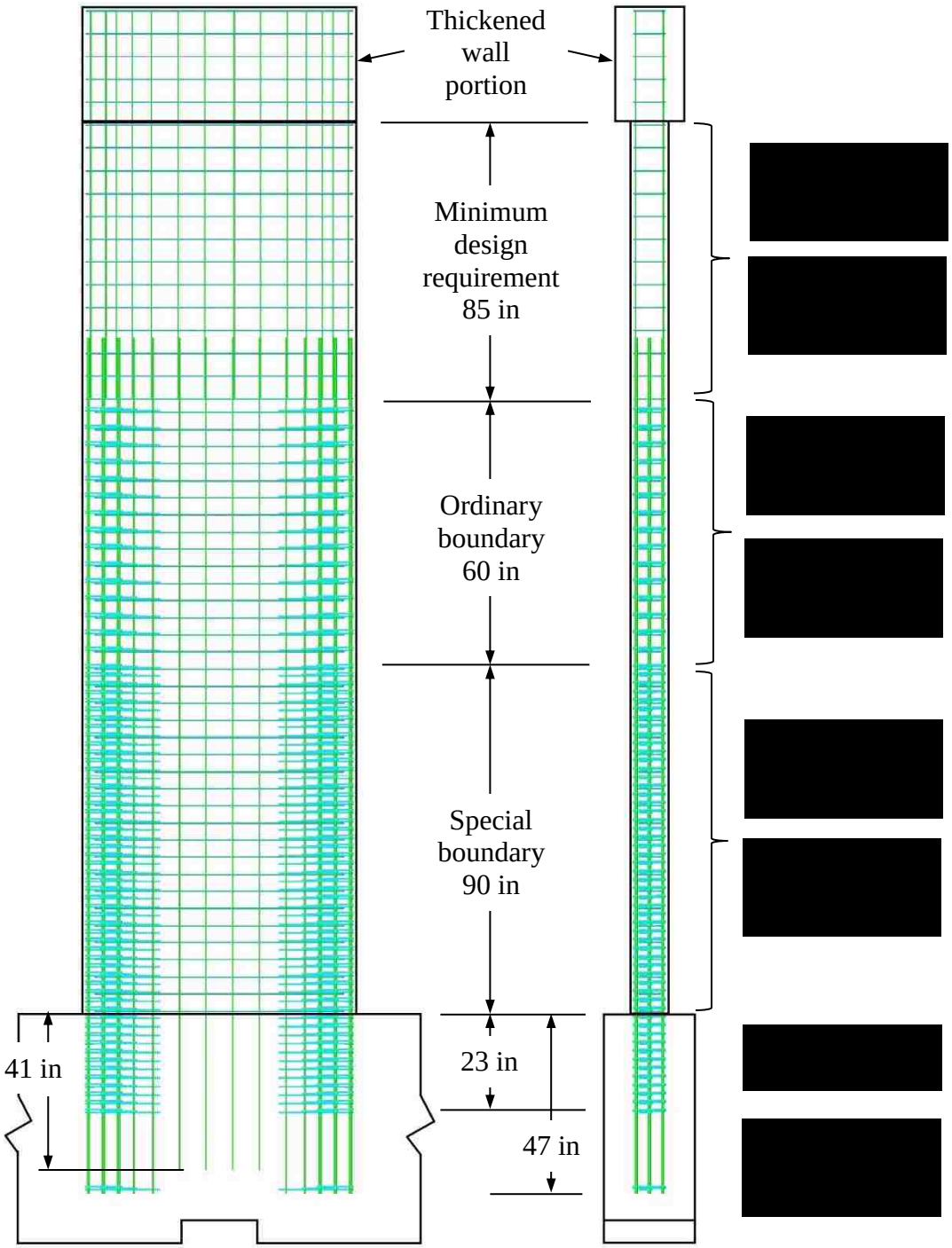

Figure 3-6: Elevation view of test wall showing steel layout at different elevations and steel layout inside the foundation (foundation steel reinforcement omitted for clarity)

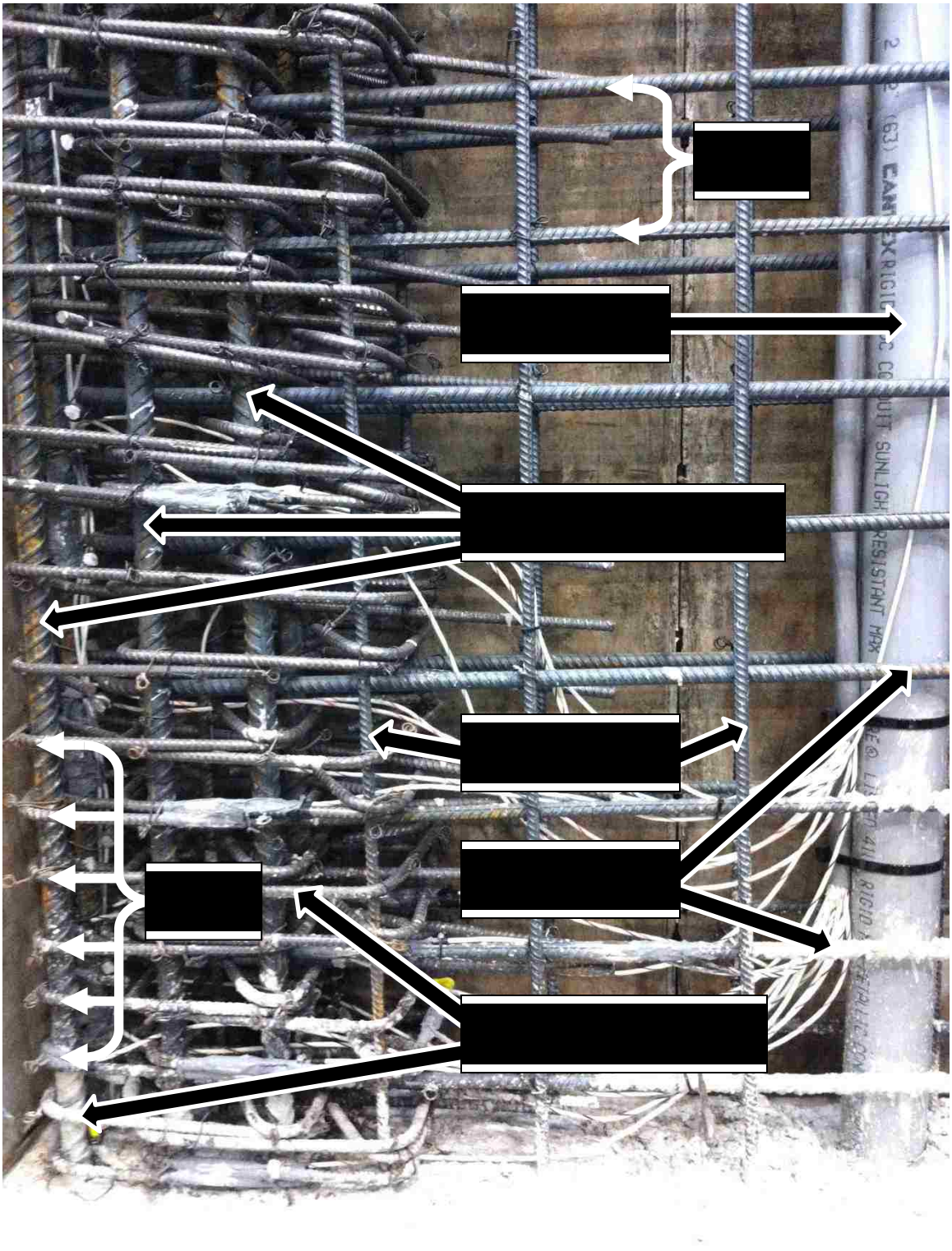

Figure 3-7 Steel layout of special boundary

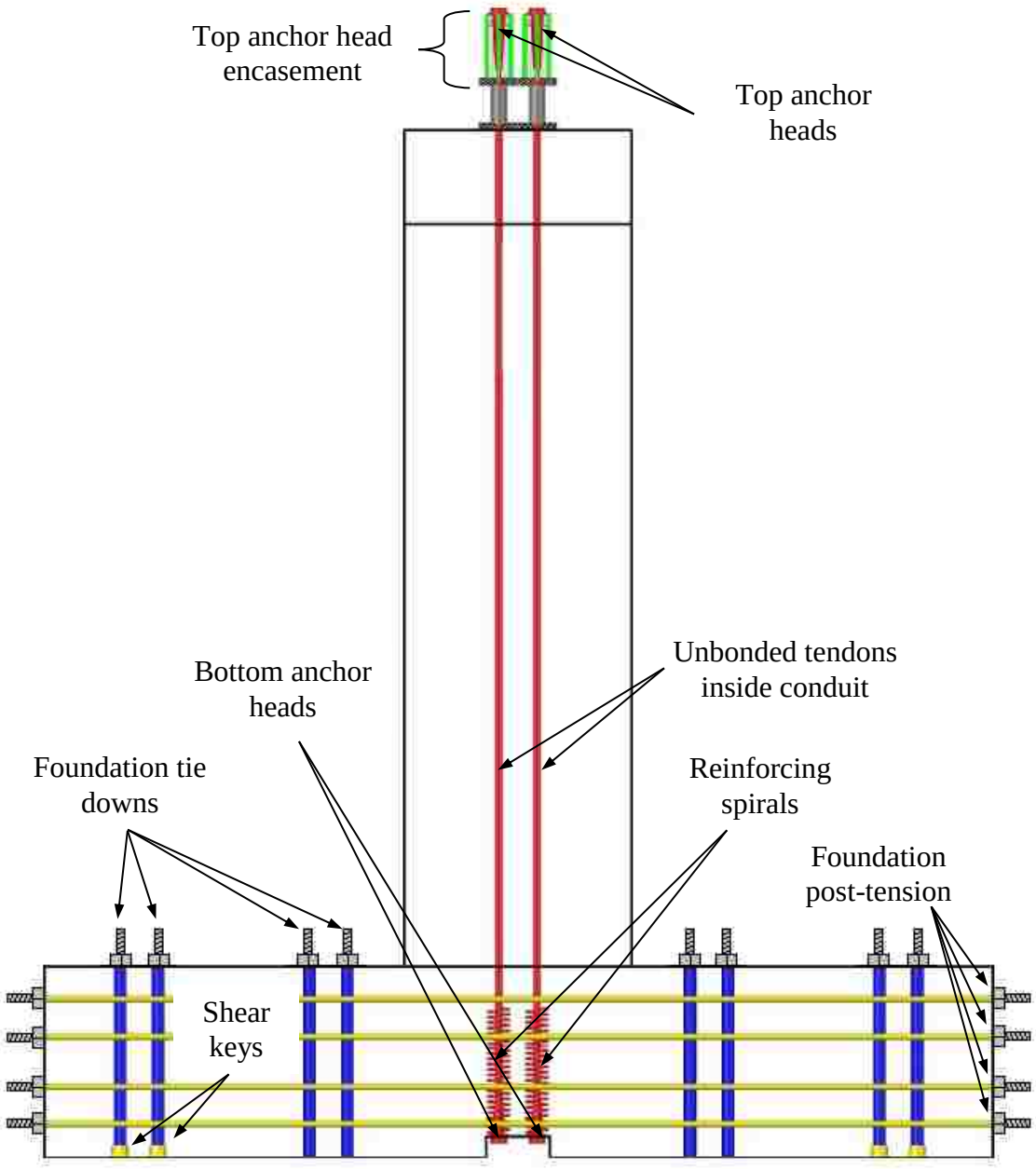

Figure 3-8: Prestressing systems for the wall and for the foundation

Figure 3-9 Anchor head components: (a) complete assembly; (b) strand wedge; (c) wedge plate; and, (d) seated strands

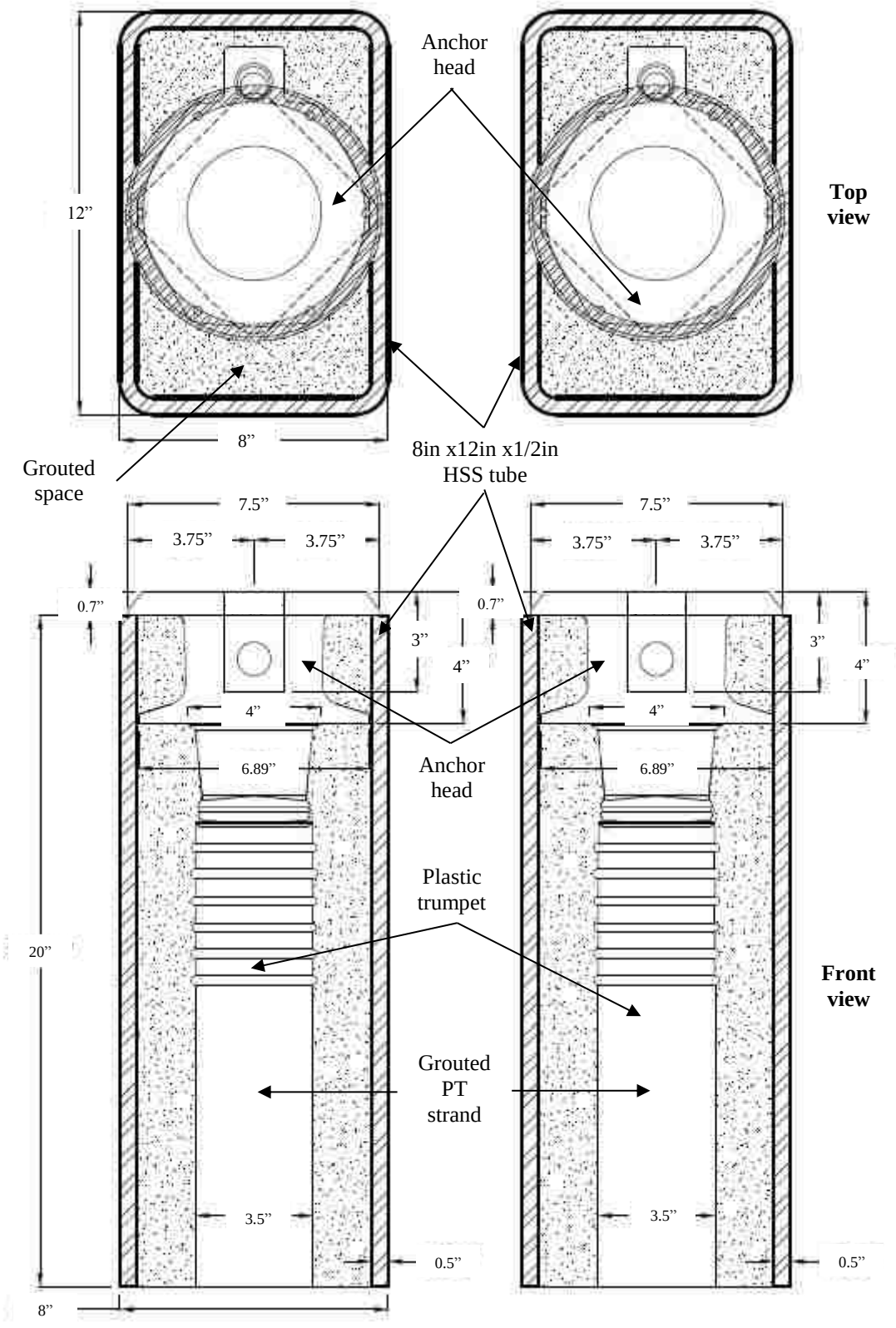

Figure 3-10 Top anchor head encasement used at the top of the wall

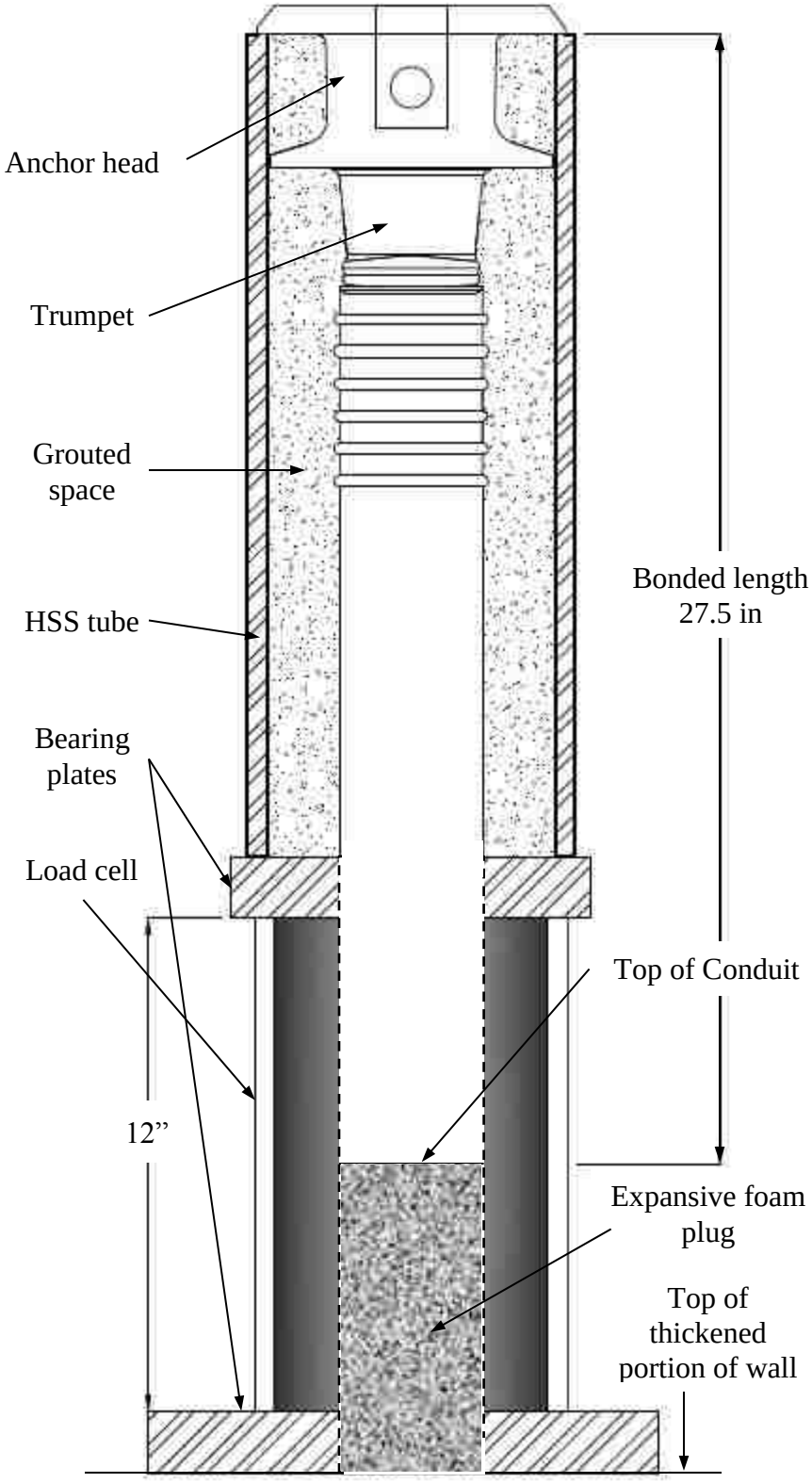

Figure 3-11 Grouted portion of strands at the top of the wall

Figure 3-12 Construction photographs of the top anchor head encasement

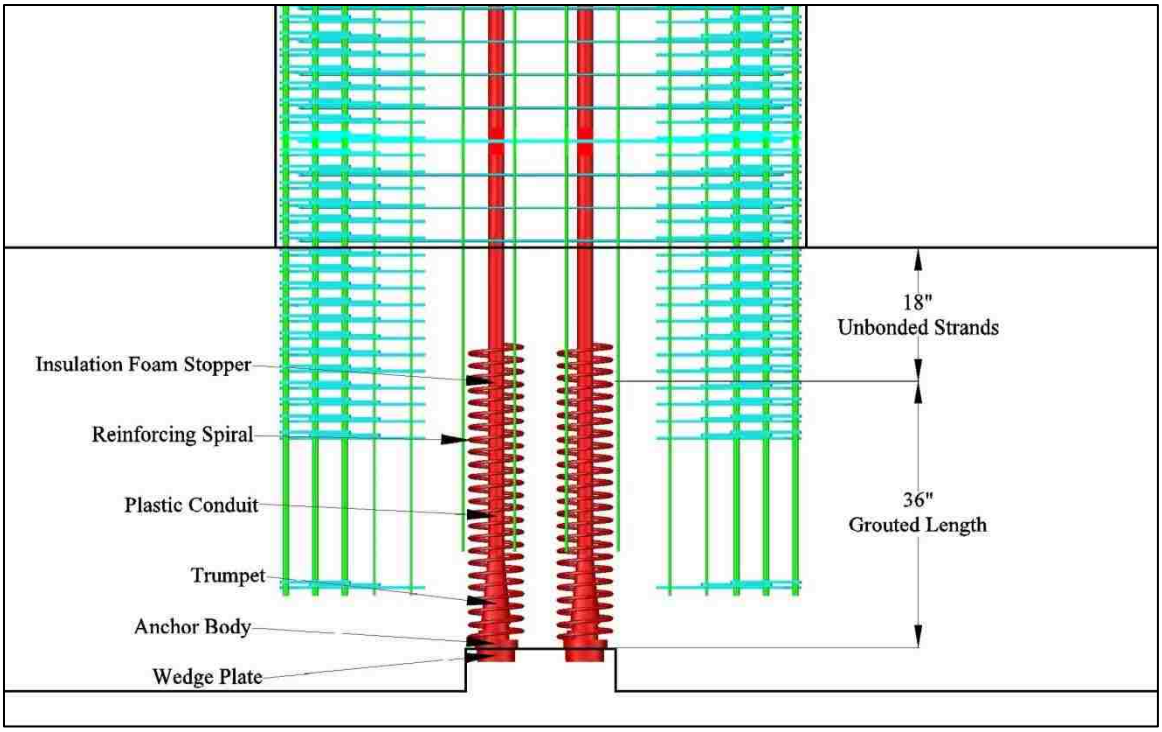

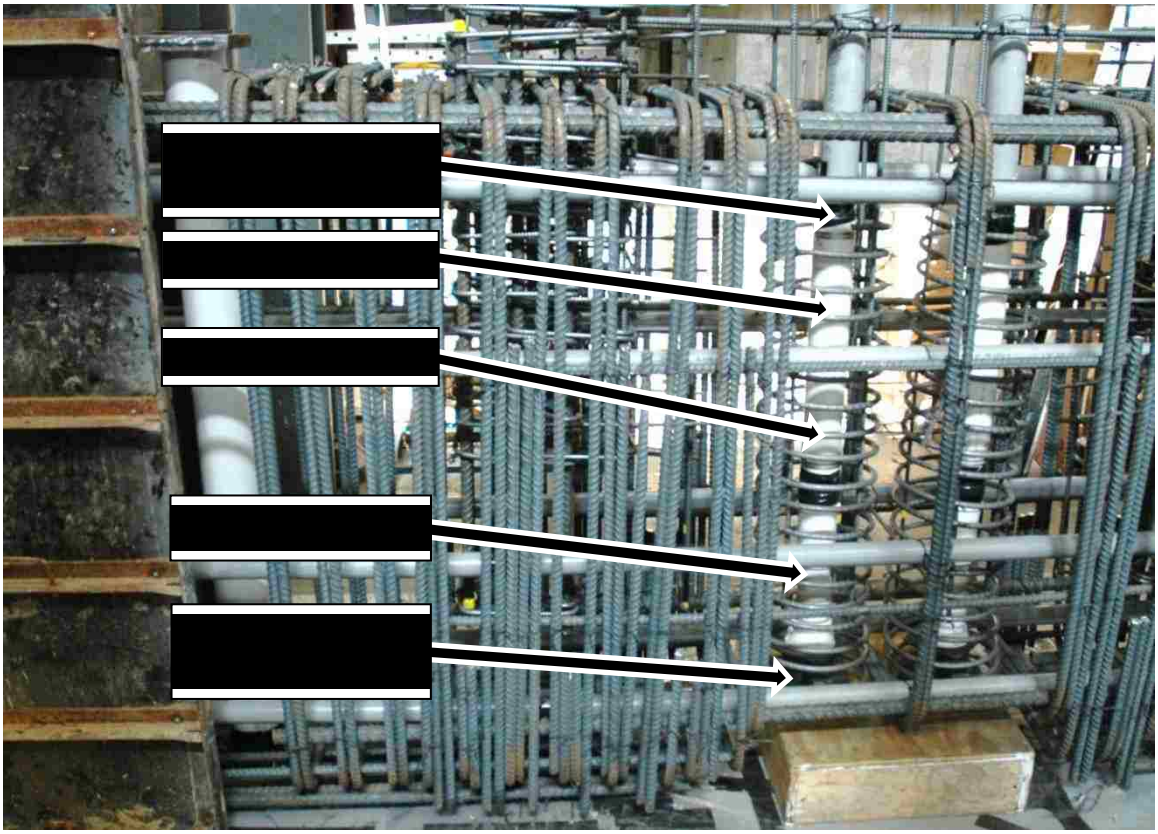

Figure 3-13 Drawing and photograph showing the grouted portion of the post-tension system at the foundation level

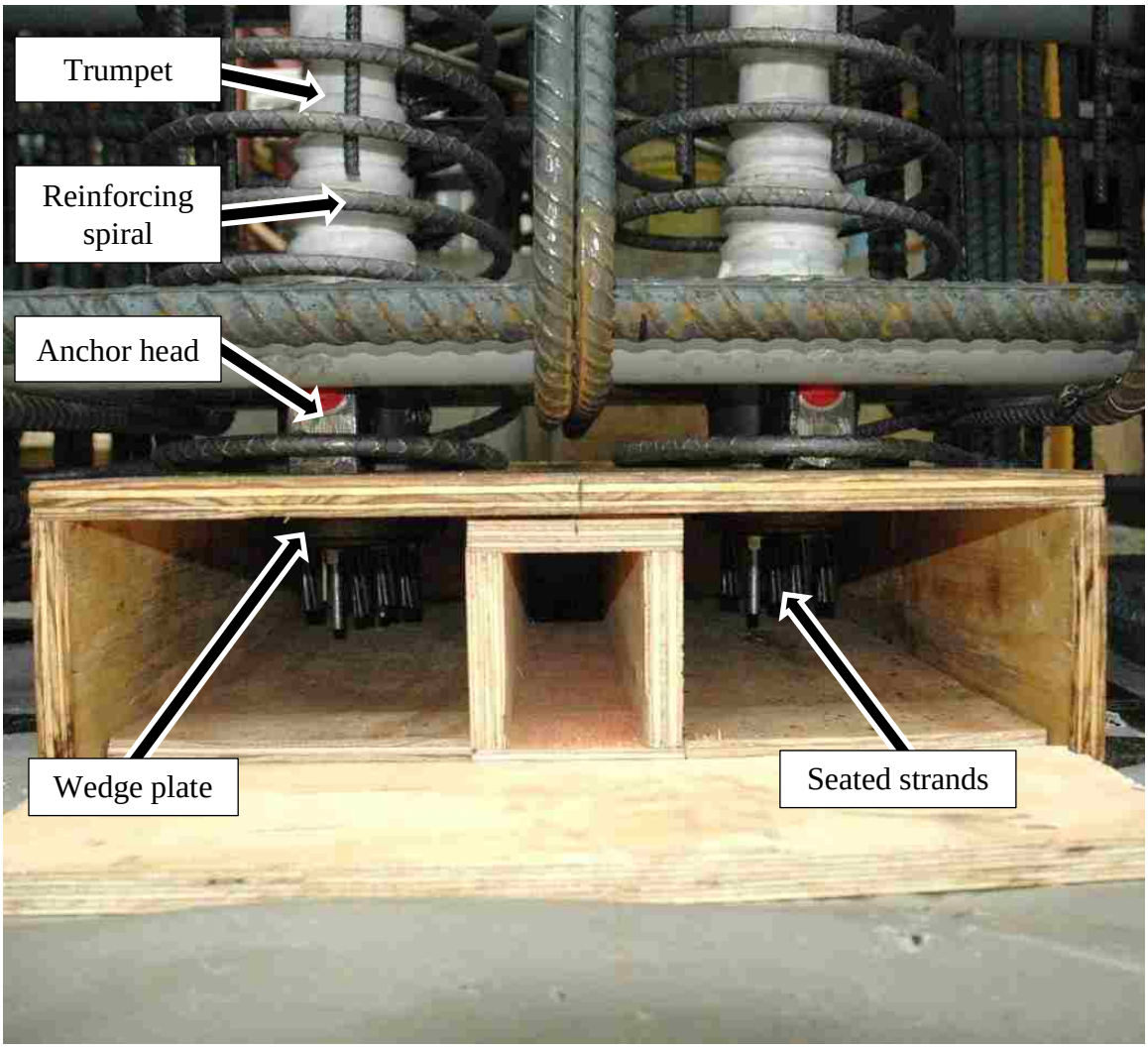

Figure 3-14 Pocket to access the wedge plates and monitor strands

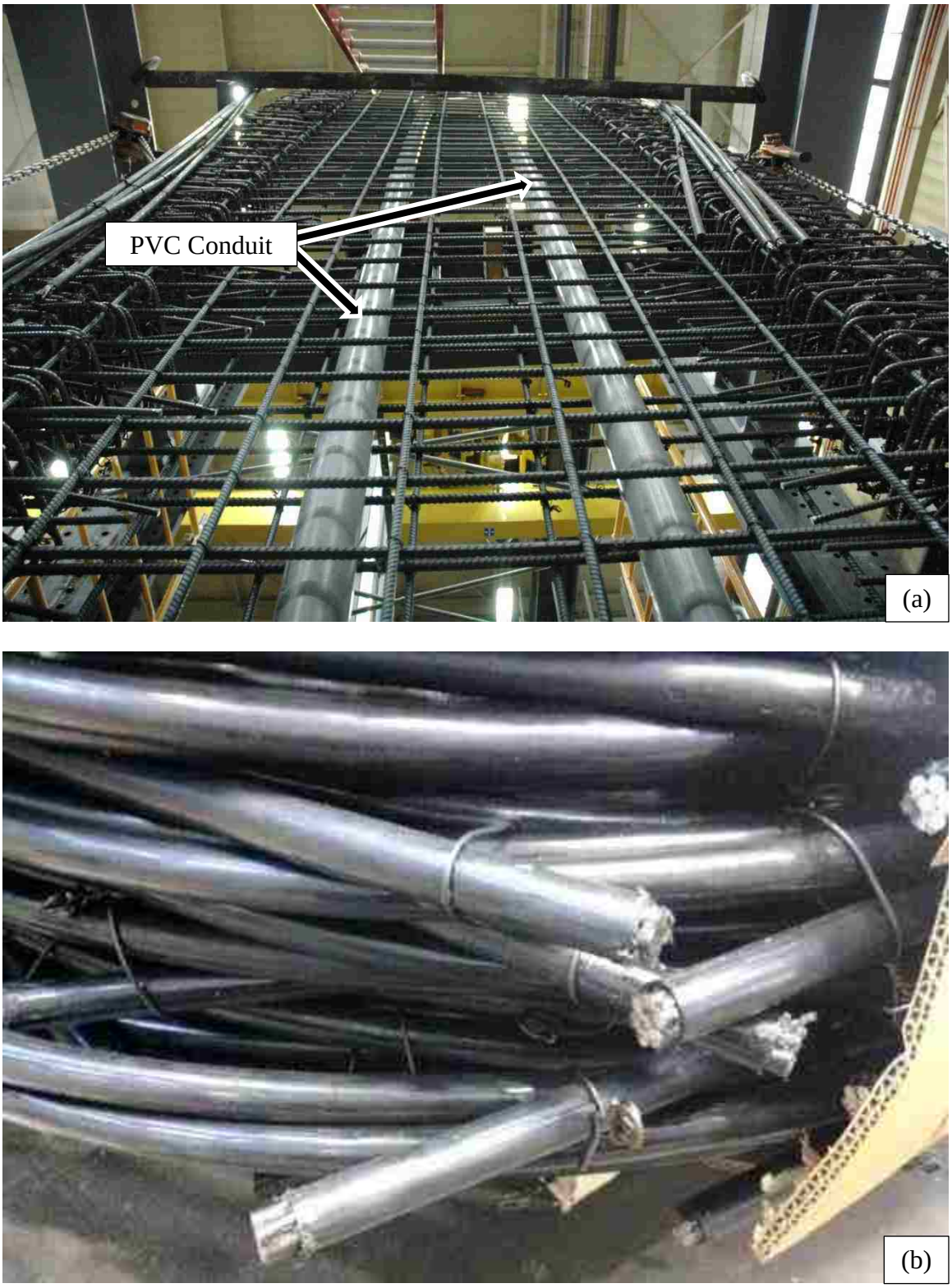

Figure 3-15 (a) PVC conduit that carries the unbonded post-tensioned tendons; and, (b) greased and sheathed strands

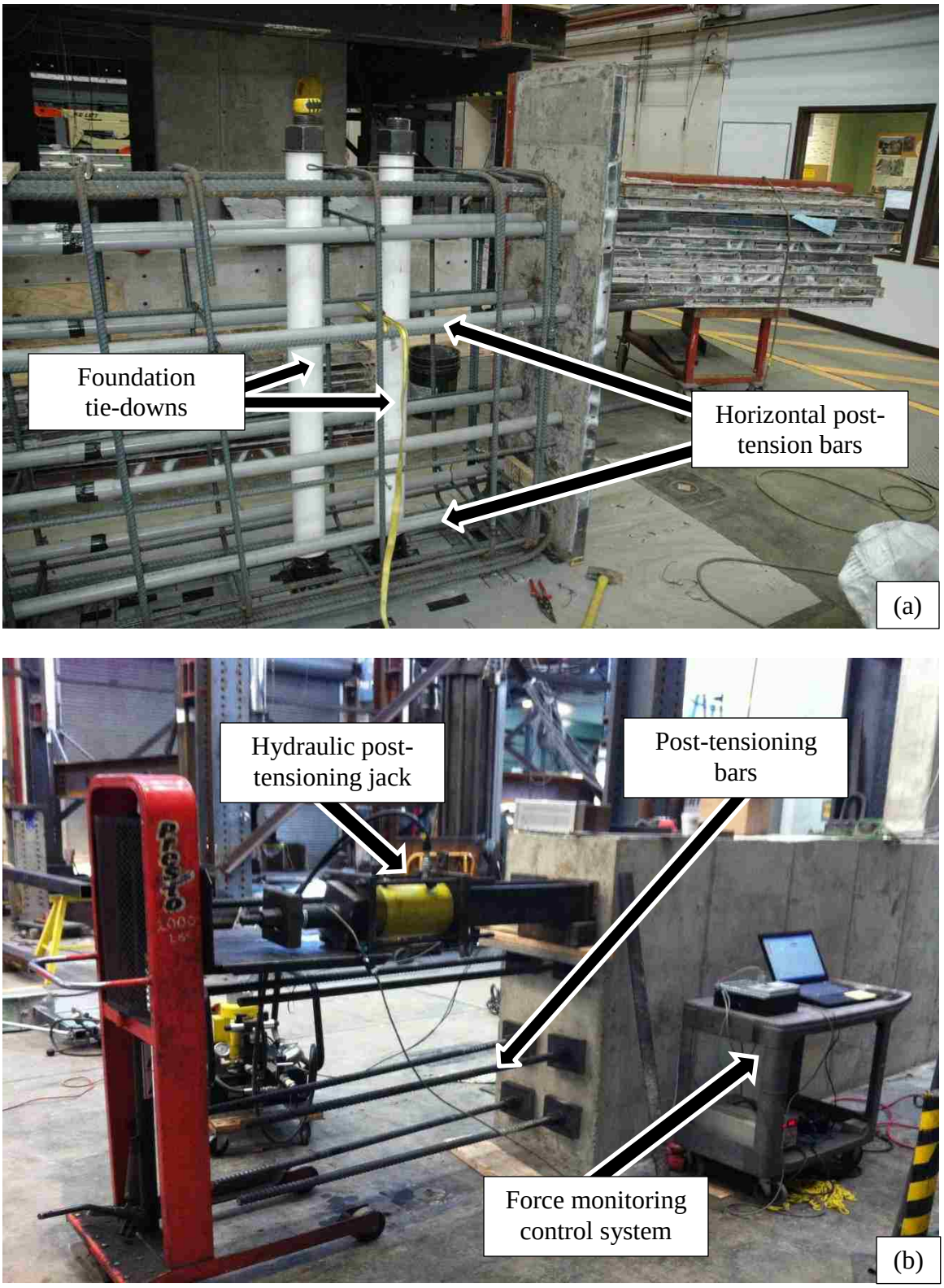

Figure 3-16 Foundation block post-tensioning systems: (a) horizontal and foundation tie-downs inside PVC conduits; and, (b) post-tensioning of the high strength horizontal bars

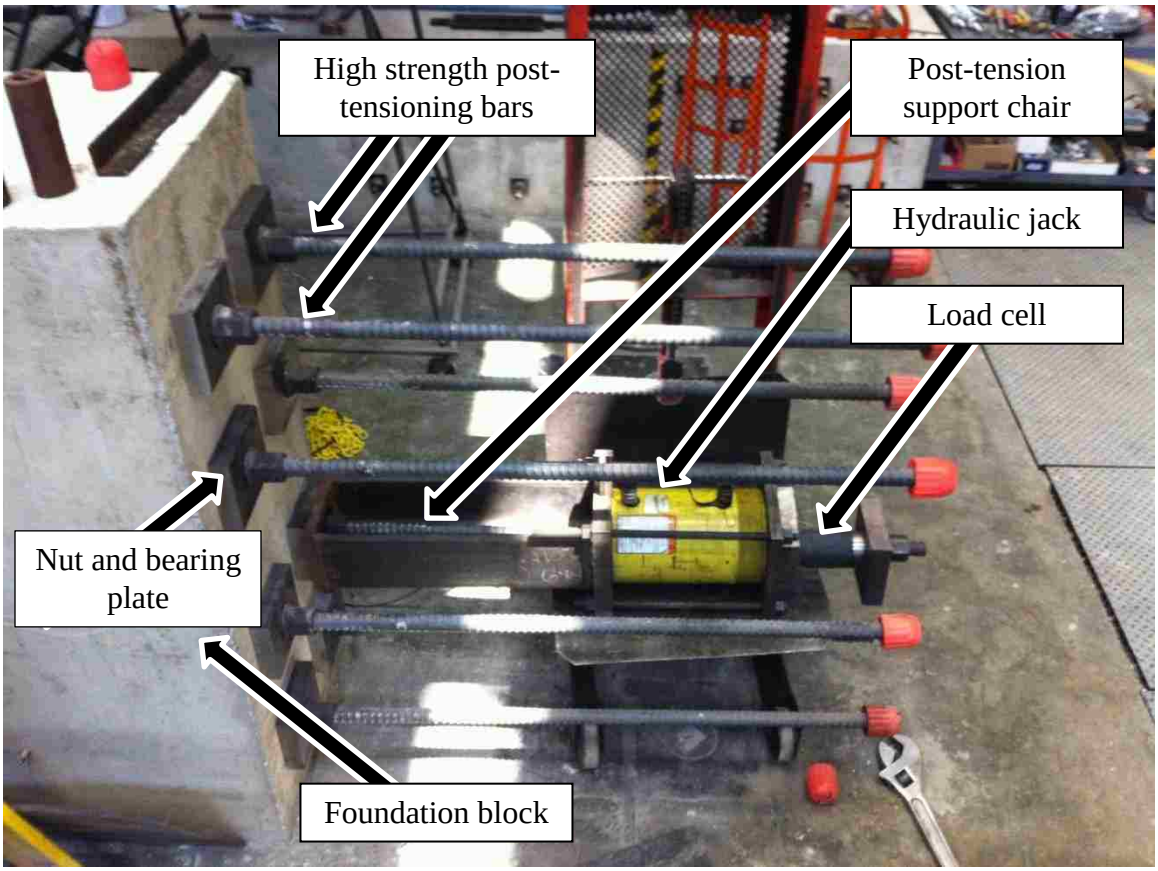

Figure 3-17 Prestressing equipment needed for post-tensioning the foundation block

Figure 3-18 Construction photographs of the steel reinforcement cage for the foundation block

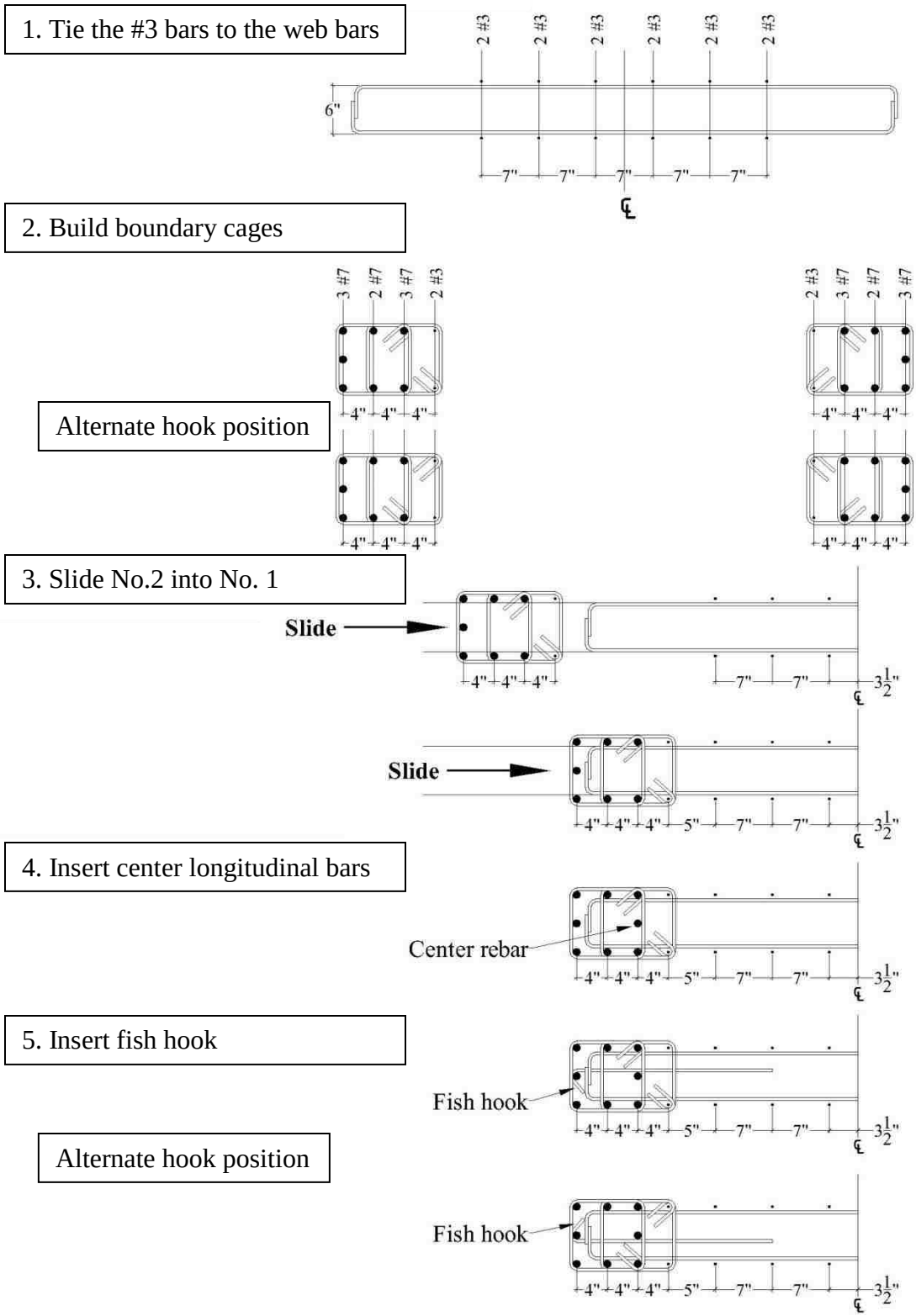

Figure 3-19 Steel reinforcing cage fabrication sequence

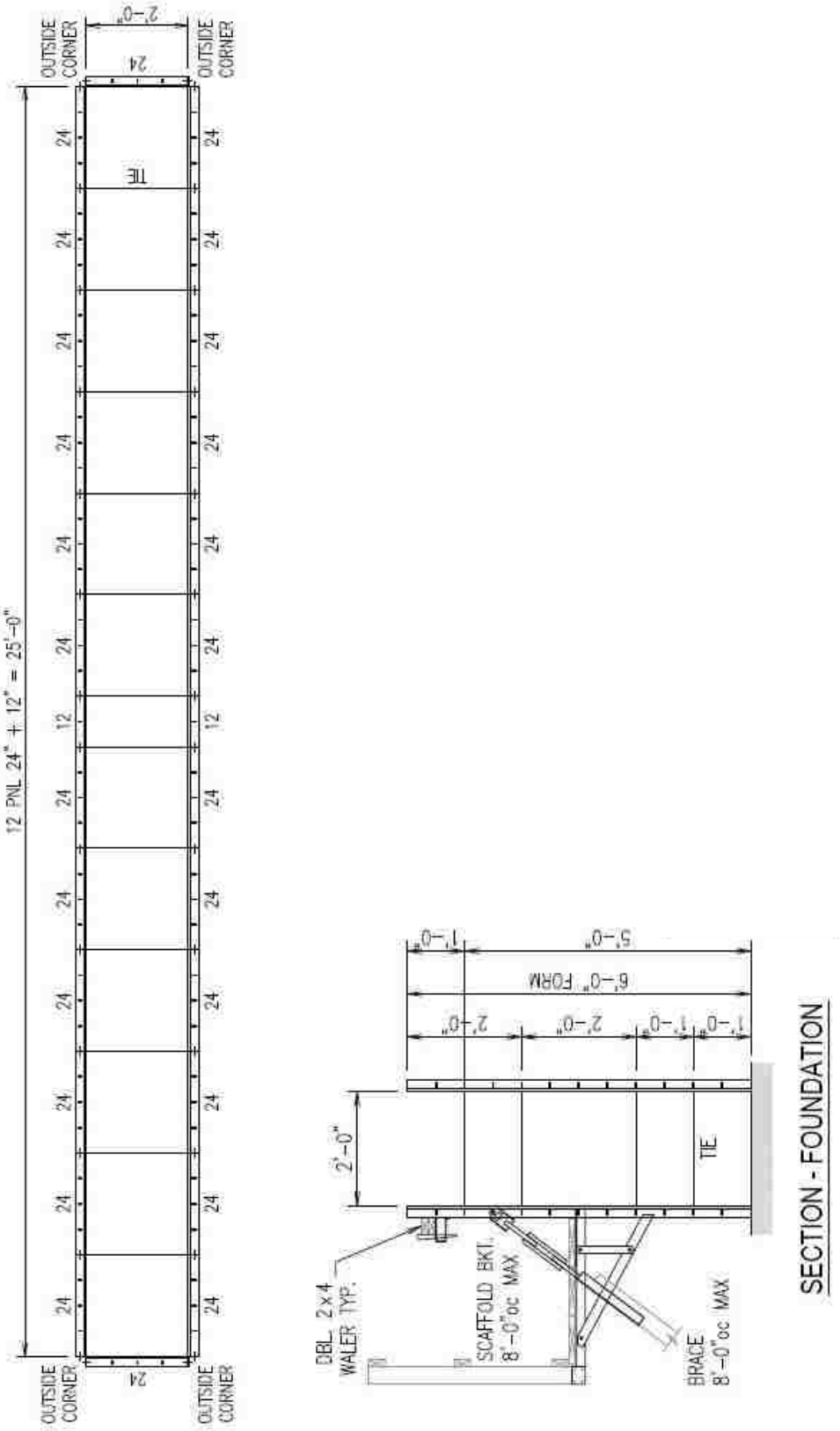

Figure 3-20: Formwork panels for foundation block

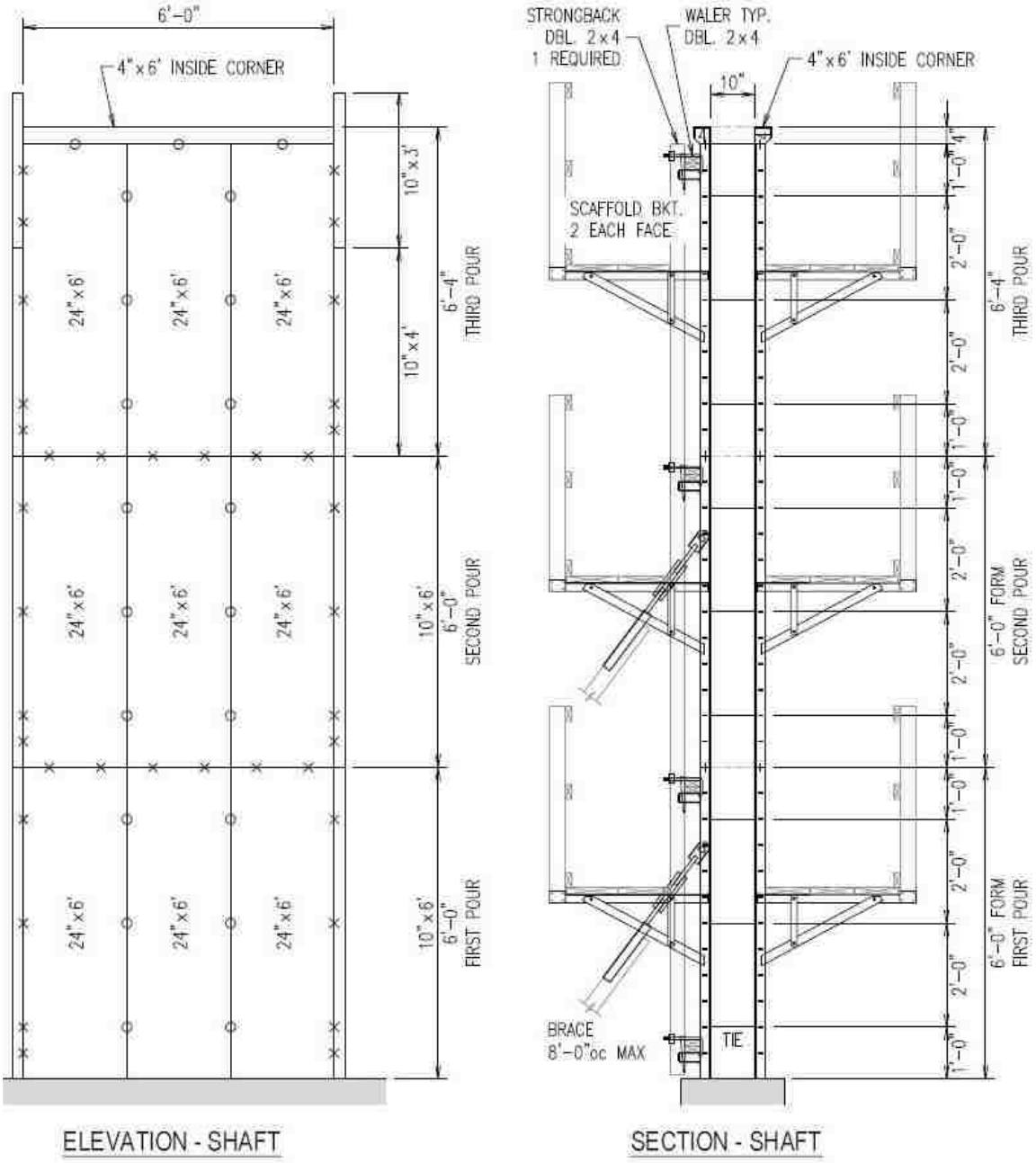

Figure 3-21: Formwork panels for wall section

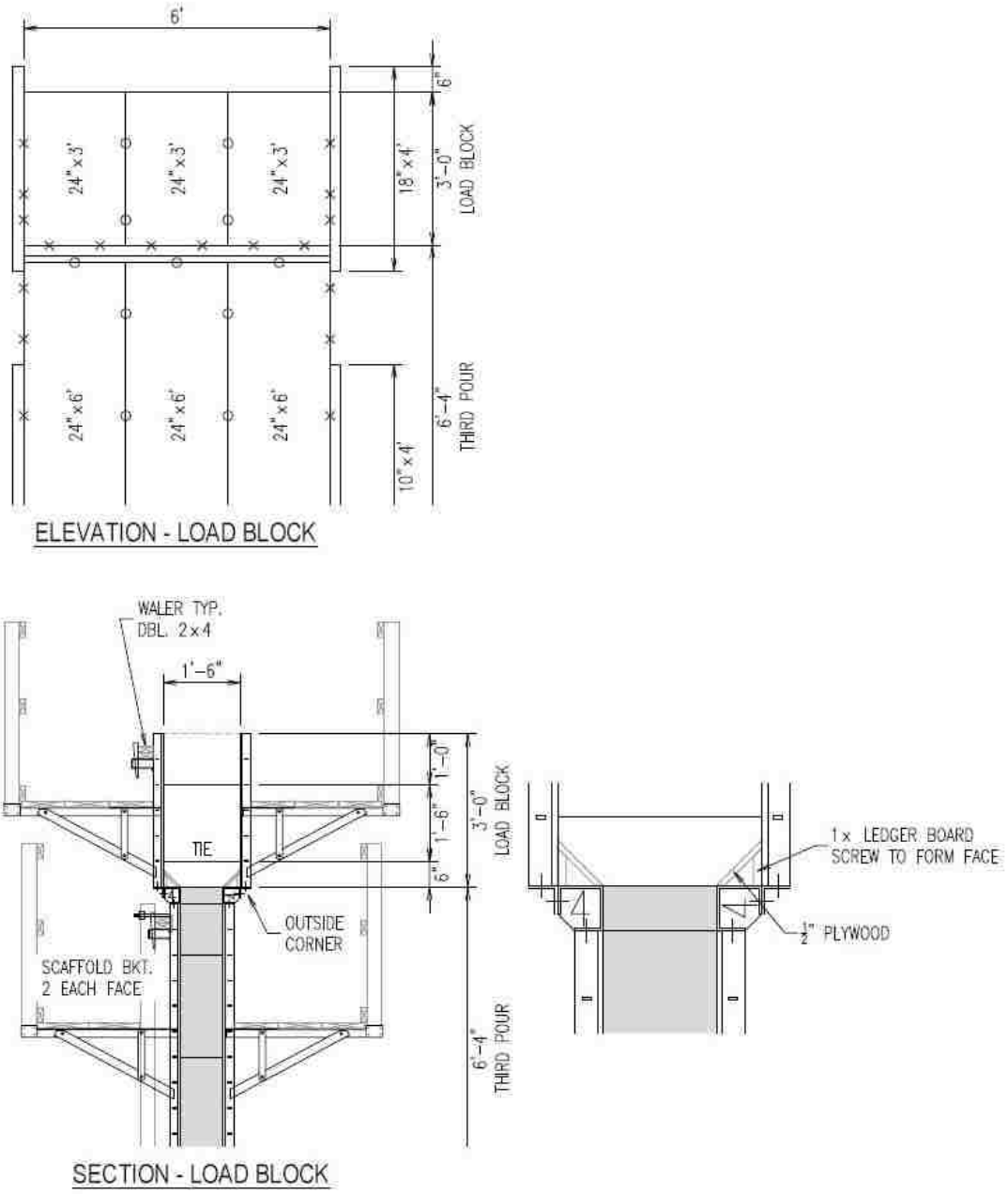

Figure 3-22: Formwork panels for thickened wall portion

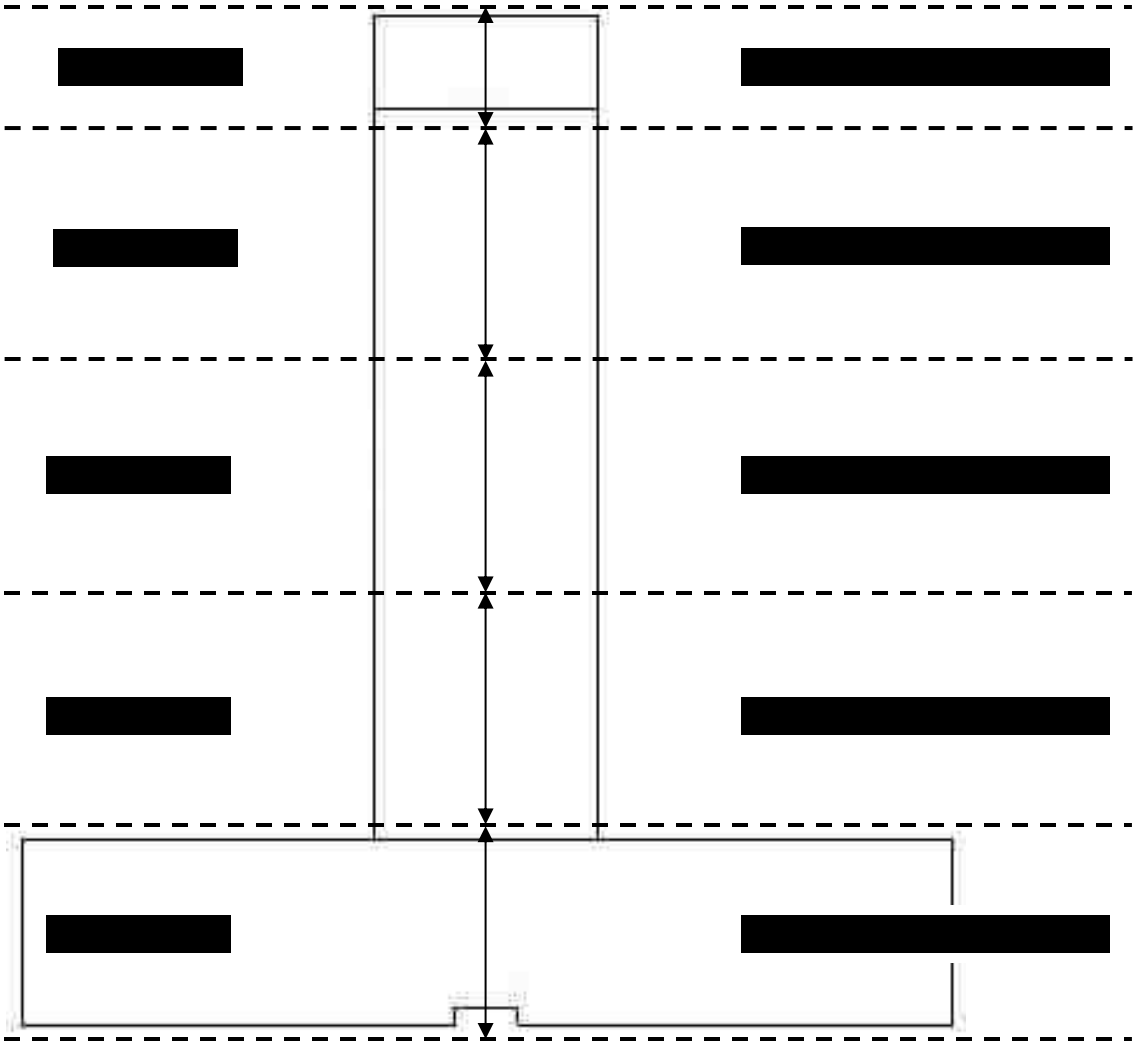

Figure 3-23 Concrete placing schedule

Figure 3-24 Additional construction photographs

Figure 3-25 Setup for seating post-tensioning anchors

Figure 3-26 Actuator support fixture

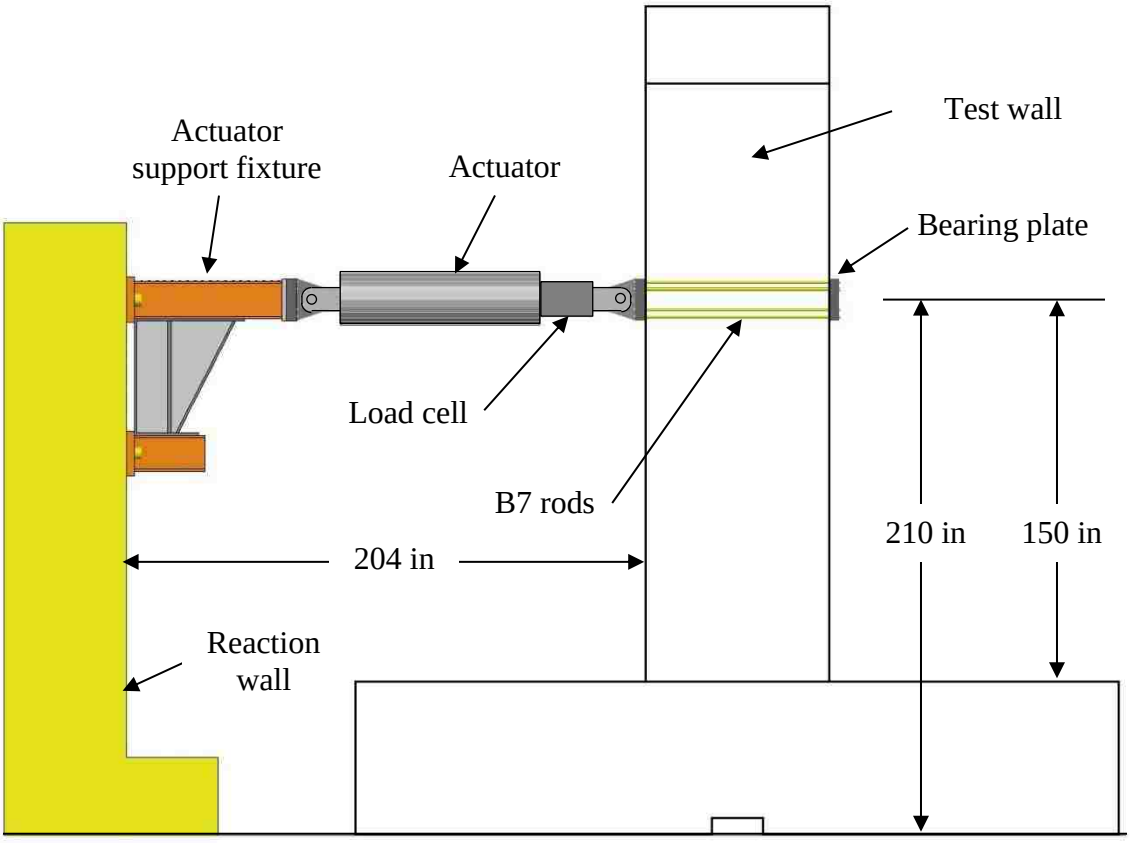

Figure 3-27 Loading apparatus setup

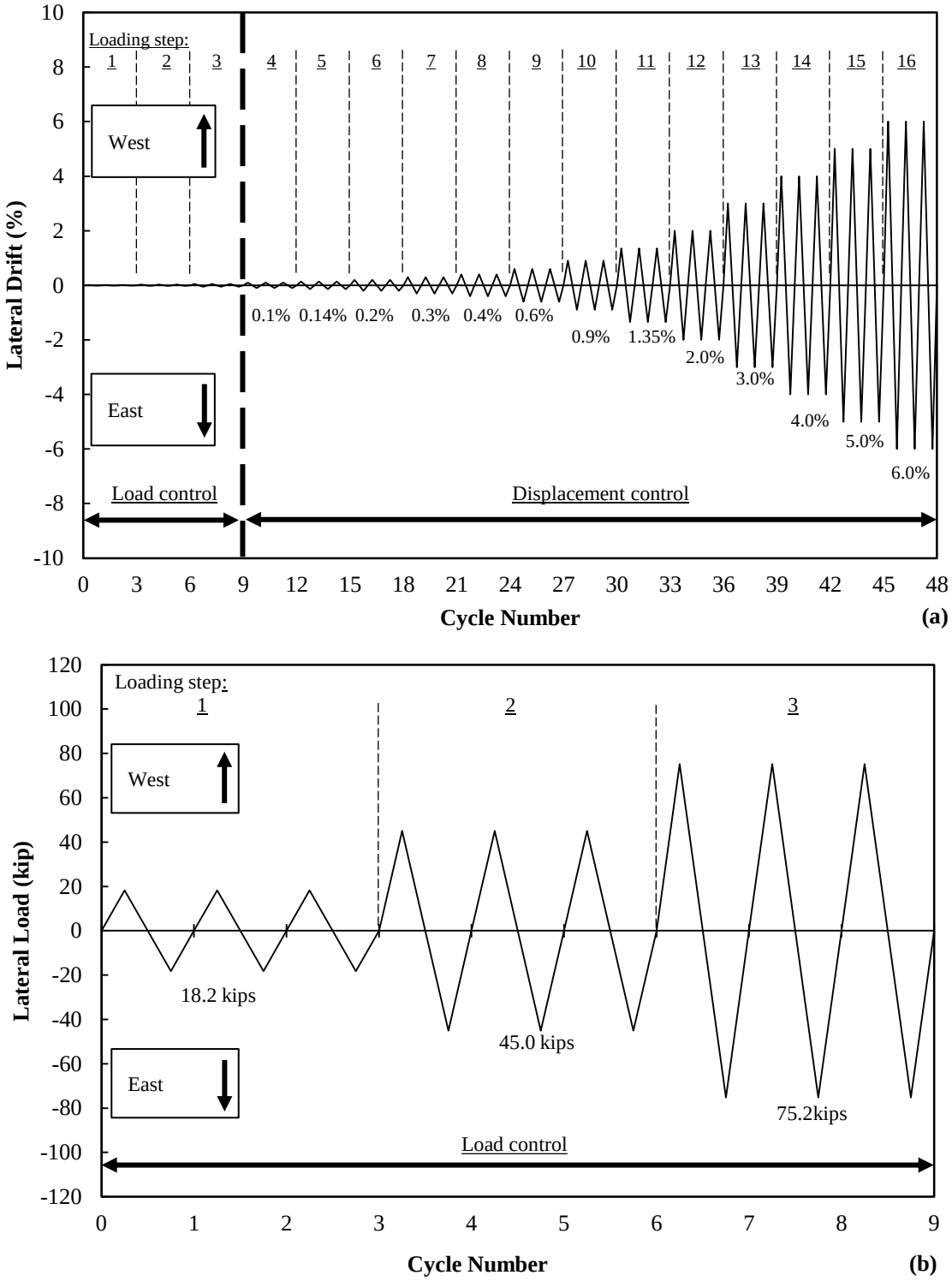

Figure 3-28 Details of loading sequence: (a) Planned loading sequence; and, (b) load control sequence (Pakiding 2014)

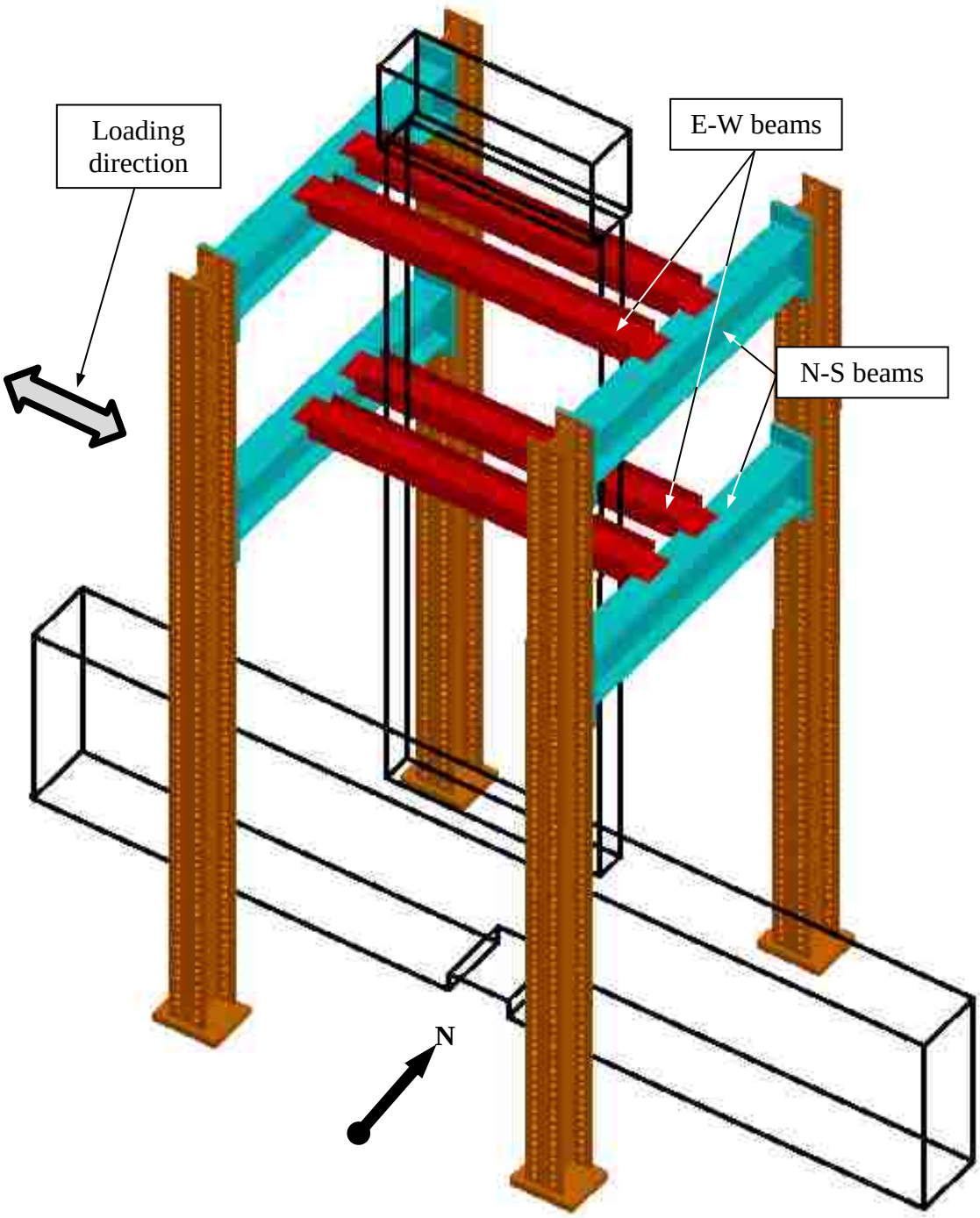

Figure 3-29 Bracing system to prevent out of plane movement

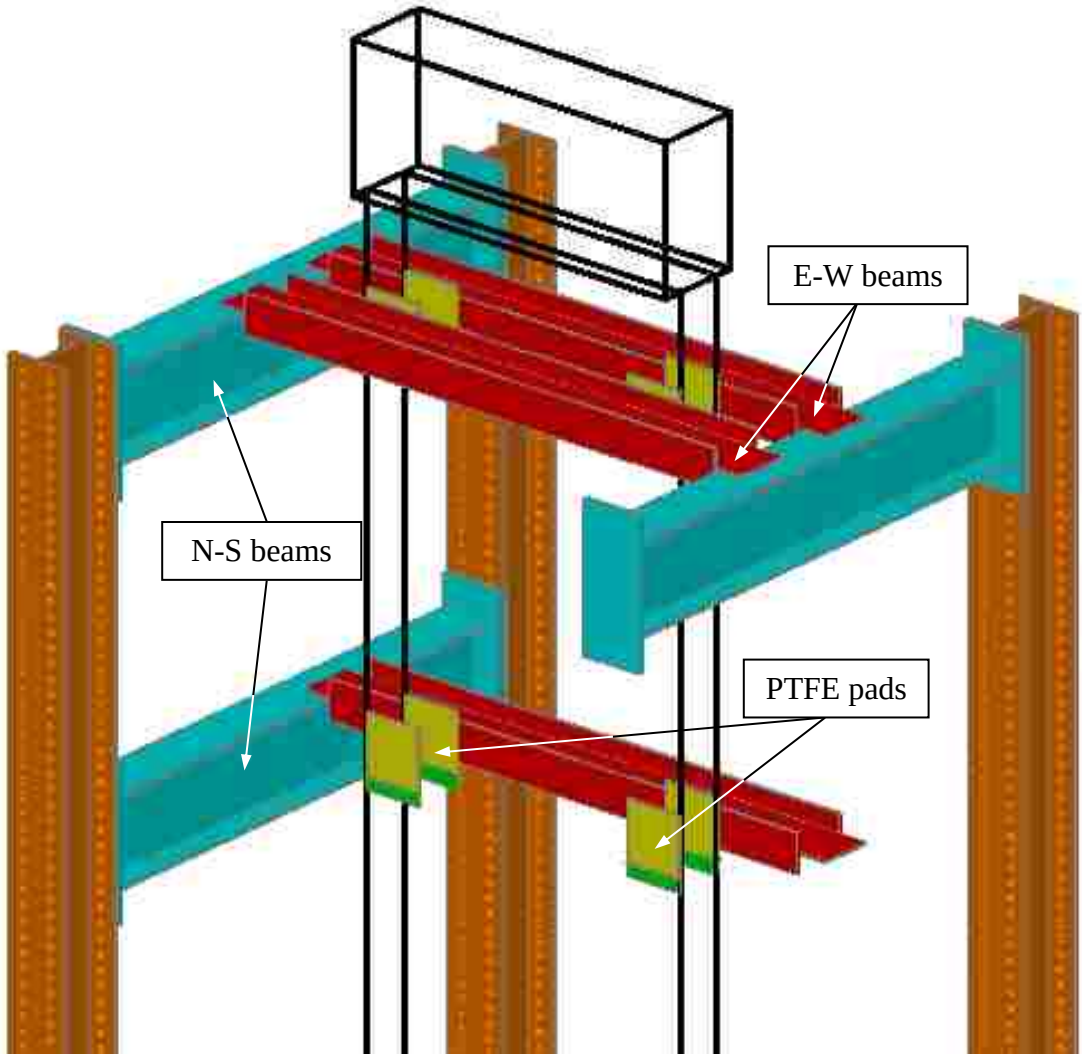

Figure 3-30 PTFE pad locations

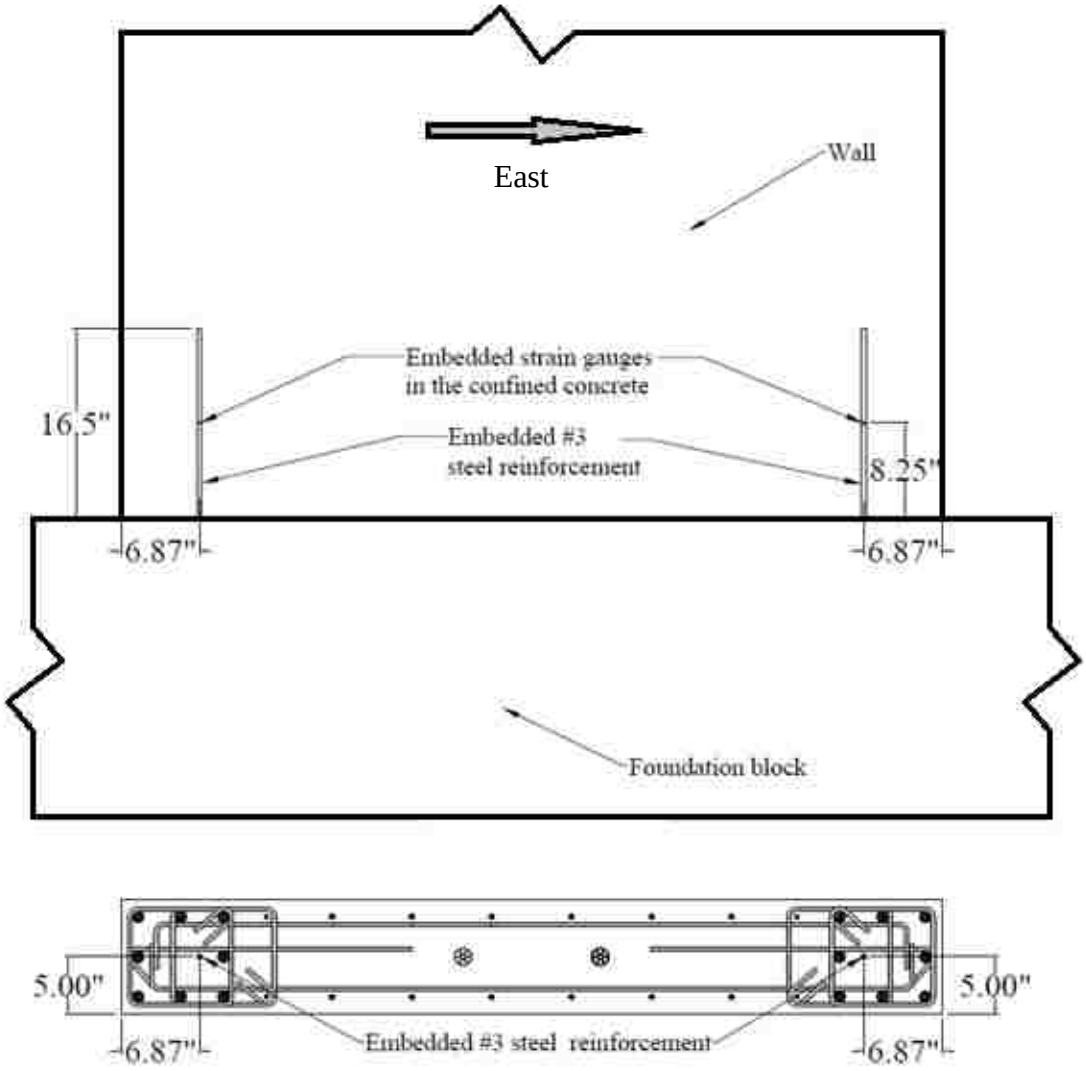

Figure 3-31 Strain gauges placed in a #3 steel bar located in the confined region

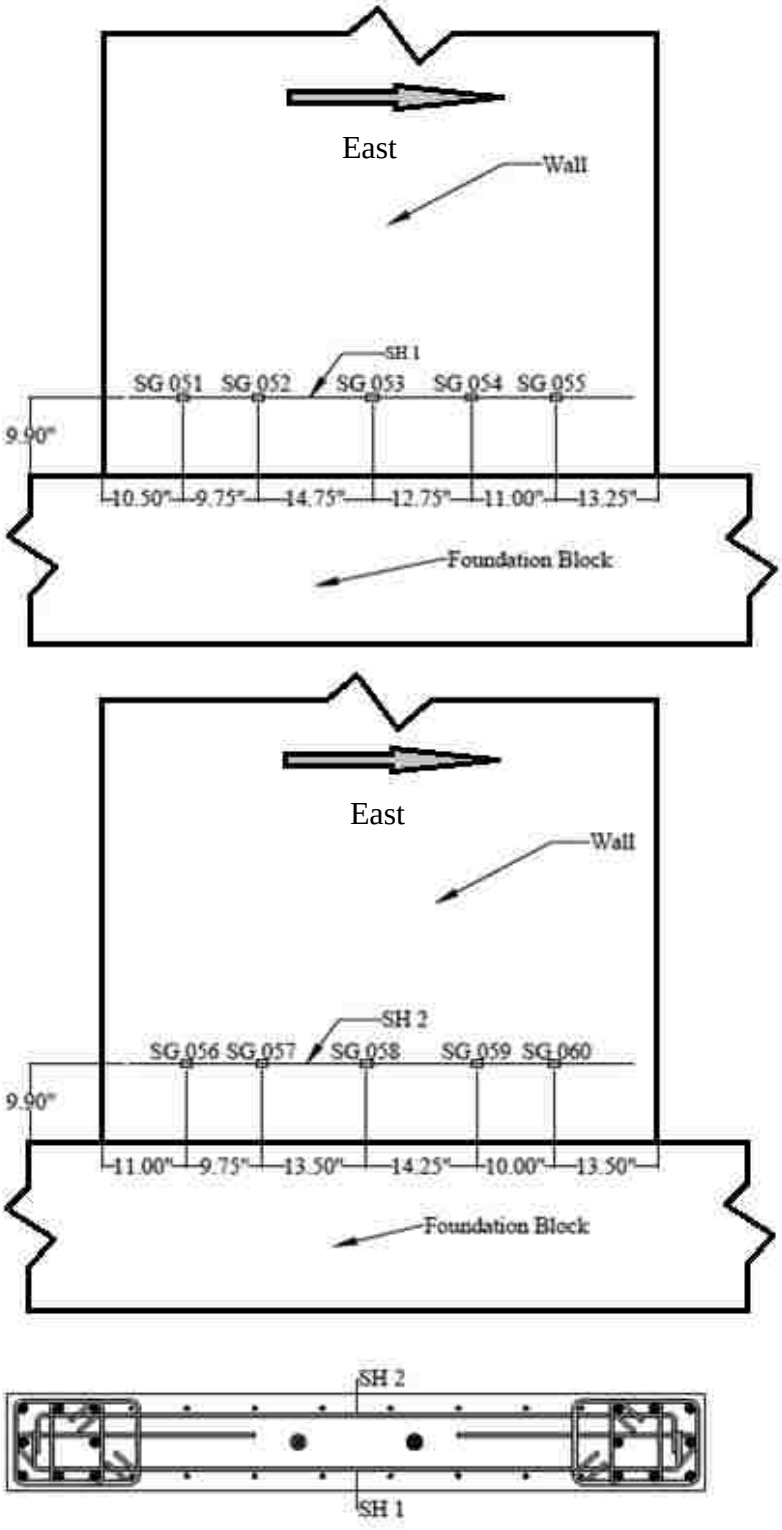

Figure 3-32 Strain gauges placed on transverse shear reinforcement #4 steel bars

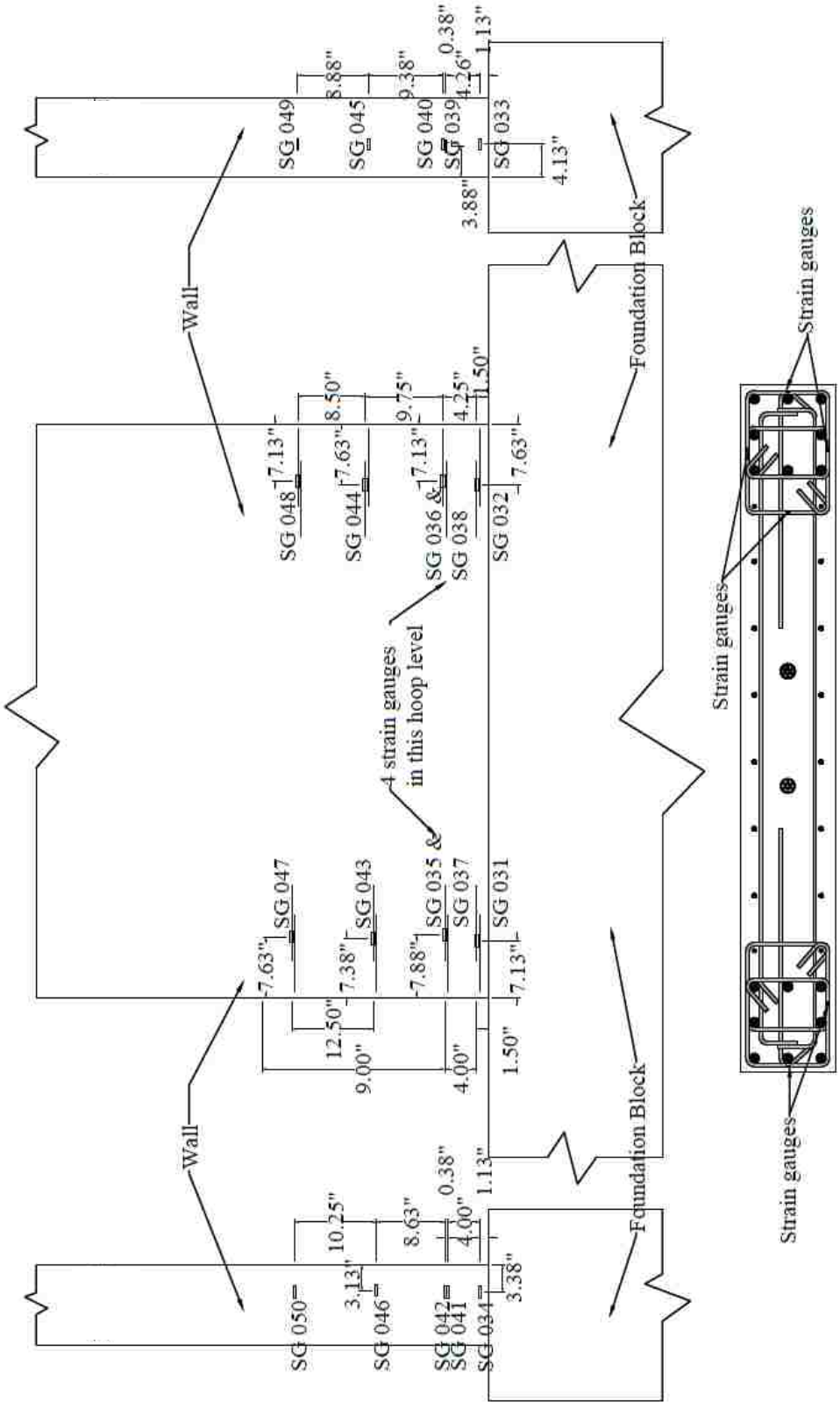

Figure 3-33 Strain gauges placed on stirrups

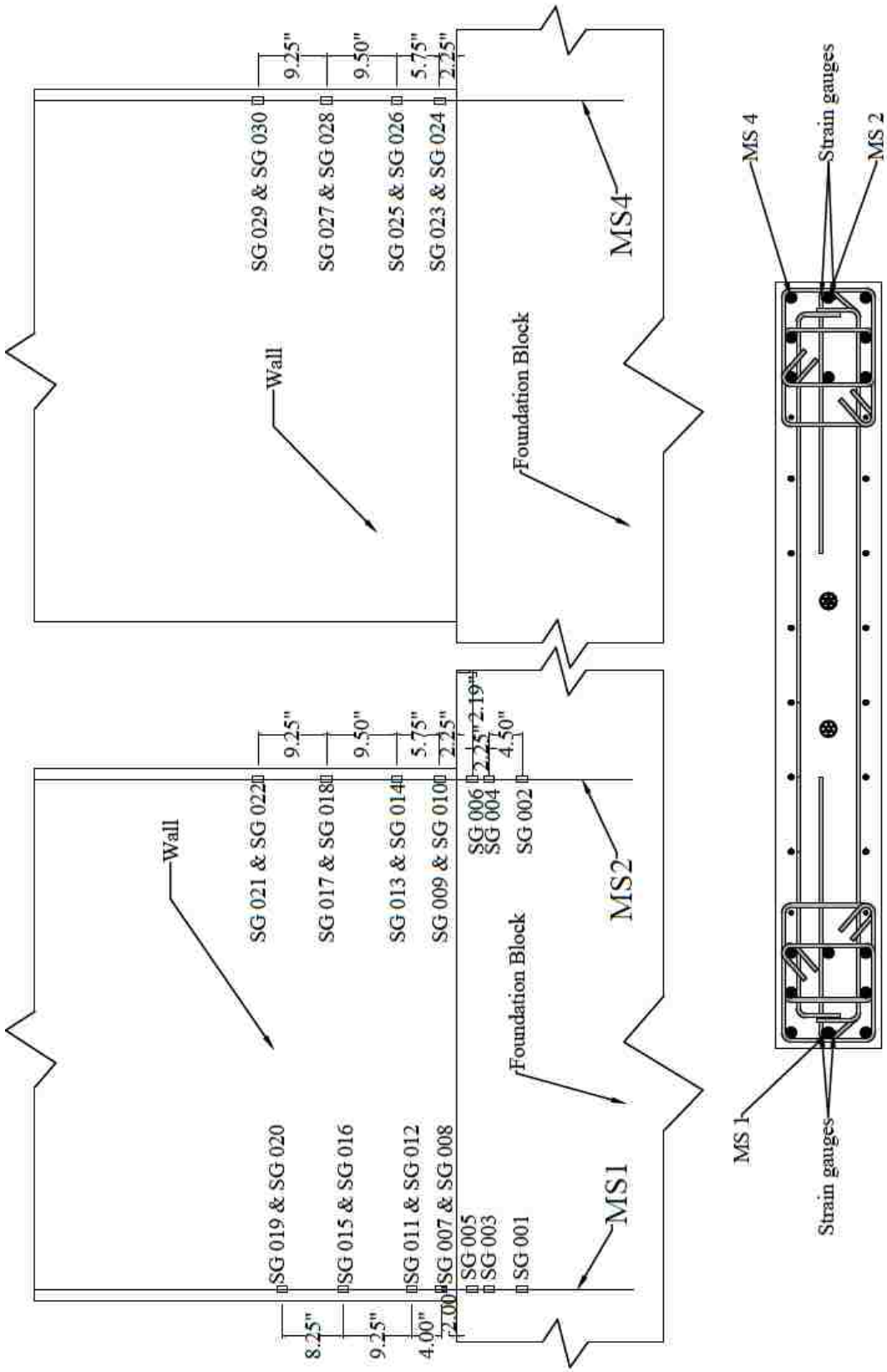

Figure 3-34 Strain gauges placed on #7 longitudinal steel bars

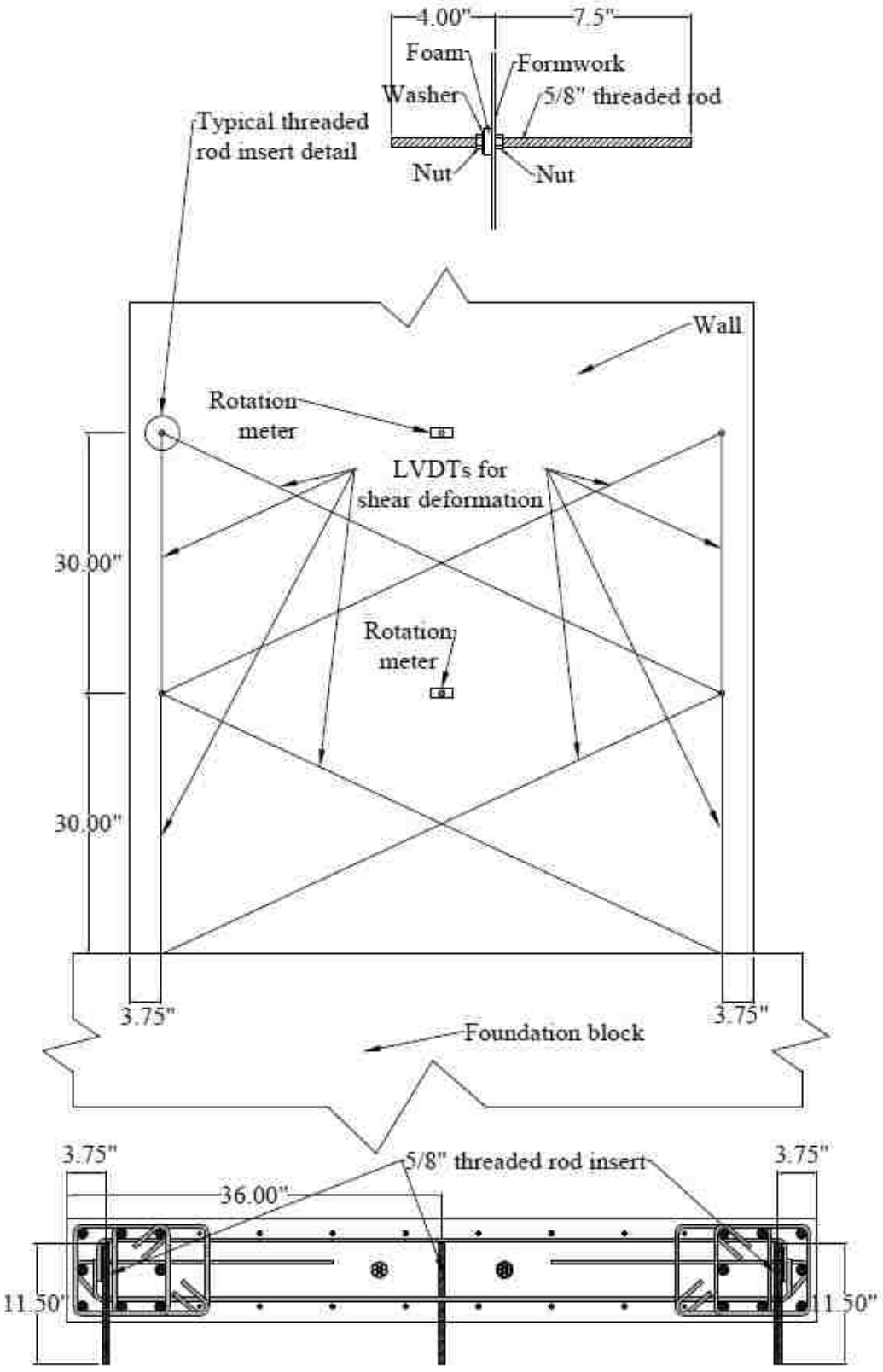

Figure 3-35 Location of LVDT transformers and rotation meters

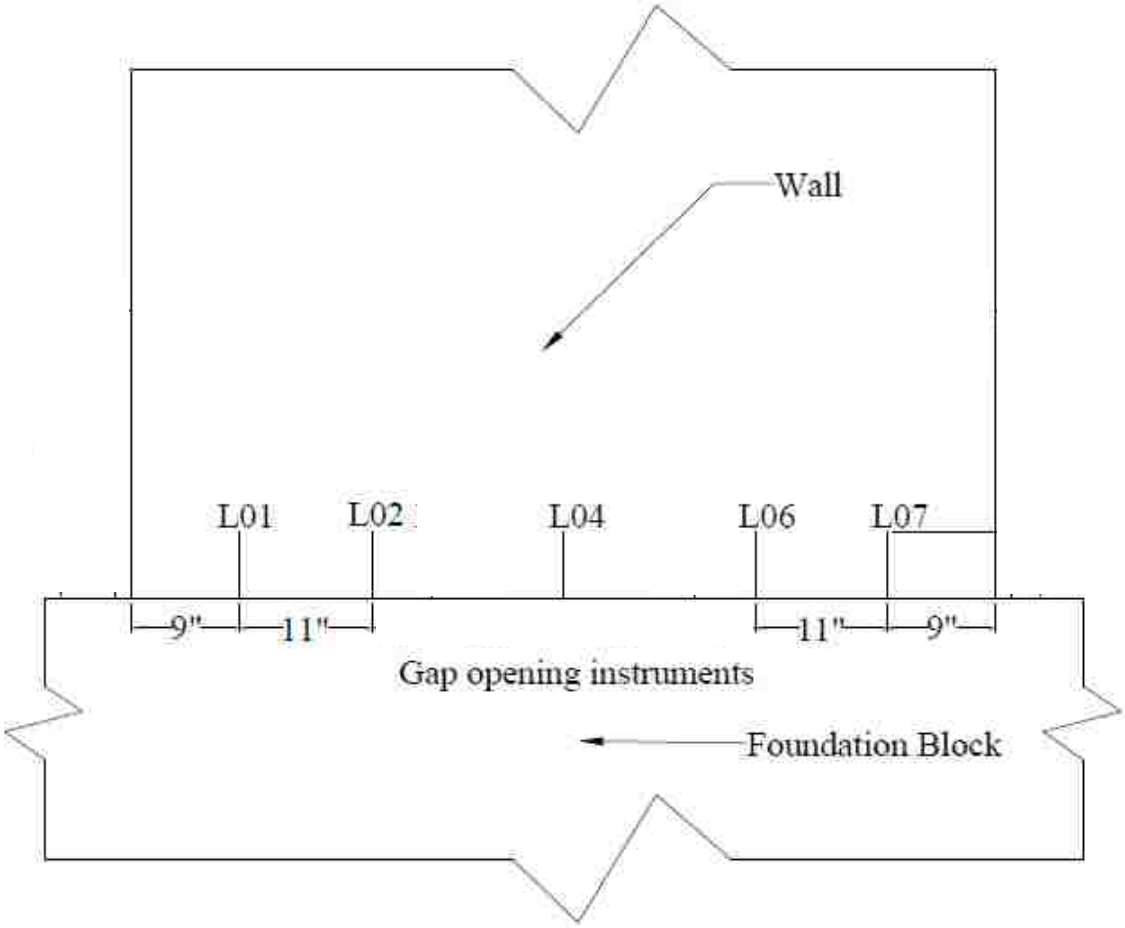

Figure 3-36 Gap opening instrumentation (conductive plastic potentiometers) located at the base of the wall

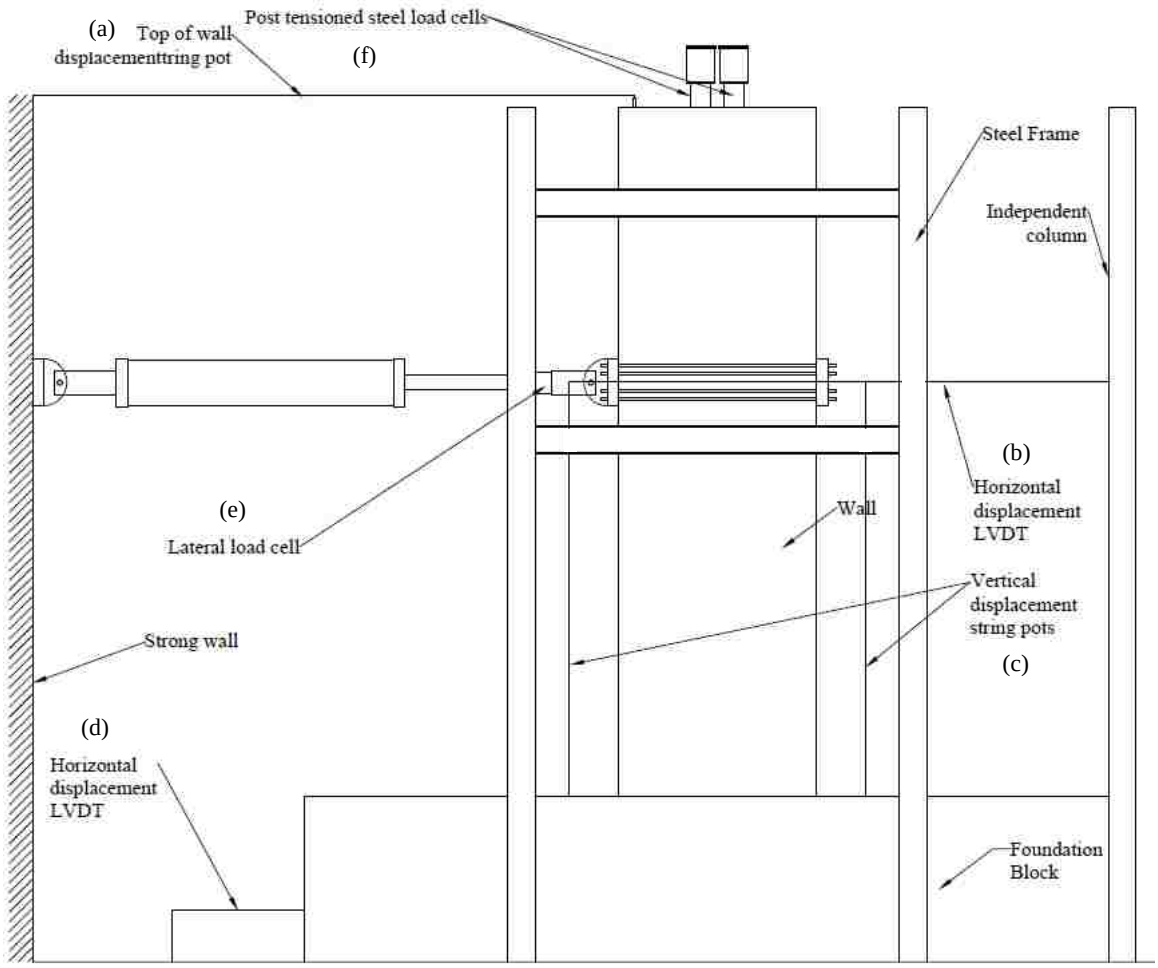

Figure 3-37 Overall view of additional instrumentation

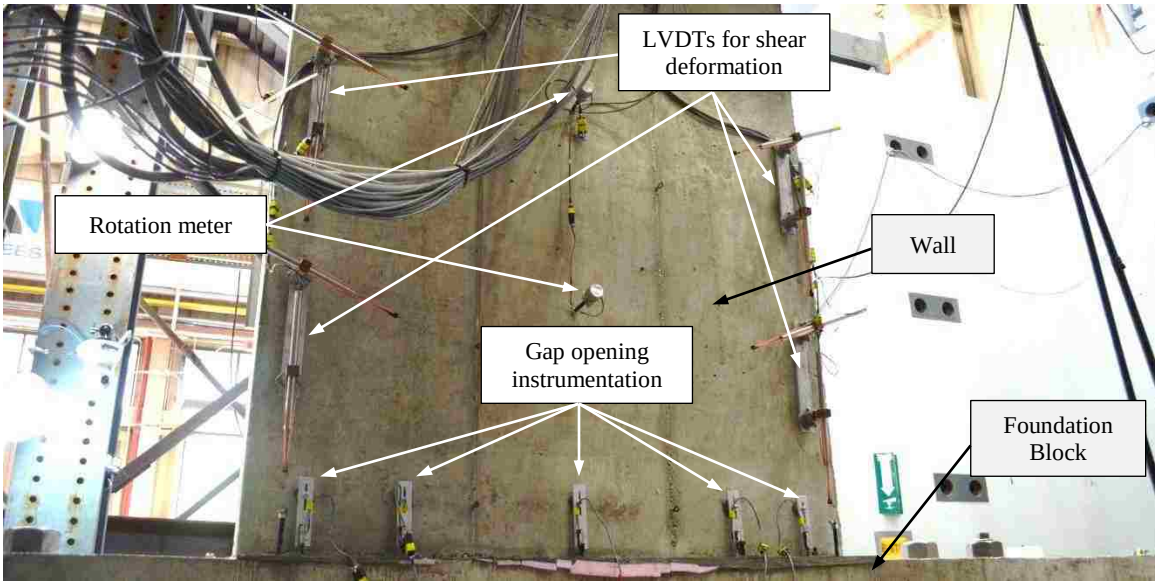

Figure 3-38 Instrumentation placed on the North side of the wall

Figure 3-39 Load cells placed between the top anchor head encasement and the top of the wall

Figure 3-40 Load cell attached to the actuator

CHAPTER 4

FOUNDATION BLOCK DESIGN

This chapter discusses the foundation block design details. Section 4.1 describes the overall design approach. Section 4.2 describes the wall forces acting on the foundation block while Section 4.3 discusses the Finite Element (FE) model used to obtain stresses in the foundation block. Section 4.4 describes the determination of longitudinal prestressing forces, and finally Section 4.5 describes the rebar sizing for tension stress.

4.1 OVERALL DESIGN APPROACH

The peak wall forces were determined based on the structural wall analysis from Pakiding (2014). The forces at the base of the wall are then transferred into the foundation block. Once these forces were obtained, a FE model using ABAQUS software was developed to analyze tension stresses in the foundation block (longitudinal, transverse, and vertical) caused by wall forces acting on the foundation block .

The FE model was also used to determine the magnitude and location of the post-tensioning (PT) forces required to minimize of eliminate tension stress in the foundation block. The location of the vertical PT forces was limited to tie-down locations. Only longitudinal and vertical PT was used (no transverse post-tensioning).

After the PT was applied, mild steel was used to carry all remaining tension stresses. Mild steel was design to carry full tension at $0.5f_y$. Temperature and shrinkage minimum required steel was also considered per ACI 318.

4.2 WALL FORCES ACTING ON FOUNDATION BLOCK

The desire to dispose of the foundation block in one piece, without to need to demolish it in to smaller pieces, coupled with 20 ton overhead crane capacity, determined the overall size of the foundation block. Based on these limitations, the preliminary foundation block dimensions are 24in x 60in x 300in. Based on a unit weight of 150 pcf, the approximate block weight is 3,750 lbs.

Figure 4-1 shows the forces transferred from the wall acting on the foundation block. These forces include point loads and distributed loads. These loads were the basis for developing the finite element model. The forces shown in Figure 4-1 correspond to an applied lateral force of 365 kips applied at 12.5 ft. from the base of the wall. This correspond to a base moment of 4,572 ft-kip

4.3 FINITE ELEMENT MODEL

Using the preliminary dimensions, a FE model was developed to investigate the location and magnitude of the prestressing forces. Once the location and magnitude of these prestressing forces was determined, the forces transferred from the wall were included to determine the regions of tensile stress.

As shown in Figure 4-2, a frictionless contact surface between the bottom face of the foundation block and top face of the laboratory floor was used to model the interface. A frictionless surface was assumed to create a least favorable condition to account for the

reduction in friction caused by plastic sheeting used to protect the laboratory floor. The bottom surface of the laboratory floor slab was modeled as fixed.

Element type C3D20, which is a second-order element, was utilized to model the foundation block and the laboratory floor. This element provides higher accuracy, and captures stress concentrations more efficiently than a similar first-order element. This element offers full integration over its 27 integrating points, which adds accuracy. It also avoids issues with volumetric locking and Hourglassing. Hourglassing is an issue related to shear deformations and typically occurs on first order and reduced integration elements such as the C3D8R. A uniform element size as shown in Figure 4-3 was used in the model.

Additionally, element C3D20 converts to element C3D27 when placed adjacent to a slave hard contact surface. This occurs to ensure matching and compatibility of integration points along this frictionless contact surface. Since no deformation is expected from the laboratory floor, the nodes on the top surface of the floor were modeled as master nodes. On the other hand, deformation of the foundation block was expected, so the nodes on the bottom surface of the foundation block were modeled as slave nodes.

Based on the location of applied loads and prestressing forces, the foundation block elements were discretized into 5in x 5in x 6in (XYZ) solid blocks, as shown in Figure 4-3. The laboratory floor was discretized into 10in x 8in x 1in solid blocks.

4.4 DETERMINATION OF LONGITUDINAL PRESTRESSING FORCES

Once the FEA model was completed and verified, the next task was to investigate the foundation block response under the transferred forces from the wall (Figure 4-1) along with the effects of vertical (tie-downs) and horizontal post-tensioning. To reduce the tensile stresses in the foundation block due loads transferred from the wall, horizontal post-tensioning forces were progressively applied. This is done by considering two approaches: a) by applying the tension force at the top of the foundation block; and b) by applying the tension force over a finite length into the foundation block to simulate force transfer through bond. Then, the magnitude of the horizontal post-tensioning force is systematically increased to reduce or eliminate tension stresses created by the wall forces.

Figure 4-4 shows how the horizontal post-tensioning forces were applied and the effect they had in reducing the longitudinal foundation block tensile stresses. This figure also shows the reduction of tensile stresses using principal (longitudinal) stresses as a measure. Additionally, the effect of transferring the wall forces deeper into the foundation block was explored. This was done by distributing point loads originally applied on the top surface of the foundation block over element nodes inside the block. The length of this distribution over the nodes was equal to 10 inches. This length corresponds to a minimum length needed to engage the foundation block steel reinforcement. This procedure was done to simulate more realistic conditions in which there is strain compatibility between the steel rebar and concrete and also to reduce stress concentrations produced by the point loads. Finally, horizontal post-tensioning forces were applied gradually until it was evident that applying more than 900 kips of total

horizontal prestressing force had no further effect in reducing the longitudinal stresses in the foundation block.

Figure 4-5 shows the application of horizontal post-tensioning forces and their effect on the longitudinal direction (S11). Figure 4-6 shows the effect of horizontal post-tensioning force and their effect on the transverse direction (S22) and Figure 4-7 shows the effect of horizontal post-tensioning and their effect on the vertical direction (S33).

Once the horizontal post-tensioning forces were determined, it was noted that some region in the foundation block still showed tensile stresses. In these areas of high tensile stress or critical sections, mild steel reinforcement is required to carry the tension stress. These critical sections are areas of the foundation block in each orthogonal direction where the tensile stresses are the highest.

Figure 4-8 shows the tensile critical sections on the longitudinal direction. One critical section is located at 120 inches from the end, where the wall's longitudinal reinforcement extends into the foundation. Although there are no forces acting on the longitudinal direction other than the prestressing forces, the stress in this section is generated by the Poisson effect. The other critical section is located at 180 inches from the end, where tensile stress in this section is generated by pure bending.

Figure 4-9 shows the tensile critical section on the vertical direction. This critical section is located 50 inches from bottom of foundation block and 120 inches from the end and is

the location where the wall's longitudinal reinforcement extends into the foundation. This stress is generated by the tensile action of the wall's longitudinal reinforcement being stressed in flexure.

Finally, Figure 4-10 shows the three tensile critical sections on the transverse direction. The first critical section is located 120 inches from the end, a place where the wall's longitudinal reinforcement extends into the foundation, which acts in compression. The critical second is located at 150 inches from the end, where the lower anchor head is embedded. The third critical section is located at 180 inches from the end, where the wall's longitudinal reinforcement on the other side of the wall extends into the foundation, which acts in tension. Although there are no forces acting on the transverse direction, the stresses at these three critical locations are generated by the Poisson effect. Load reversal was considered for all the critical sections, which made the steel reinforcement layout symmetrical.

To obtain the design demand forces, the stresses obtained from these critical sections are multiplied by the area on which they act upon. These forces are then used to design the steel reinforcement according to ACI 318.

4.5 REBAR SIZING FOR TENSION STRESS

Once the tensile stresses in each orthogonal direction were identified, mild steel reinforcement was used to carry the tension forces in these areas. As a safety measure, the steel reinforcement was designed not to exceed $0.5f_y$.

The provided areas of steel reinforcement were calculated by dividing the tensile forces obtained from the critical sections by 30 ksi, the desired maximum stress. Minimum percentage of steel reinforcement was checked in all critical sections according to ACI 318 Section 10.5.1. Minimum steel reinforcement ratio was also verified against the minimum required by shrinkage and temperature per Section 7.12. Section 7.6 was followed for spacing limits for reinforcement, as well as Section 7.2 for minimum bend diameters. Clear cover surrounding the steel reinforcement was provided as per Section 7.2.2.

Figure 4-11 shows an overlay of the tensile stresses obtained from the FEA model and the steel reinforcement required provide adequate capacity in the longitudinal direction. Subsequently, Figure 4-12 and Figure 4-13 show overlays of the tensile stresses obtained from the FEA model and the steel reinforcement required to provide adequate capacity in the transverse and vertical direction, respectively.

In addition to the forces transferred by the wall, there is the horizontal force that the actuator exerts on the wall and ultimately on the foundation block. To keep the foundation block in place, the laboratory is equipped with shear keys that are attached to the floor tie-downs. These shear keys have a capacity of 500 kips of shear force per anchor set. Therefore, shear collectors were placed at the bottom section of the foundation block to facilitate the transfer of horizontal forces directly to the shear keys. The area of the steel reinforcement provided to transfer the shear forces was obtained by using the maximum expected force exerted by the actuator during testing. As a safety

measure and due to symmetry, two sets of shear keys were placed on the tie-downs. Ultimately, Figure 4-14 shows the final foundation block steel reinforcement layout that includes the steel reinforcement in all three orthogonal directions, tie downs, horizontal post-tension, and shear collectors.

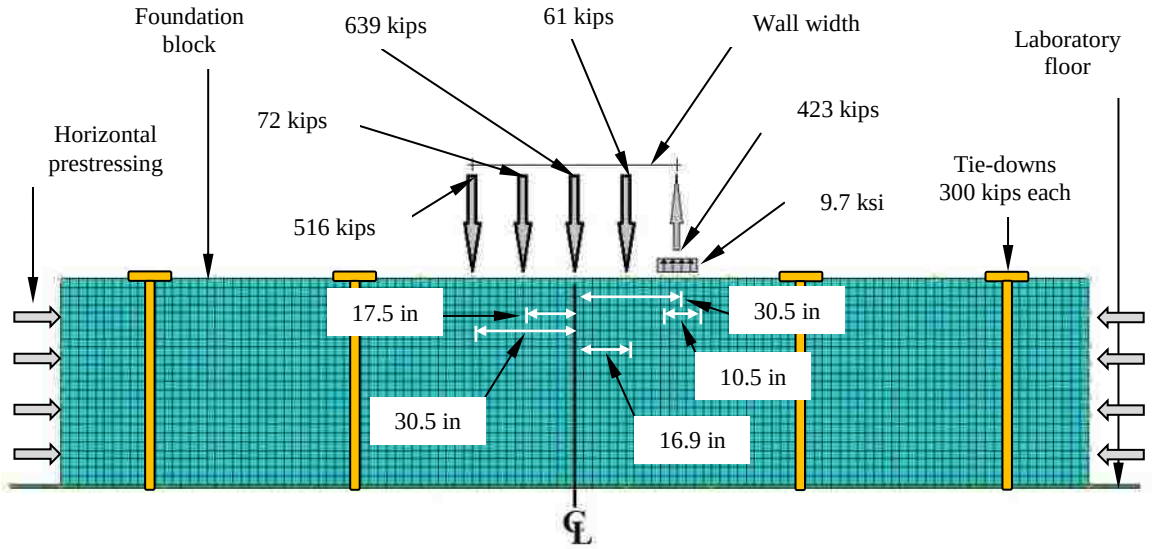

Figure 4-1 Forces transferred from the test wall to the foundation block and horizontal prestressing forces

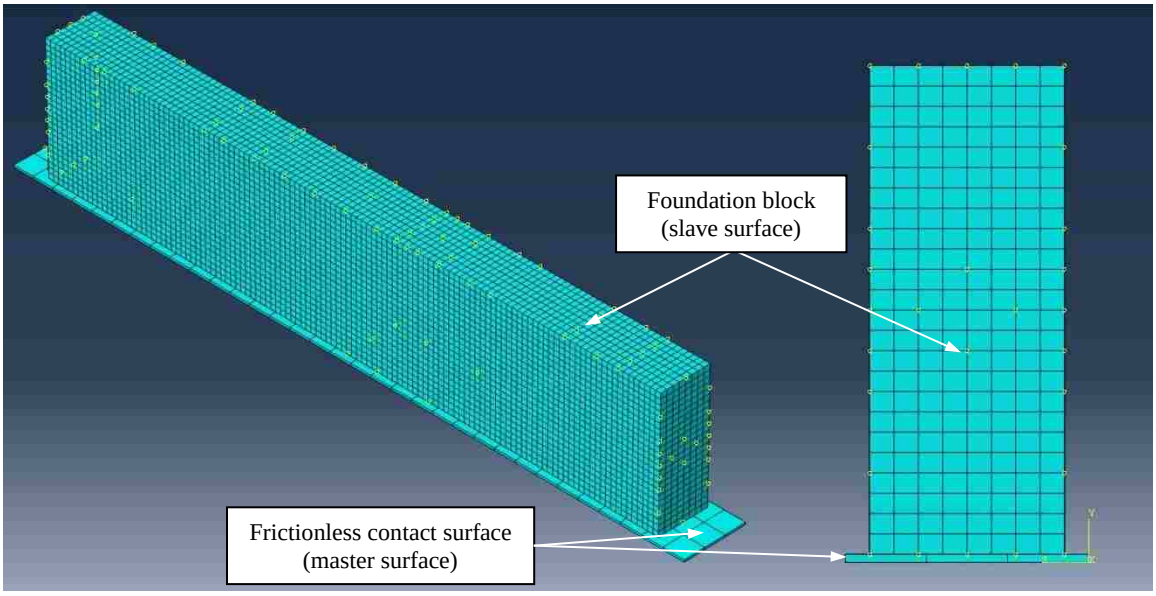

Figure 4-2 Finite element analysis model of the foundation block and floor simulating frictionless contact

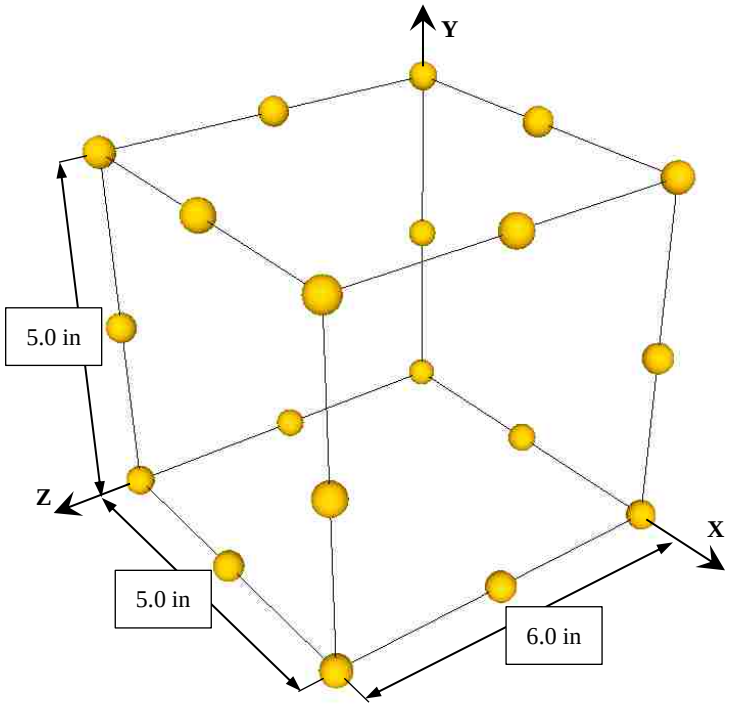

Figure 4-3 C3D20 ABAQUS element and its dimensional discretization

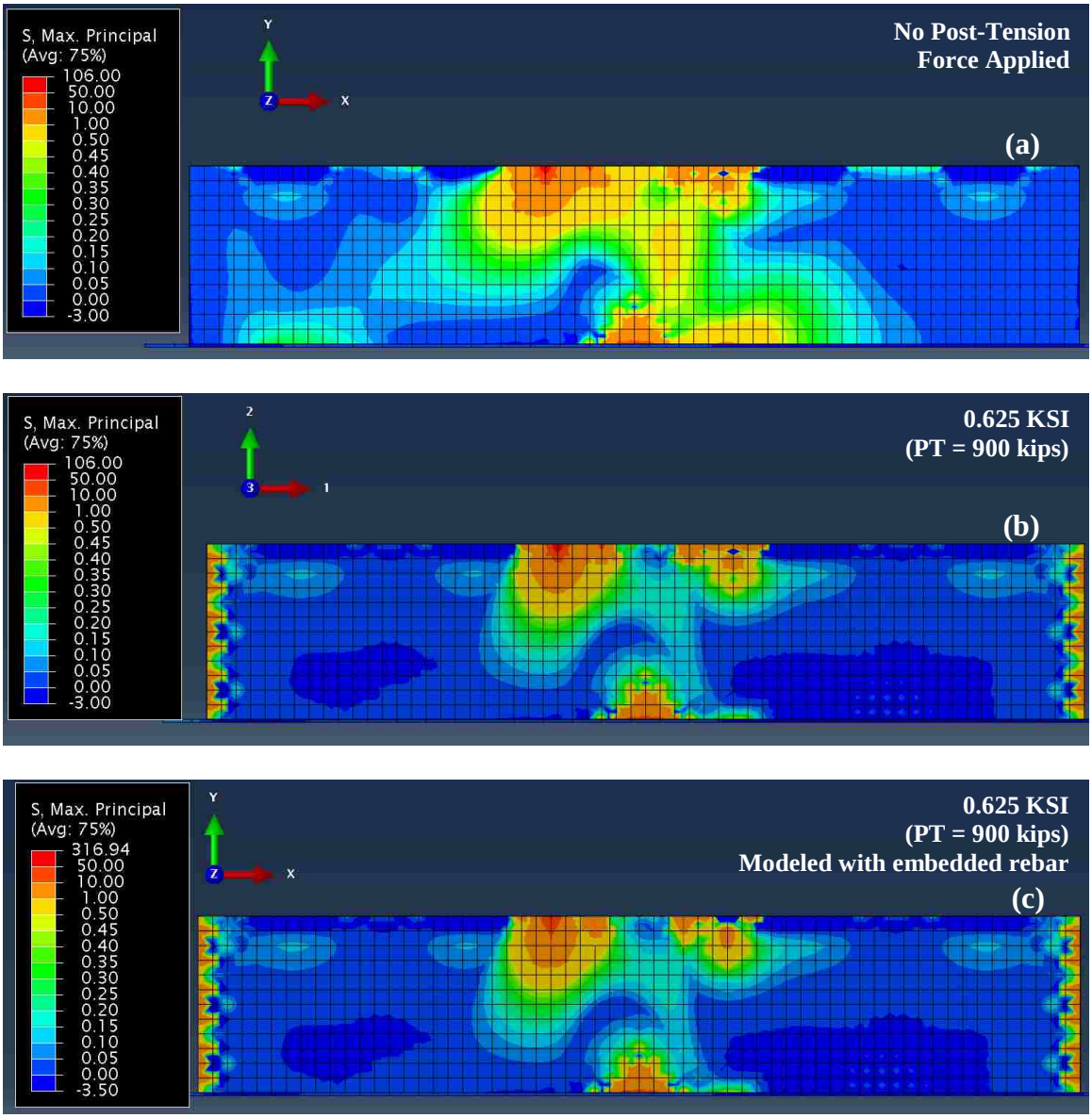

Figure 4-4: Application of horizontal post-tensioning forces: (a) no horizontal post-tensioning force applied (only wall forces); (b) 900 kips of horizontal PT force applied with wall forces applied at the top of the wall; (c) 900 kips of horizontal PT force applied with wall forces distributed over 10 inches into foundation block

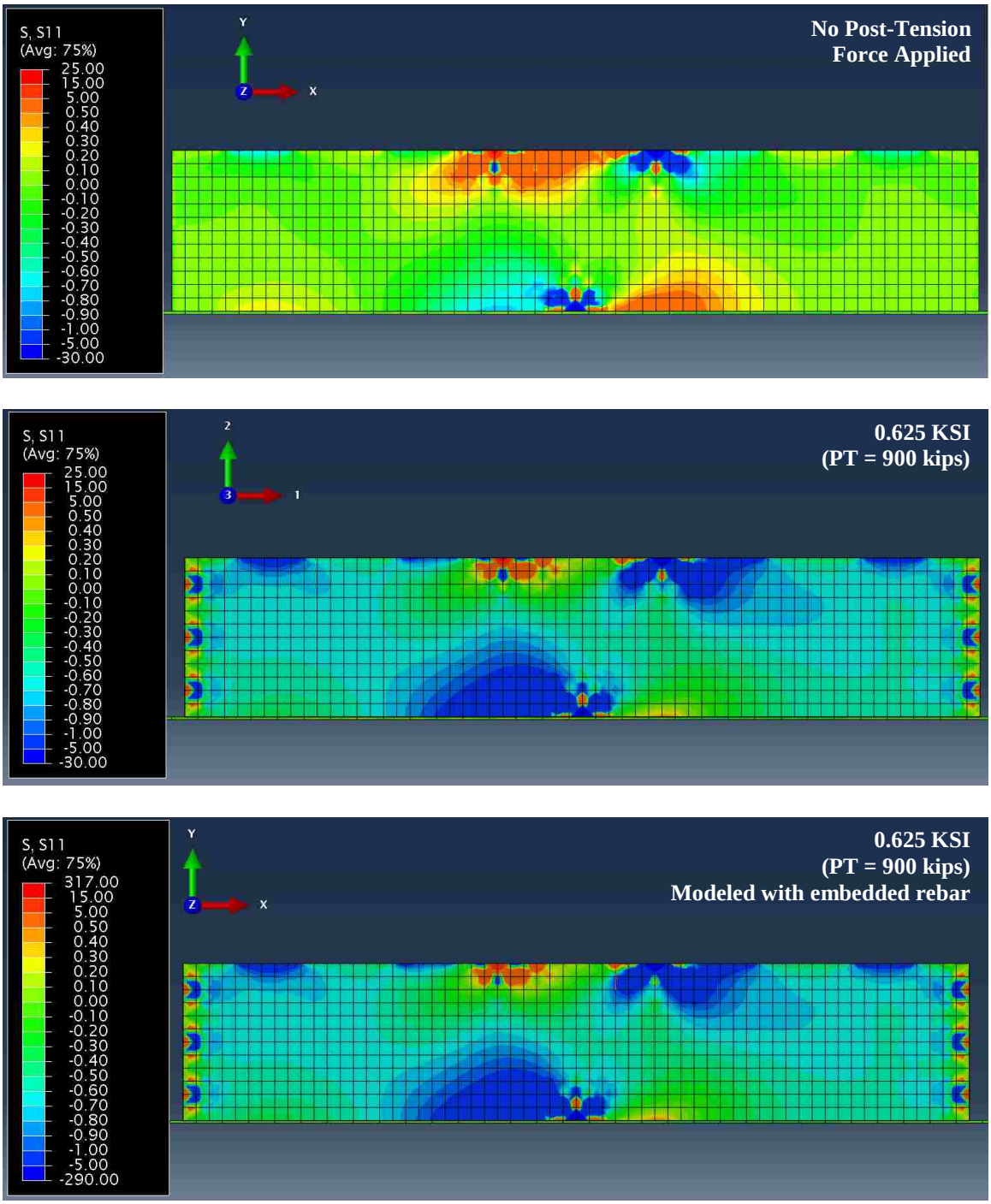

Figure 4-5: Effect of post-tensioning force on the longitudinal direction (tensile longitudinal stresses)

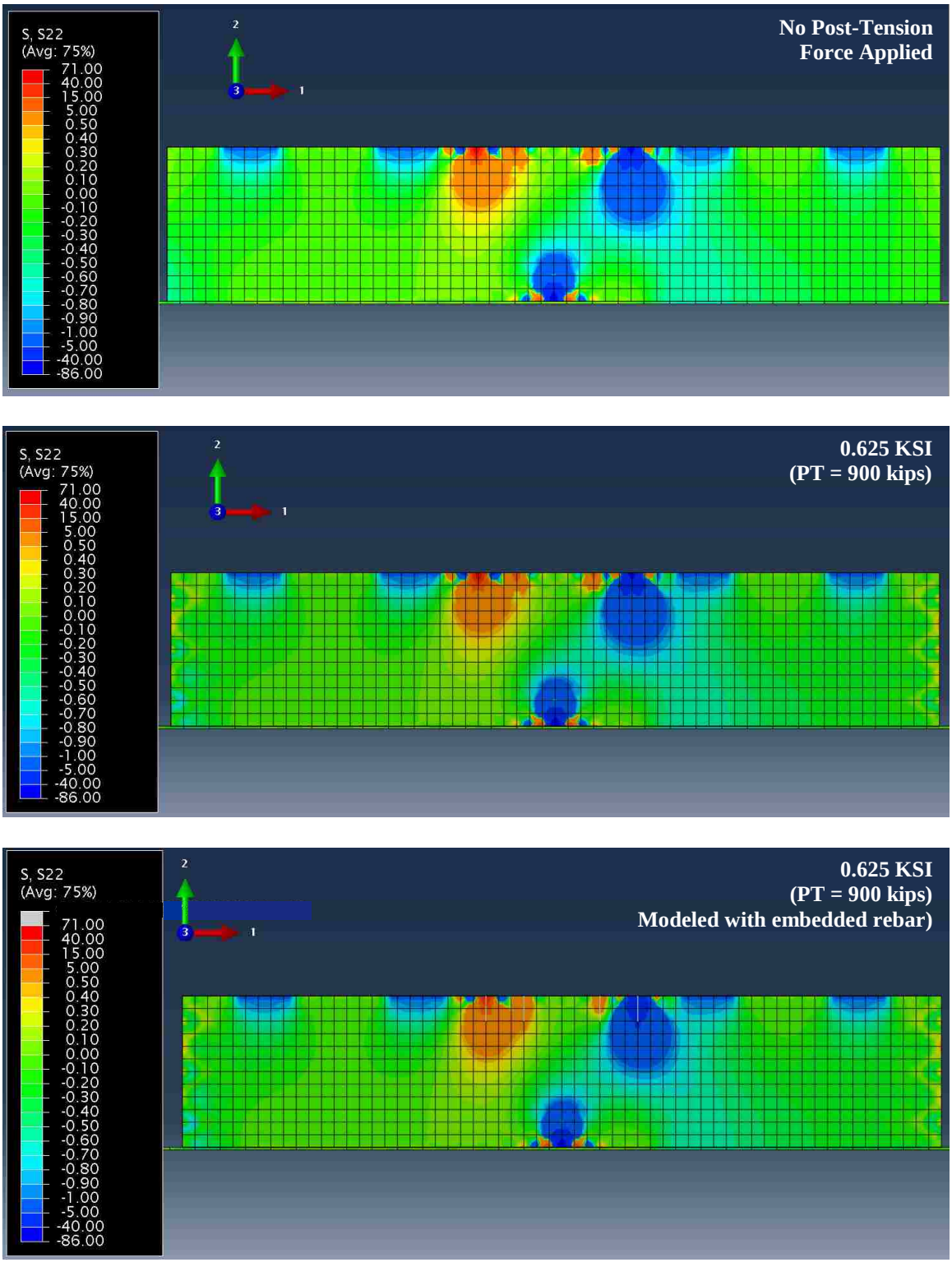

Figure 4-6: Effect of post-tensioning force on the transverse direction (tensile transverse stresses)

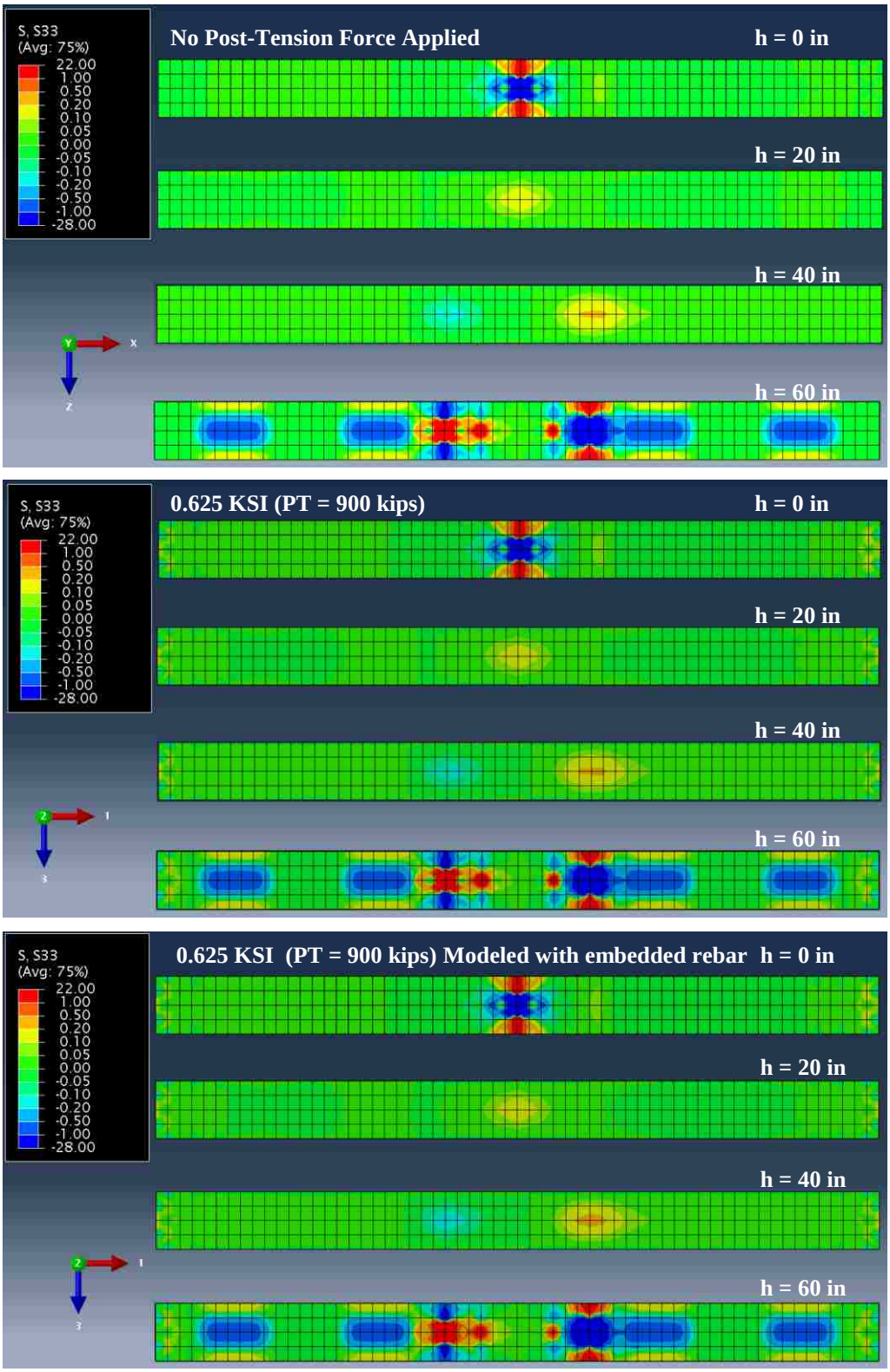

Figure 4-7: Effect of post-tensioning force on the vertical direction (tensile vertical stresses

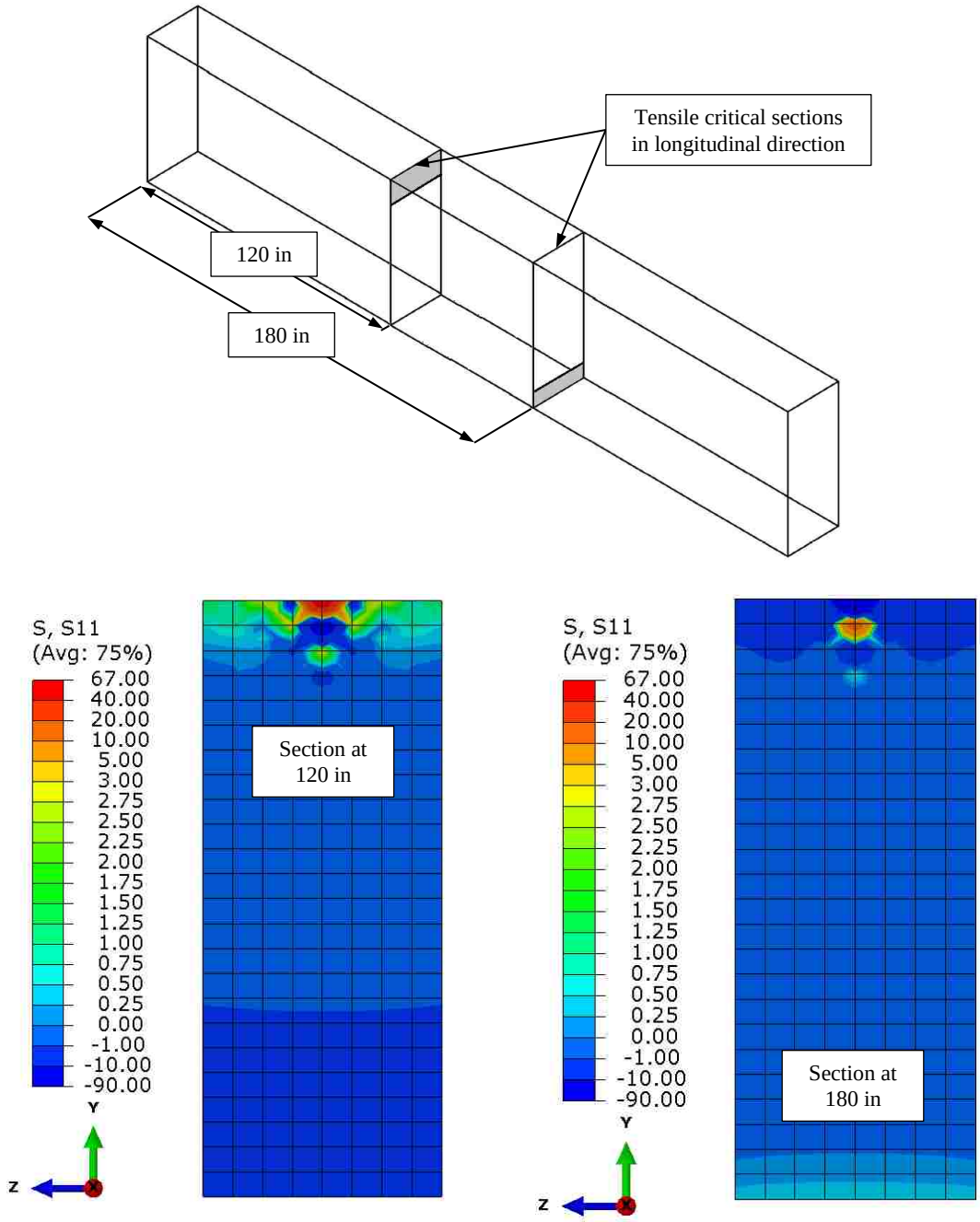

Figure 4-8 Critical sections in the longitudinal direction (tensile longitudinal stresses)

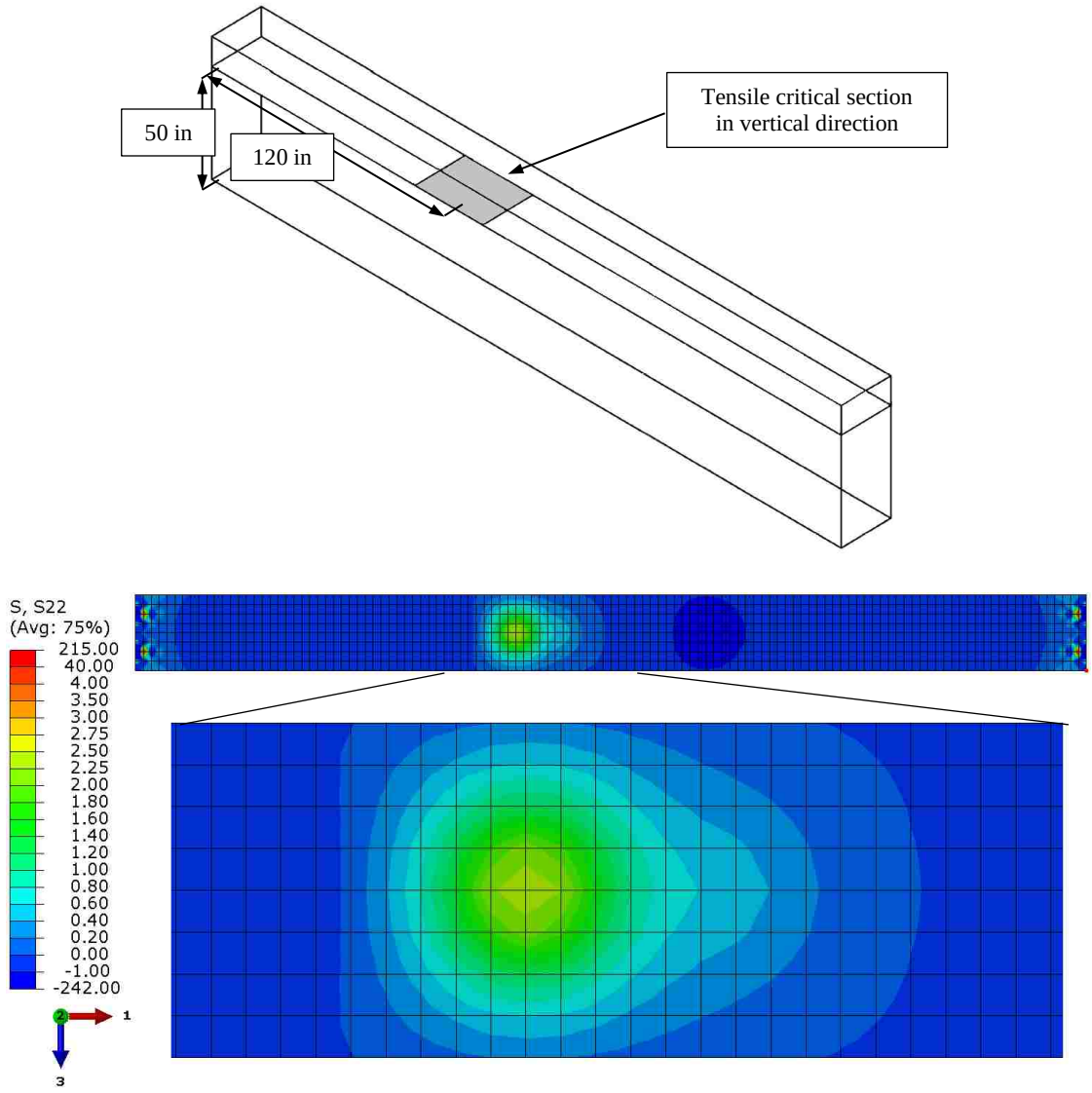

Figure 4-9 Critical section in the vertical direction (tensile vertical stresses)

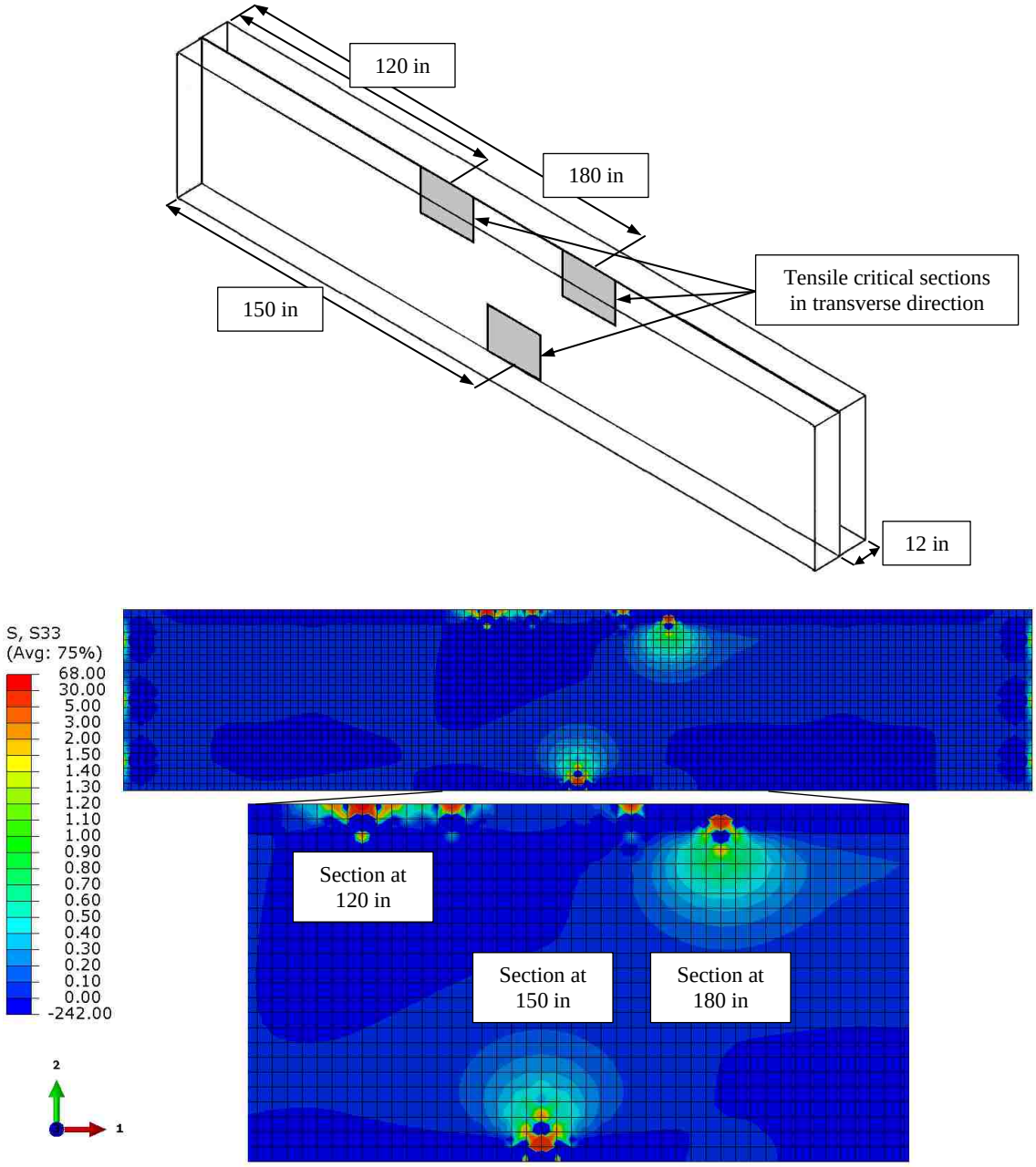

Figure 4-10 Critical sections in the transverse direction (tensile transverse stresses)

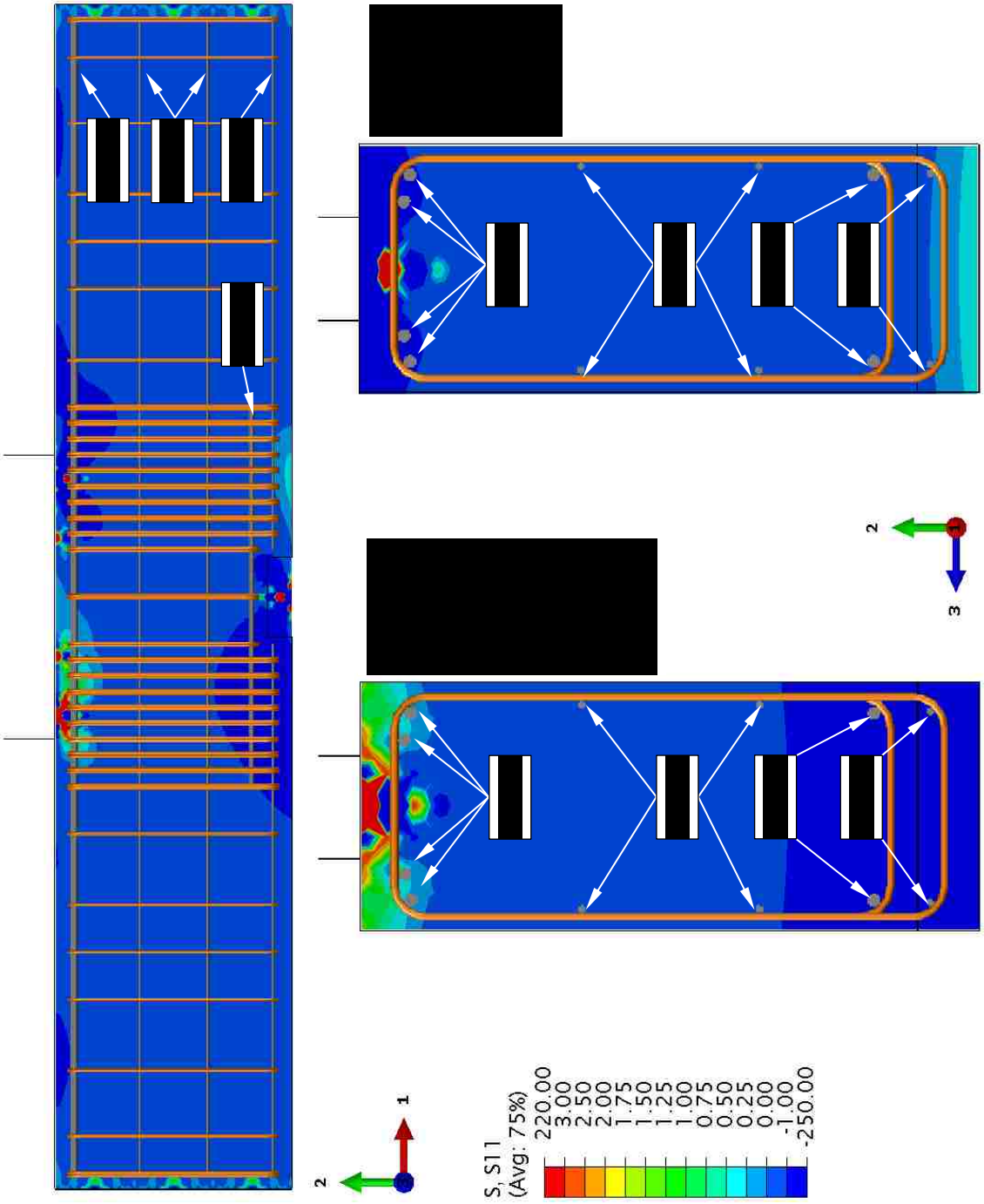

Figure 4-11: Steel reinforcement required carry tensile stresses in the longitudinal direction

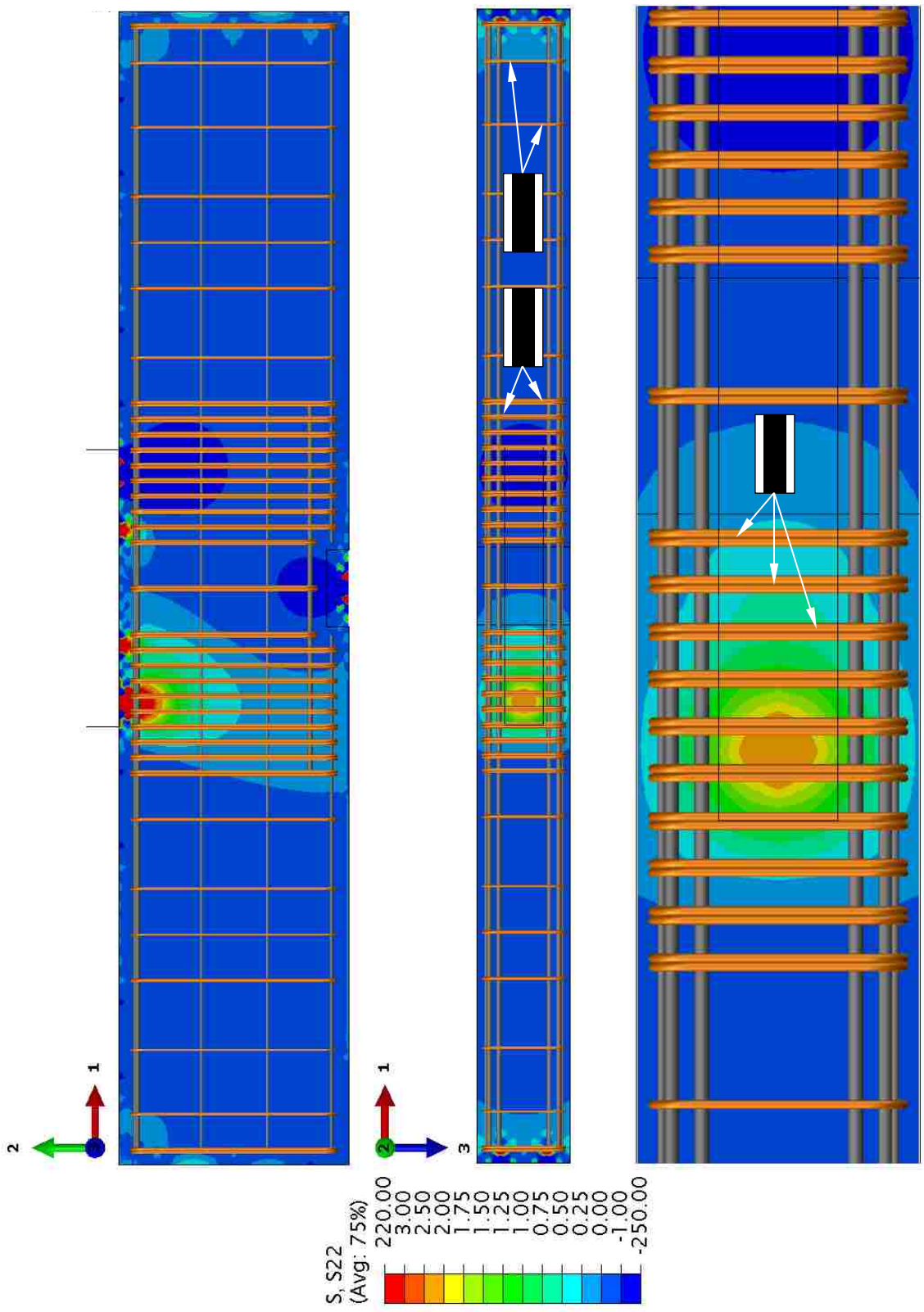

Figure 4-12: Steel reinforcement required to carry tensile stresses in the transverse direction

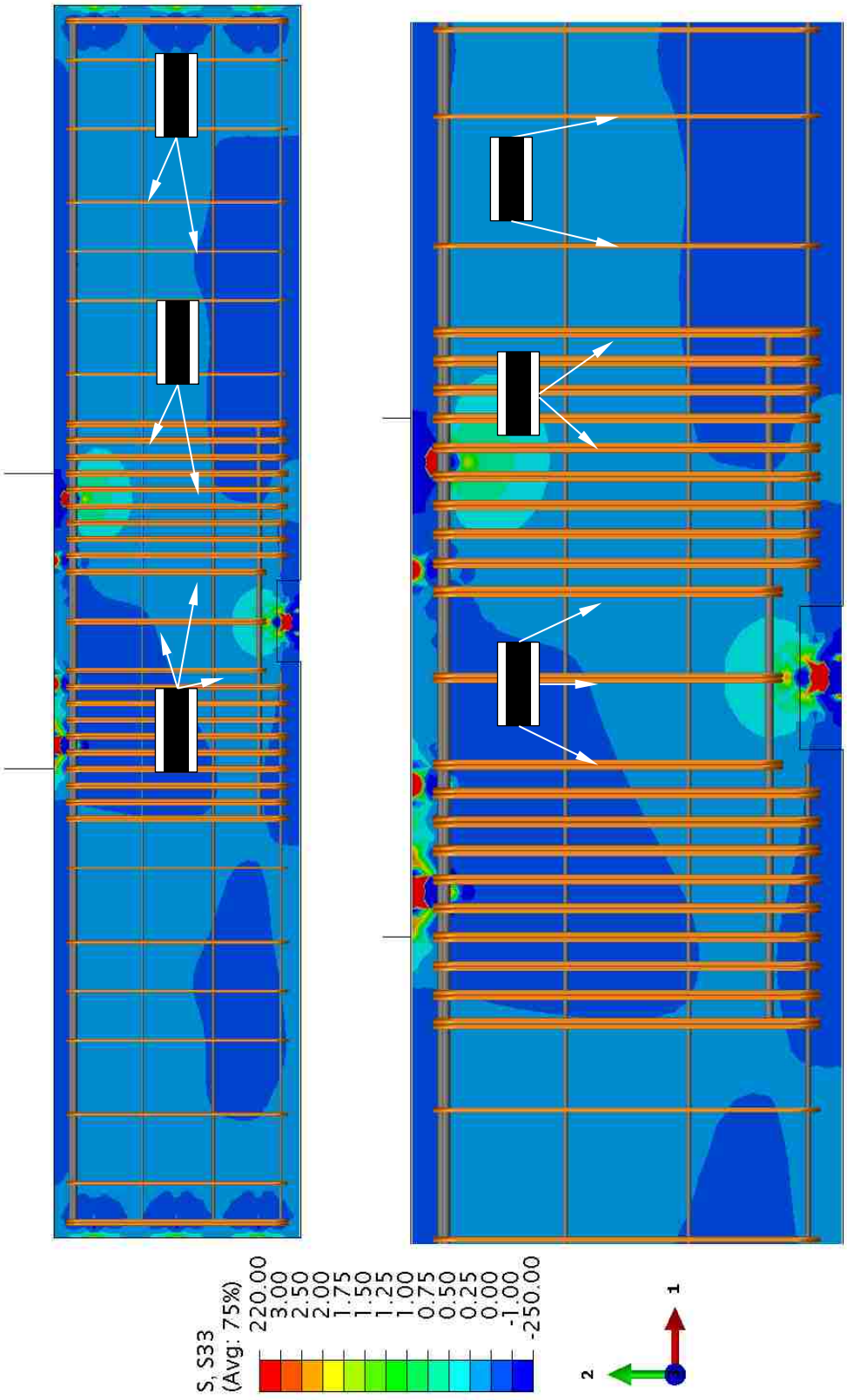

Figure 4-13: Steel reinforcement required to carry tensile stresses in the vertical direction

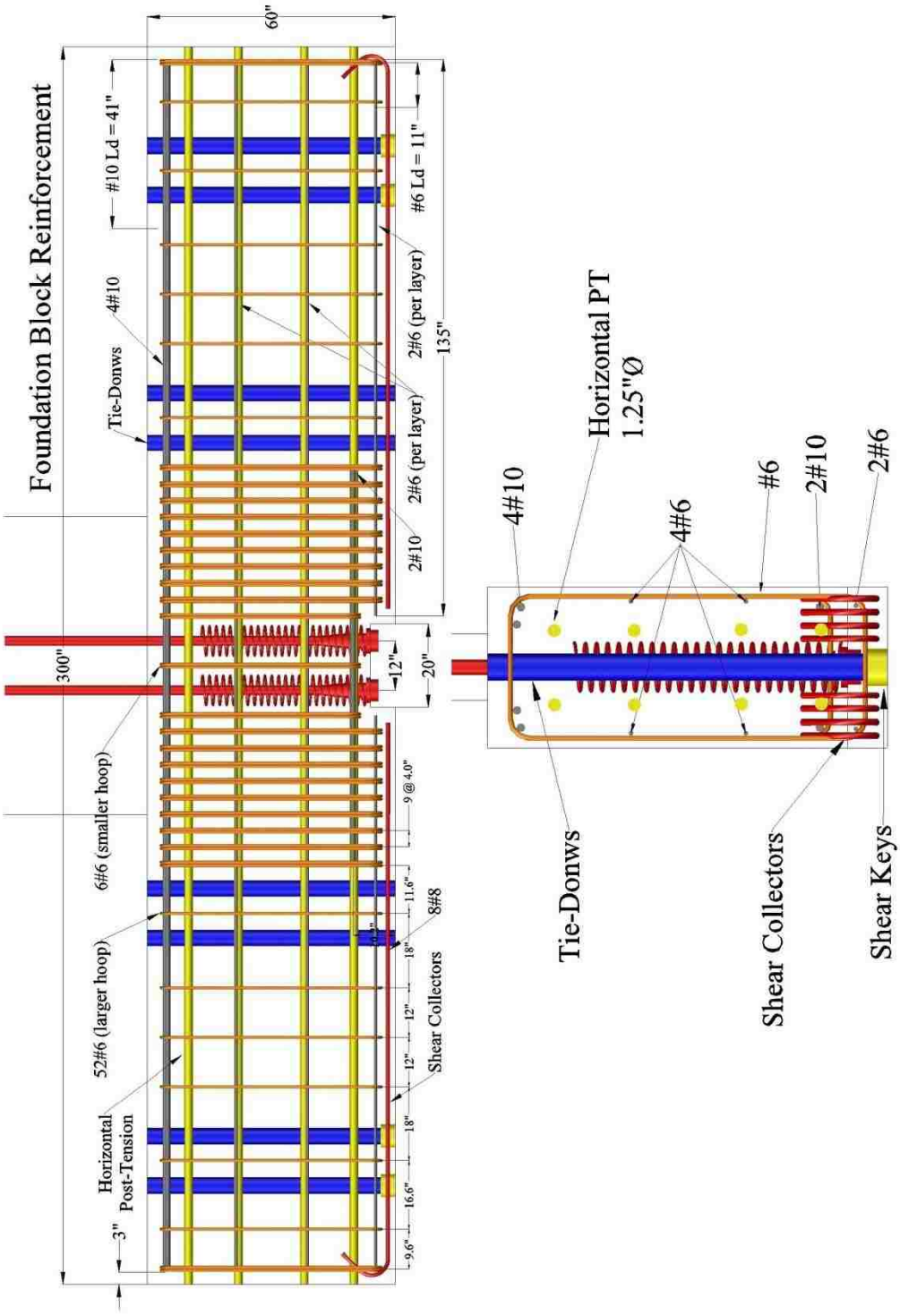

Figure 4-14: Final steel reinforcement layout of the foundation block

CHAPTER 5

EXPERIMENTAL RESULTS

This chapter presents the experimental results for the lateral load test of Wall 1. Section 5.1 describes the loading history for both the load and displacement control portions of the loading sequence. Section 5.2 identifies various response quantities that describe the global behavior of the test wall as well as observed limit states that occurred during testing. Section 5.3 describes the initiation of concrete cracking. Section 5.4 presents the yielding of the longitudinal bars during testing. Section 5.5 shows the initiation of observed concrete spalling. Section 5.6 describes the complete response of the post-tensioning. Section 5.7 presents the fracture of the longitudinal steel reinforcement bars. Section 5.8 describes the response of the confined concrete. Finally, Section 5.9 describes the failure mode of the test wall.

5.1 LOADING HISTORY

Figure 5-1 and Figure 5-2 show the test wall in its displaced configuration when it is loaded eastward and westward, respectively. As shown in Figure 5-1 and Figure 5-2, the lateral force actuator applied a vertical component of force in the displaced position. This vertical force component is small and is not included in the presentation of results in this report. In this report, actuator forces are positive in tension, loading westward, and negative in compression, loading eastward. Similarly, lateral displacements are also positive when displaced westward, and negative when displaced eastward. Lateral displacements were obtained at the actuator level from two LVDTs, one attached to the actuator, and another connected to an independent column as shown in Figure 3-37.

Figure 5-3 shows the complete loading history planned for the test wall. The loading sequence was obtained from ACI ITG 5 and is further explained by Pakiding (2014). The complete loading history was divided into 16 loading steps and each loading step has three full cycles. The wall was loaded up until Loading Step 15, Cycle 1. At that point failure occurred and the test was ended.

At the start of the test, the first three loading steps are applied under load control, and the remaining 13 loading steps are applied under displacement control. Figure 5-4 shows the portion of the load history under load control. Displacements collected during the load control portion of the load history were obtained from the LVDT connected to the independent column, and displacements collected during the displacement control portion of the load history were obtained from the LVDT attached to the actuator.

Figure 5-5 superposes the planned load over the actual load for the load control portion of the load history. This figure shows the accuracy of the actual load at every cycle. In this figure, load is plotted verses record number. The record number is increased by 1 each time data is saved. In this experiment data was saved every 2 seconds. Figure 5-5 shows the accuracy of the applied loads at every cycle.

Figure 5-6 superposes the planned displacement over the actual displacement for the displacement control portion of the load history. Again, the control parameter (displacement in this case) is plotted versus record number. This figure also shows the accuracy of the actual displacement at every cycle.

Figure 5-7 shows a plot of the base moment versus record number. Base moment is calculated by the applied actuator force times the height of wall to the actuator level. Similarly, Figure 5-8 shows a plot of the base shear versus record number. Base shear is equal to the applied actuator force. These plots also show the overall uniformity of load and displacement applied during the test as well as the displacement increase every three cycles.

5.2 LATERAL LOAD RESPONSE

Figure 5-9 shows a plot of the base moment versus lateral drift showing the complete experimental response of Wall 1. As explained in Section 5.1, failure occurred during Loading Step 15, after 43 cycles of load. The lateral drift is calculated as the ratio of lateral displacement at the actuator height divided by the height of the wall at the actuator level.

Figure 5-10 shows a plot by Srivastava (2013) that describes the limit states of an unbonded post-tension cast-in-place structural wall. These limits states are decompression (DEC), effective linear limit (ELL), yielding of mild steel (YMS), fracture of mild steel (FMS), yielding of PT (LLP), and crushing of confined concrete (CCC). These limit states are identified for Wall 1 in subsequent sections.

5.2.1 Stiffness Degradation

Figure 5-11 shows a plot of the experimental envelope curve using base moment versus lateral drift. This envelope curve shows key components of the structural response during

the test. These components are concrete cracking, yielding of the mild steel, observed concrete spalling, yielding of PT, and observed fracture of the longitudinal bars. Detailed comparison of analytical versus experimental limit states is presented in Pakiding (2014).

Figure 5-12 and Figure 5-13 show the stiffness degradation versus the loading steps and lateral drift, respectively. The lateral stiffness was obtained by taking the slope of the hysteresis curve for each loading step. This was done by first, selecting data ranging from $\Theta = \pm 0.015$ to $\Theta = \pm 0.040$, and then obtaining the regression line slope from this data. This range was selected to avoid data close to zero drift due to excessive static noise and to avoid the nonlinear portion of the lateral force-lateral drift curve. The initial lateral stiffness at Loading Step 1 was 1,254 kip/in. At Loading Step 2, the lateral stiffness decreased 4.03% to 1,202 kip/in. This trend continued throughout the loading steps. The stiffness at the final loading step was 37 kip/in, a 97.1% reduction compared to the initial stiffness.

5.2.2 Strength Deterioration

Figure 5-14 describes a plot of the lateral strength deterioration exhibited during each loading step (loaded eastward). In this plot, the second and third cycles are compared with the first cycle of that loading step. This plot shows that during the elastic portion of the test, the strength deterioration at Cycles 2 and 3 is almost negligible. However, after the effective linear limit (ELL) state, the lateral strength deterioration ranges from 2.0% to 3.7% for the second cycle and from 2.4% to 16.7% for the third cycle.

5.2.3 Energy Dissipation

Figure 5-15 shows a plot of the normalized cumulative hysteretic energy dissipation ($E_d/E_{d,max}$). The energy dissipation values (E_d) were obtained from the area enclosed by the cycle of the force-displacement curve. These values were normalized by $E_{d,max}$ which is calculated as 20,761 kip-in This number is obtained by adding the area of all of the hysteresis loops. These normalized values are plotted versus the lateral drift. From Figure 5-15, it is evident that cycles after the effective linear limit (ELL) found in Figure 5-10, dissipate larger amounts of energy. This dissipation, among other factors, is due to concrete cracking, yielding of longitudinal bars, shear sliding along cracks, yielding of PT, fracture of longitudinal bars, and nonlinear compression in concrete.

5.3 CONCRETE CRACKING

Figure 5-16 shows a plot of the concrete strains versus the lateral drift. The concrete strain is normalized by the strain at which the concrete is predicted to crack under tension. The strain at which the concrete was predicted to crack was obtained by dividing the concrete modulus of rupture (f'_r) by the concrete modulus of elasticity (E_c). In this research, the predicted concrete cracking strain is calculated as follows: $f'_c = 7.5\sqrt{6{,}000} = 581$ psi, $E_c = 5700\sqrt{6{,}000} = 441{,}520$ psi, therefore $\text{strain} = 131\mu\varepsilon$.

Using strain gauges embedded in the confined section of the wall, the concrete on the East end of the wall was found to crack during Cycle 13W. The measured drift at this point was recorded at $\Theta_{ccr} = 0.023\%$. Figure 5-17 shows a photograph at the end of Cycle 13W, where cracks can be observed on the East end of the wall.

Figure 5-18 shows a plot of the concrete strains versus the lateral drift. The concrete strain is normalized by the strain at which concrete cracks under tension. The strain at which the concrete cracks was obtained by dividing the concrete modulus of rupture (f_r) by the concrete modulus of elasticity (E_c). Using strain gauges embedded in the confined section of the wall, the concrete on the West end of the wall was found to crack during Cycle 13E. The measured drift at this point was recorded at Θ_{ccr} = -0.016%. Figure 5-19 shows a photograph at the end of Cycle 13E, where cracks can be observed on the West end of the wall.

5.4 LONGITUDINAL BAR YIELDING

Figure 5-20 shows the strains in the midface longitudinal bar in the extreme fiber of the East toe of the wall. For clarity, the bar location is illustrated in the wall section and a photo included in the figure. The strain is normalized by the yield strain (ε_{msy_n} = 0.0026), and plotted versus the lateral drift. The yield strain for the #7 reinforcing bar was obtained from a tensile test following ASTM A370 guidelines.

The #7 rebar tested was a cut-off section of the bar adjacent to where the strain gauge is located. The recorded strain from the strain gauge was then divided by the yield strain. From this figure, it can be shown that the middle bar reached its nominal yielding strain at about Θ_{msy_n} = 0.57%. This occurred during Cycle 28W. Figure 5-21 shows the again the steel bar strain normalized by the yield strain, but now versus the cycle numbers. In this figure, it is easier to appreciate the yielding of this middle bar during this cycle.

Figure 5-22 shows the strains in the North corner of the East toe of the wall. For clarity, the bar location is illustrated in the wall section and a photo included in the figure. The strain is normalized by the yield strain, and plotted versus the lateral drift. The yield strain for the #7 reinforcing bar was obtained from a tensile test following ASTM A370 guidelines.

From this figure, it can be shown that the corner bar reached its yielding strain at about Θ_{msy_n} = 0.43%. This also occurred during Cycle 28W. Figure 5-23 shows the again the steel bar strain normalized by the yield strain, but now versus the cycle numbers. In this figure, it is easier to appreciate the yielding of this corner bar during this cycle.

Other strain gauges were located on the West side of the wall. However, those strain gauges were either disturbed during the concrete placing or became inoperable after only a few cycles, never reaching the rebar nominal yielding strain.

5.5 CONCRETE SPALLING

Figure 5-24 shows photographs of both the West and East ends of the wall showing the initiation of concrete spalling. Concrete spalling was observed to occur at the end of Cycle 31, West and East respectively, during Loading Step 11. Concrete spalling was observed to occur at a measured at drift of Θ_{spl} = 1.35%. Figure 5-25 shows the loading step and cycle at which concrete spalling was observed.

5.6 POST-TENSIONING RESPONSE

Figure 5-26 shows the complete response of the unbonded post-tension (UPT) tendon on the East side identified as UPT 1 in the figure. The PT force is normalized by the PT yielding force. In this figure, it can be seen that only actuator westward lateral forces bring the tendon to yielding, while eastward lateral forces bring the tendon to only about 85% yielding. Figure 5-27 shows the UPT force and the normalized yielding peaks. In total there were four yielding peaks. These yielding peaks occurred at Cycles 37W, 40W, 41W, and 42W. Yielding peak during Cycle 37W was measured at Θ_{llp_n} = 3.04%, while the other three yielding peaks were measure at Θ_{llp_n} = 3.98%, Θ_{llp_n} = 4.00%, and Θ_{llp_n} = 4.00%, respectively.

Figure 5-27 also shows the loss of prestressing forces that occurred on the PT after its first yielding peak. As mentioned before, the first yielding of UPT 1 occurred at the end of Cycle 37W. At this applied drift (Θ = 3.0%), the PT force for UPT 1 at Cycle 37W was recorded at 239.6 kips. Subsequent cycles during this applied drift, 38W and 39W, show a loss in prestressing force recorded at 237.6 kips and 236.6 kips, respectively. This loss in prestressing force becomes more prominent during the following applied drift. During the three cycles at this next applied drift of Θ = 4.0%, the prestressing forces decrease from 252.6 kips at Cycle 40W, to 249.6 kips at Cycle 41W, to finally 241.9 kips at Cycle 42W. At the last applied drift of Θ = 5.0%, during Cycle 43W, the prestressing force was recorded at 227.5 kips. From this loss of prestressing forces due to the yielding of UPT 1, it is evident that self-centering capabilities are greatly diminished.

Figure 5-28 shows the complete response of the UPT tendon on the East side identified as UPT 2 in the figure. The PT force is normalized by the PT yielding force. In this figure, it can be seen that only actuator eastward lateral forces bring the tendon to yielding, while westward lateral forces bring the tendon to only about 95% yielding. Figure 5-29 shows the UPT force and the normalized yielding peaks. In total there were five yielding peaks. These yielding peaks occurred at Cycles 37E, 38E, 39E, 40E, and 41E. Yielding peak during Cycle 37E was measured at Θ_{llp_n} = -2.99%, while the other four yielding peaks were measure at Θ_{llp_n} = -2.99%, Θ_{llp_n} = -2.99%, Θ_{llp_n} = -3.99%, and Θ_{llp_n} = -3.98%, respectively.

Figure 5-29 also shows the loss of prestressing forces that occurred on the PT after its first yielding peak. As mentioned before, the first yielding of UPT 2 occurred at the end of Cycle 37E. At this applied drift (Θ = -3.0%), the PT force for UPT 2 at Cycle 37E was recorded at 243.1 kips. Subsequent cycles during this applied drift, 38E and 39E, show a loss in prestressing force recorded at 240.7 kips and 239.6 kips, respectively. This loss in prestressing force becomes more prominent during the following applied drift. During the three cycles at this next applied drift of Θ = -4.0%, the prestressing forces decrease from 256.6 kips at Cycle 40E, to 248.8 kips at Cycle 41E, to finally 208.7 kips at Cycle 42E. At the last applied drift of Θ = -5.0%, during Cycle 43E, the prestressing force was recorded at 194.2 kips. From this loss of prestressing forces due to the yielding of UPT 2, self-centering capabilities are greatly reduced.

5.7 LONGITUDINAL BAR FRACTURE

Figure 5-30 shows a plot of the last three loading cycles in which the buckling and fracture of the extreme fiber longitudinal bars was observed. At the end of Cycle 41E, buckling of the longitudinal bars B1E and B3E was observed. Subsequently, before reaching the end of Cycle 42W, bars B1E, B2E, and B3E fractured (see Figure 5-31) while straightening out from the buckled concfiguration. The fracture of these bars was recorded at a drift of Θ = 3.56%. At the end of this cycle (42W), buckling of the longitudinal bars B1W and B3W was observed. Subsequently, before reaching the end of Cycle 42E, bars B1W, B2W, and B3W fractured (see Figure 5-31). The fracture of these bars was recorded at a drift of Θ = -3.35%.

A detail inspection of the test wall was performed at the conclusion of the test. It was found that no other rebar, longitudinal or otherwise, had fractured.

5.8 CONFINED CONCRETE RESPONSE

Figure 5-32 shows the response of the confined concrete under compression at the East end of the wall. The strain gauge is located in the center of this confined region, as shown in Figure 5-22, and gauge provided data until it failed at the end of Cycle 19. From this figure, nonlinear response of the confined concrete can be observed as the slope of the hysteretic loops becomes smaller and the unloading path differs from the loading path. Figure 5-33, the response of the confined concrete at the West end of the wall is similar. This strain gauge provided data until it failed at the end of Cycle 16.

5.9 FAILURE MODE

From experimental observation, it was concluded that the failure mode of the test wall was shear. Figure 5-34 shows photographs of the progression of this failure mode. As shown in the photographs, shear cracks (those seen on the web portion of the wall) developed as early as Cycle 13 along with flexure cracks (those seen on the confined regions of the wall). During this cycle, at which shear cracks were first observed, the lateral drift was Θ = 0.14%. As larger displacements were applied, more and larger flexure cracks develop as well as shear cracks. Eventually, shear cracks dominated over flexure cracks the concrete in the web portion of the wall spalled, exposing the shear steel reinforcement. After this point (during Cycle 43), the test wall lost its shear strength.

Figure 5-35 shows a photograph of the test wall after the broken concrete was removed from the web portion of the wall. This photograph also shows the flange portion of the wall and validates the importance of the confined concrete in the boundary elements of the wall.

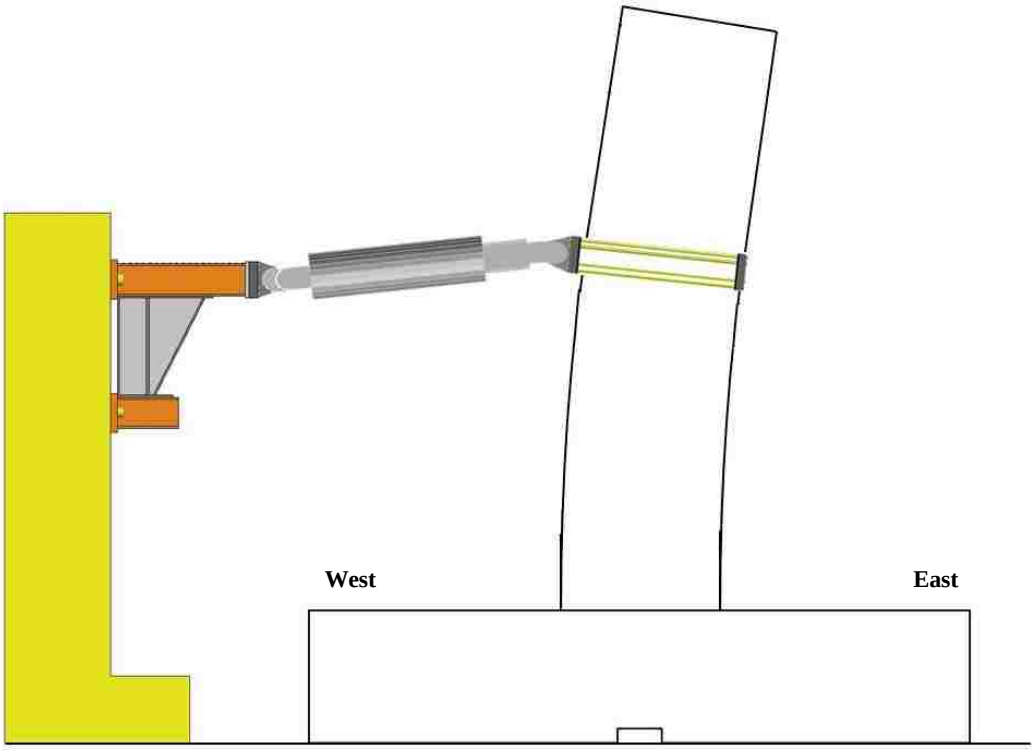

Figure 5-1 Displaced state of test wall loaded east

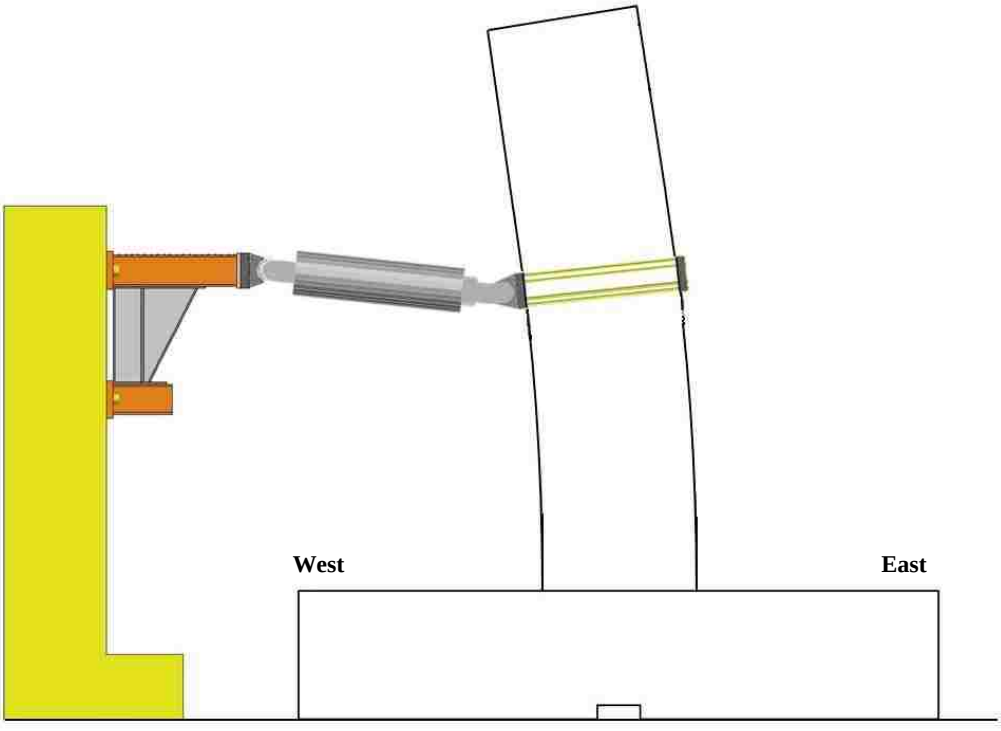

Figure 5-2 Displaced state of test wall loaded west

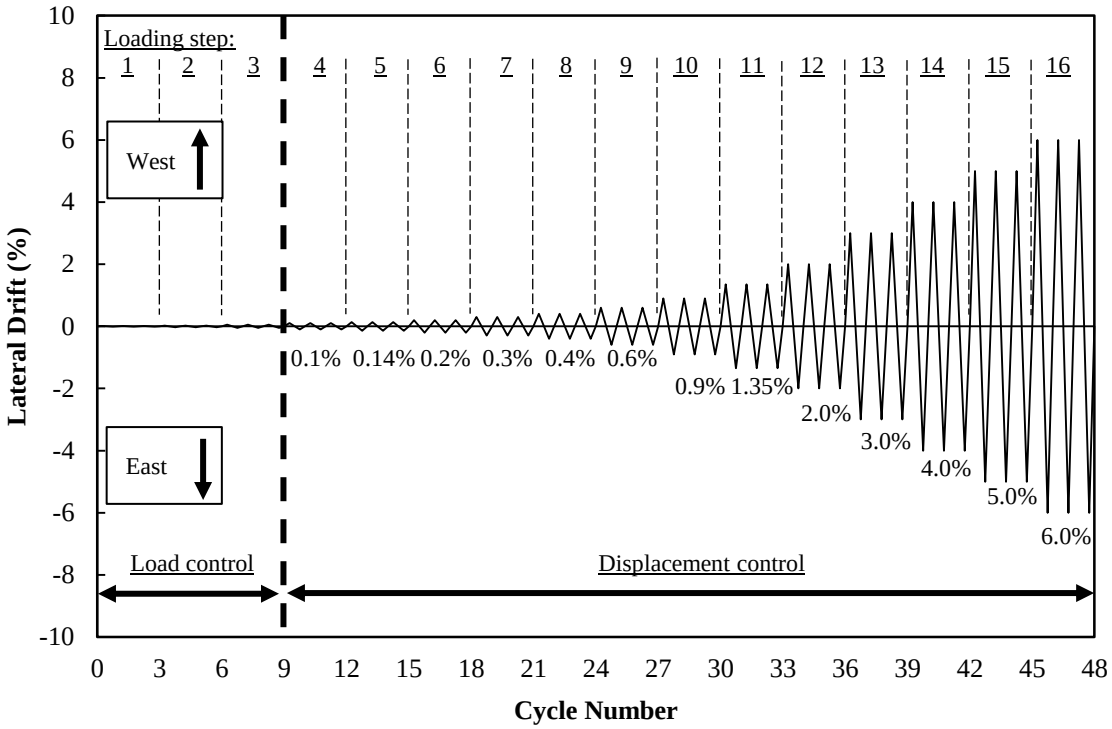

Figure 5-3 Complete planned loading history

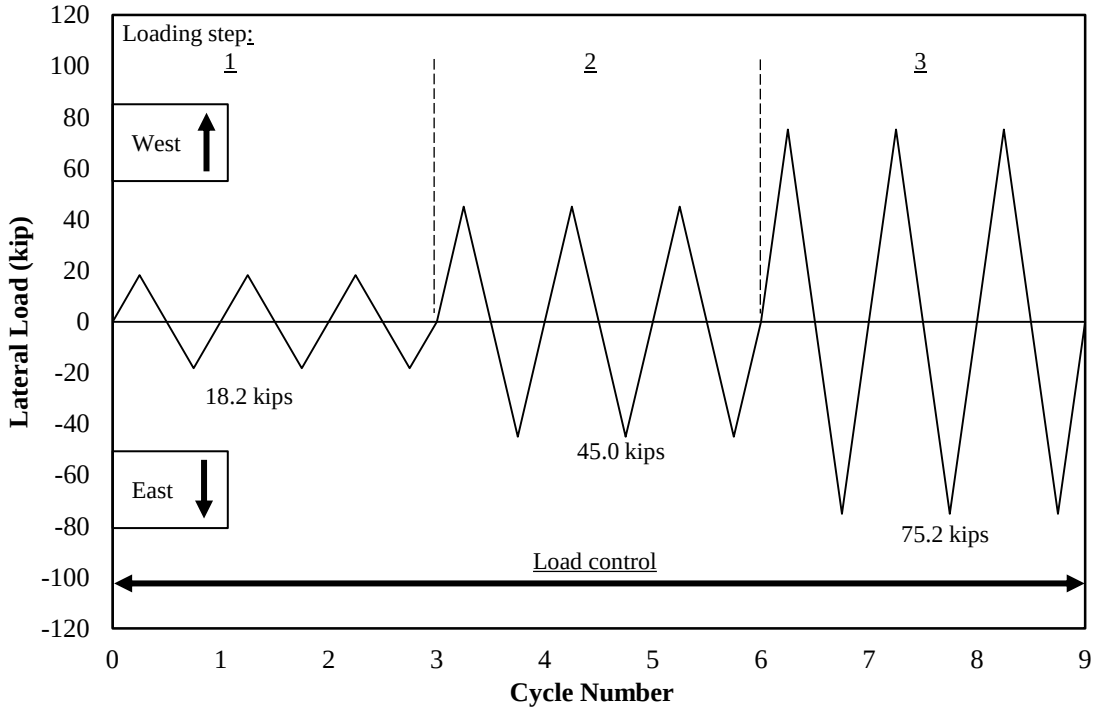

Figure 5-4 Loading history - load control portion

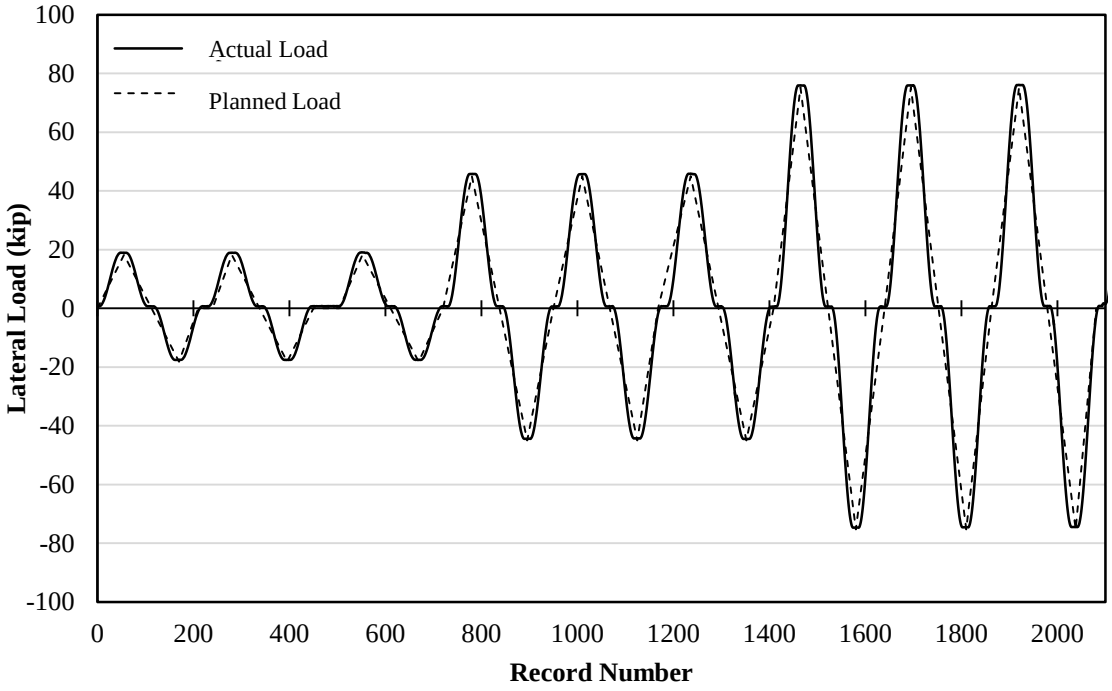

Figure 5-5 Actual load history superposed with planned load history for the load control portion of the loading history

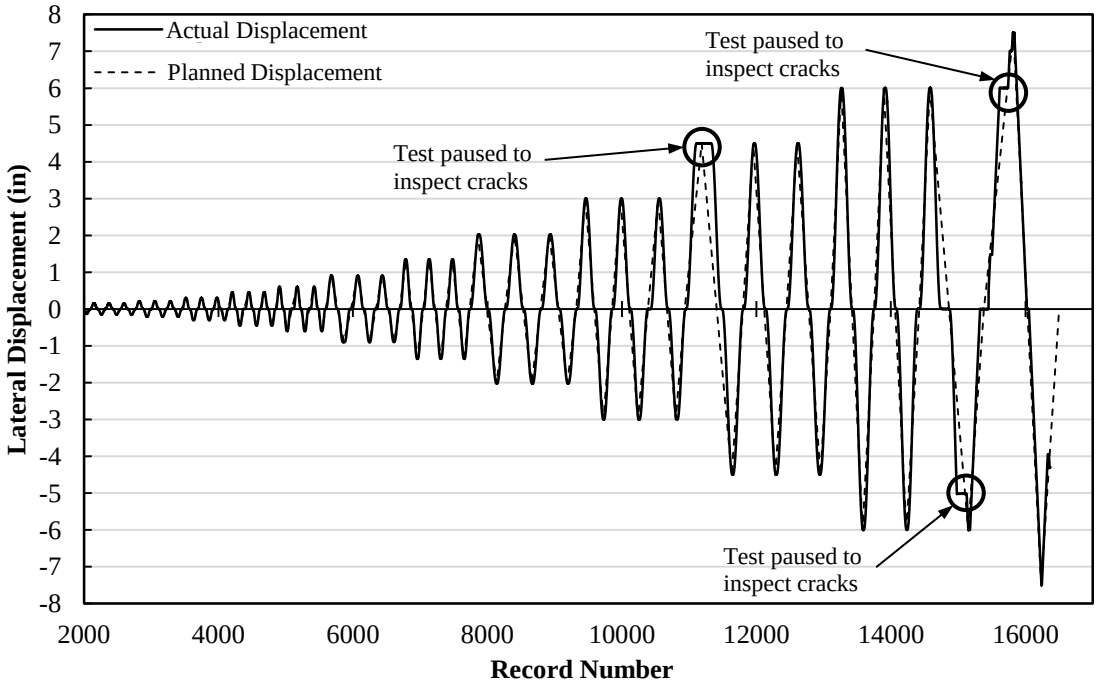

Figure 5-6 Actual displacement history superposed with planned displacement hystory for the displacement control portion of the loading history

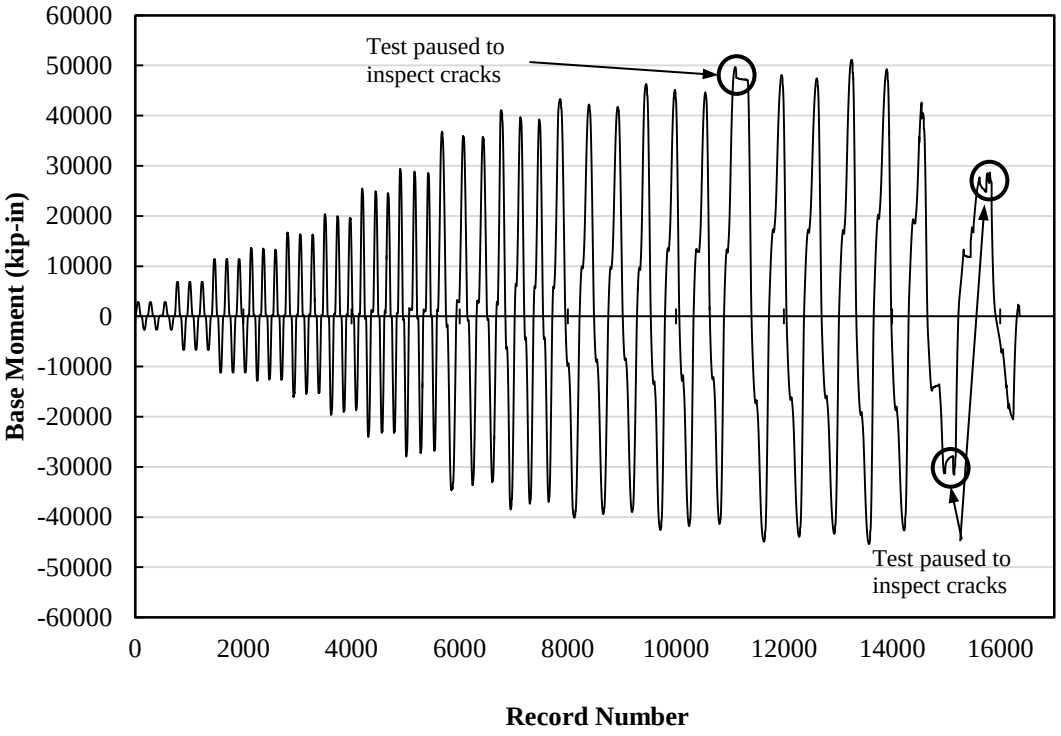

Figure 5-7 Base moment versus record number

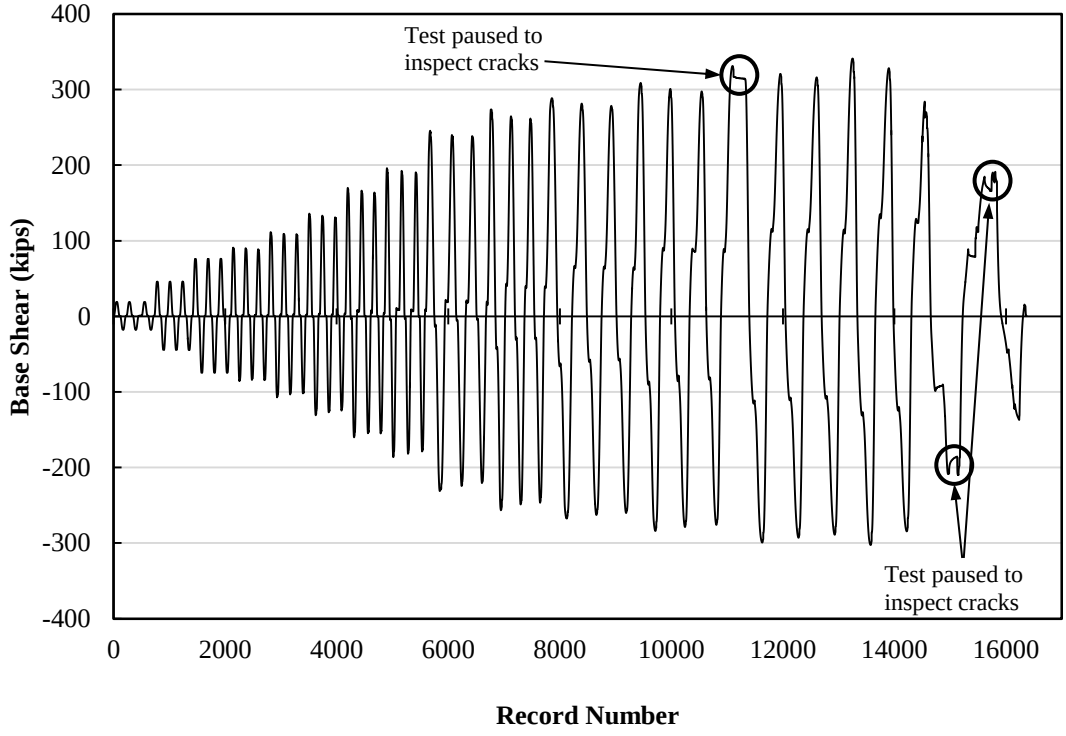

Figure 5-8 Base shear versus record number

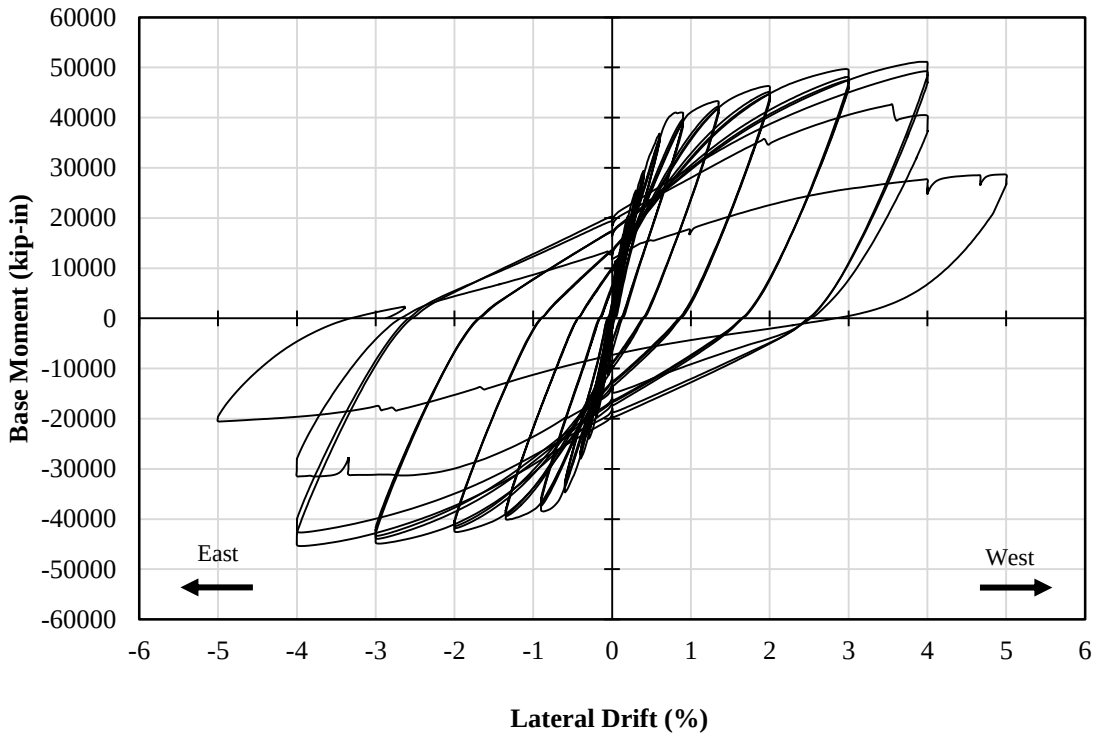

Figure 5-9 Complete experimental response - base moment versus lateral drift

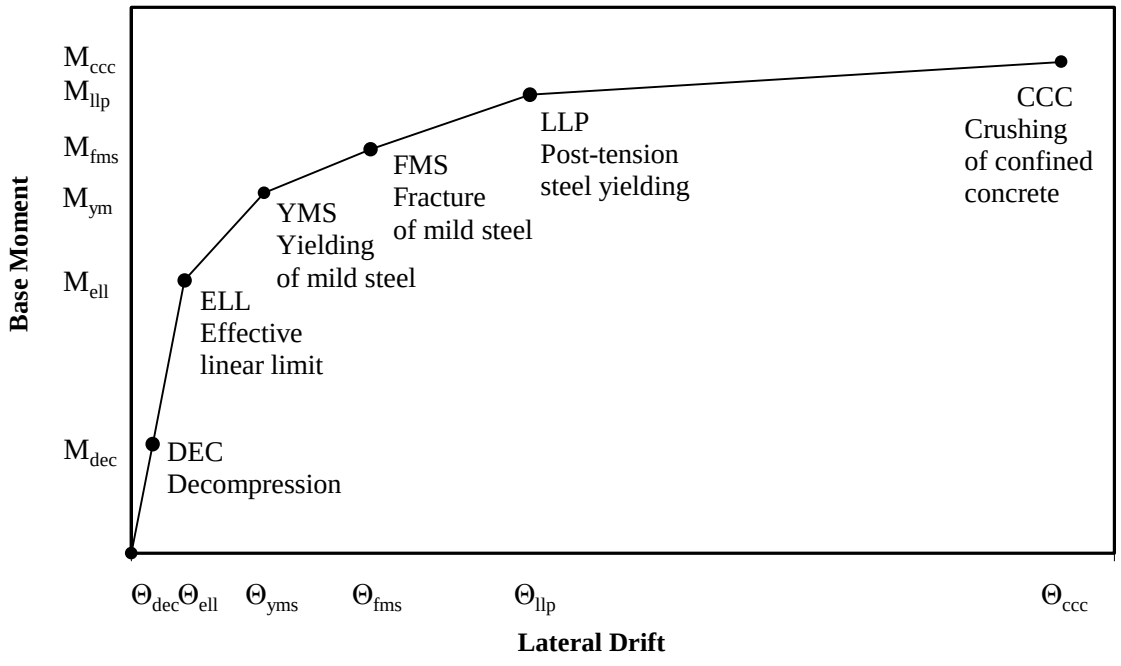

Figure 5-10 Structural limit states (Srivastava (2013))

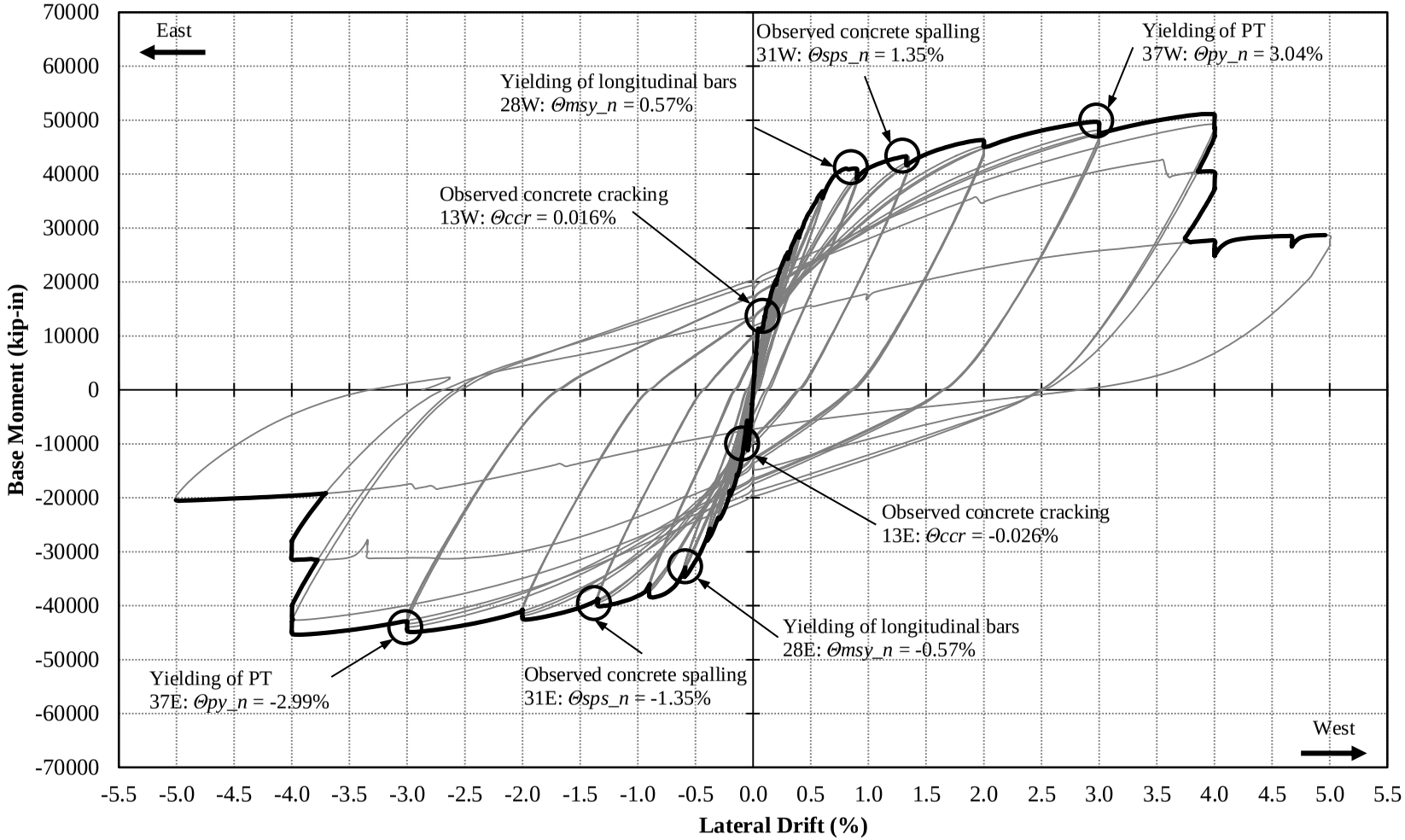

Figure 5-11 Experimental envelope curve and complete hysteresis including observed wall behavior and limit states

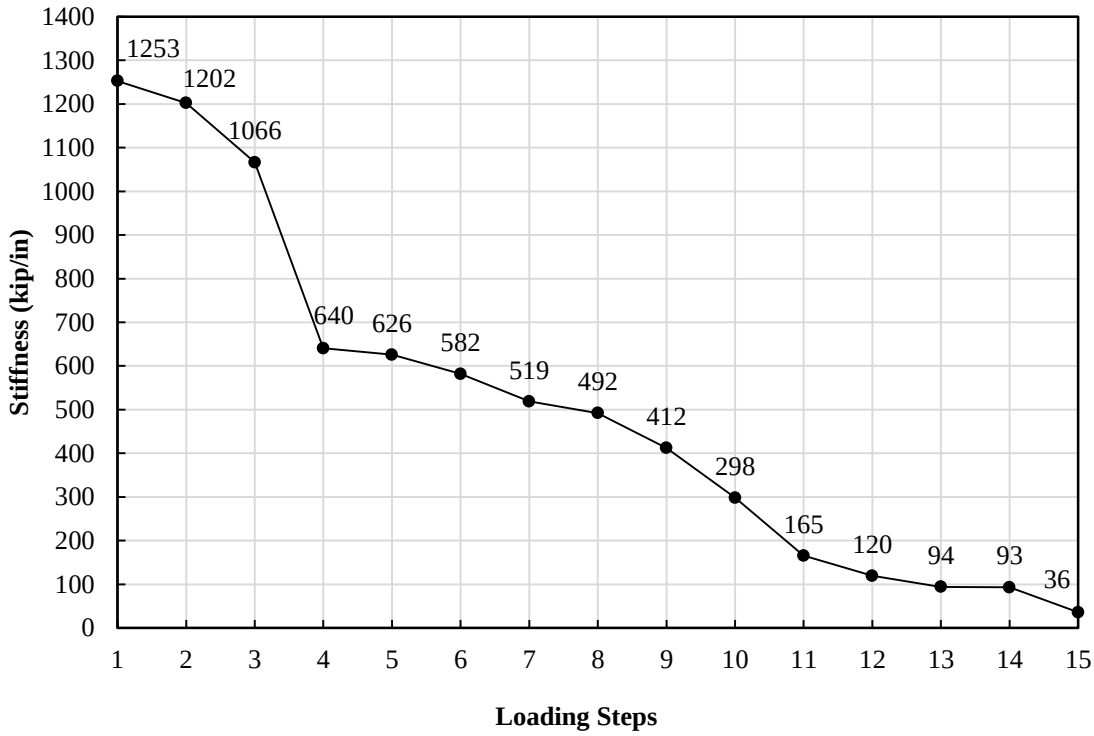

Figure 5-12 Stiffness degradation (per loading step increase) versus loading steps

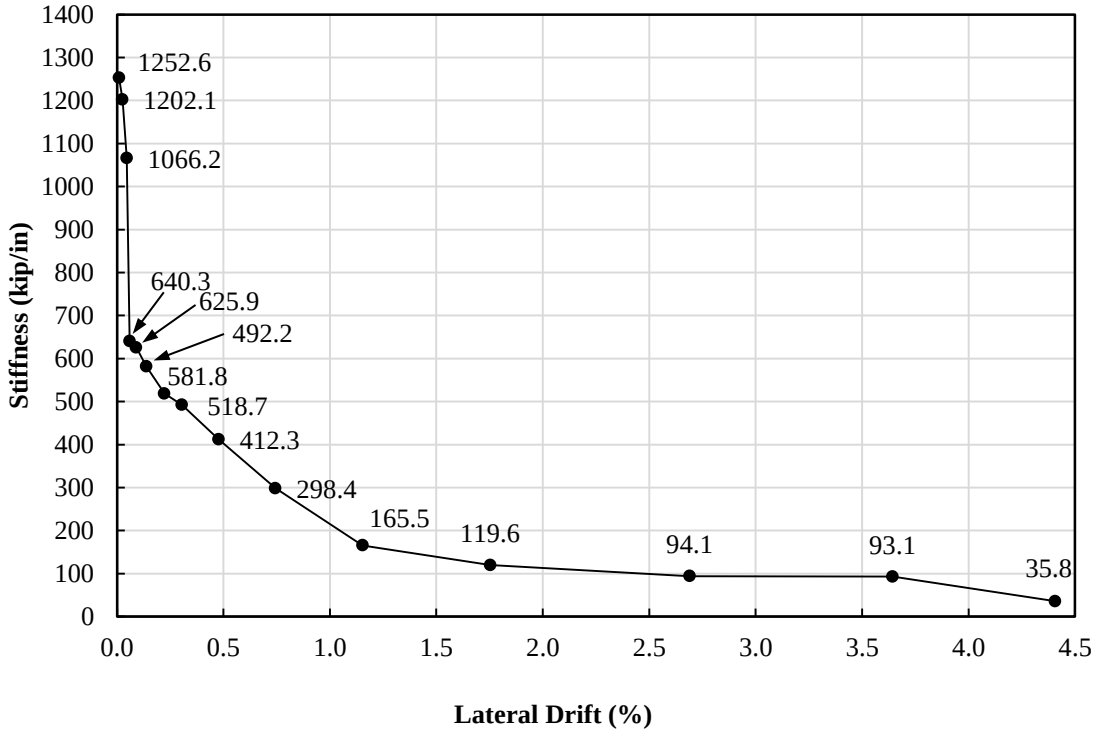

Figure 5-13 Stiffness degradation (per loading step) versus lateral drift

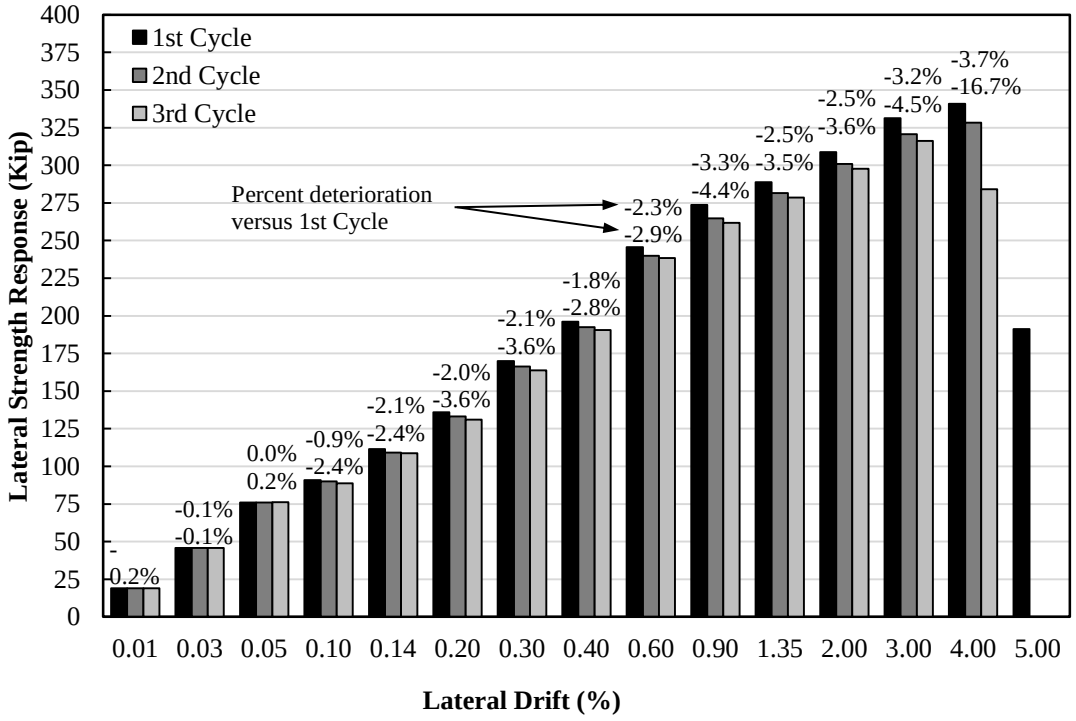

Figure 5-14 Strength deterioration per cycle at applied lateral drift

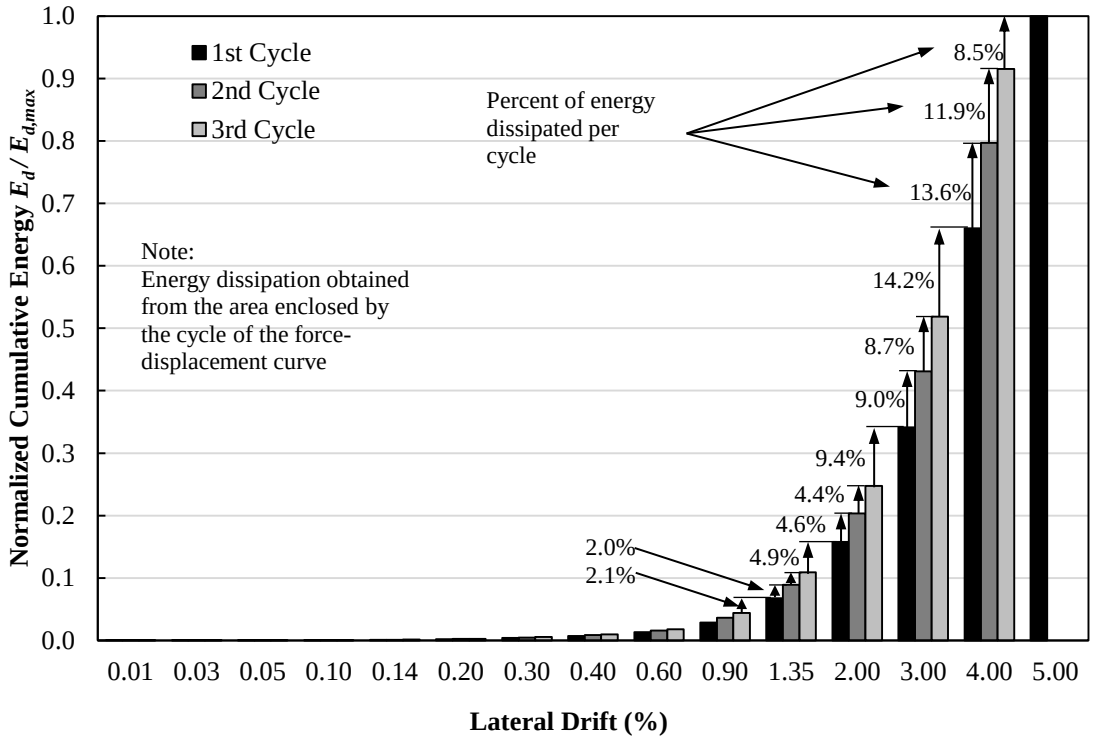

Figure 5-15 Normalized cumulative hysteretic energy dissipation

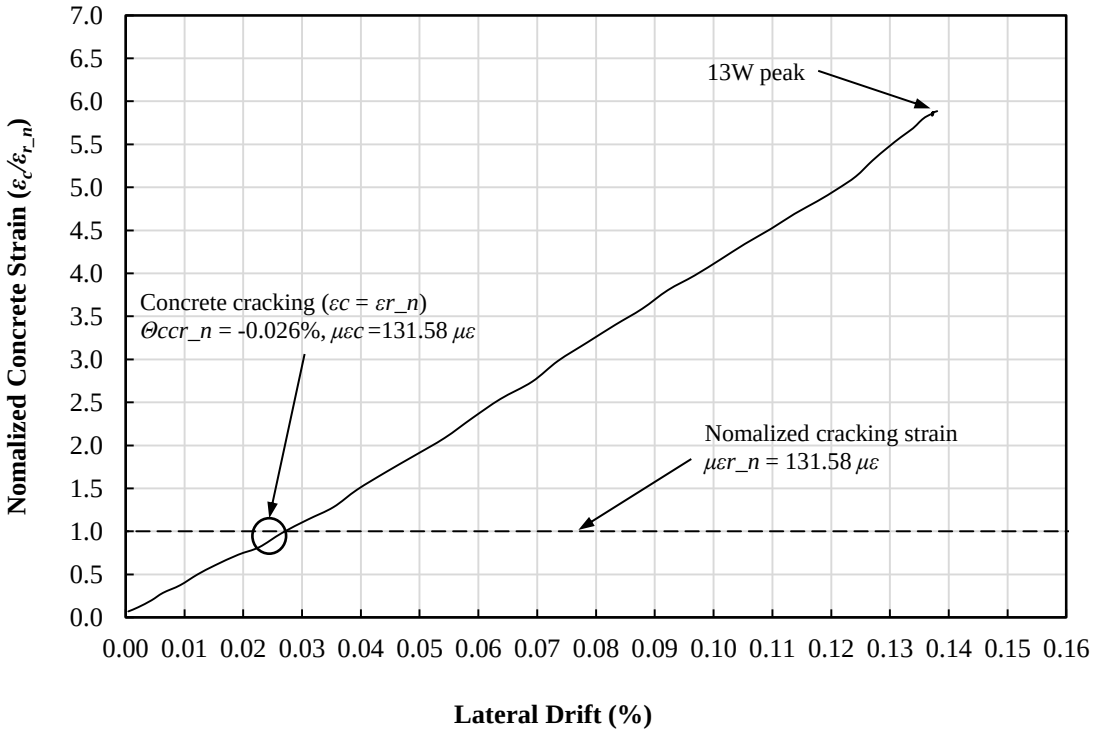

Figure 5-16 Concrete cracking strain versus lateral drift (East side)

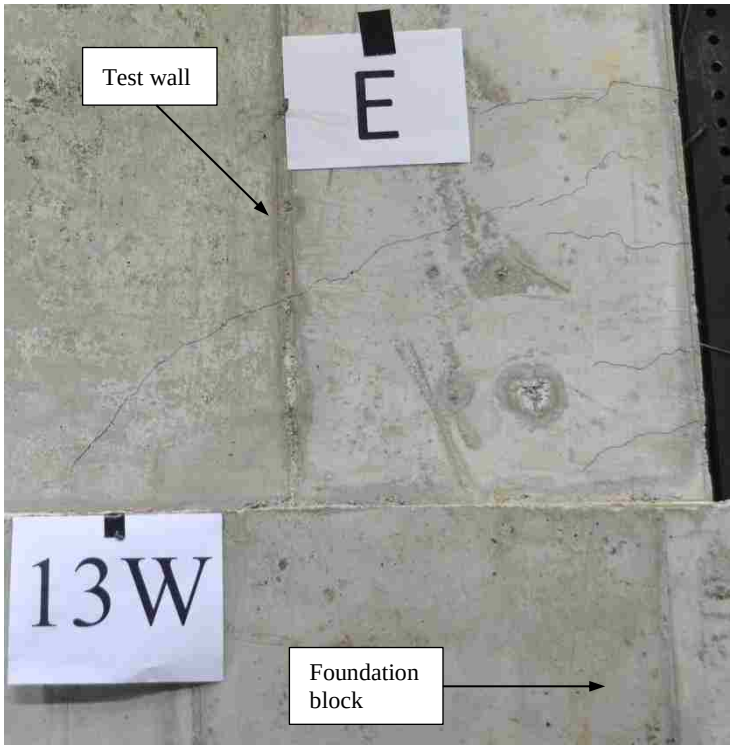

Figure 5-17 Photograph of observed initiation of concrete cracking on the East side

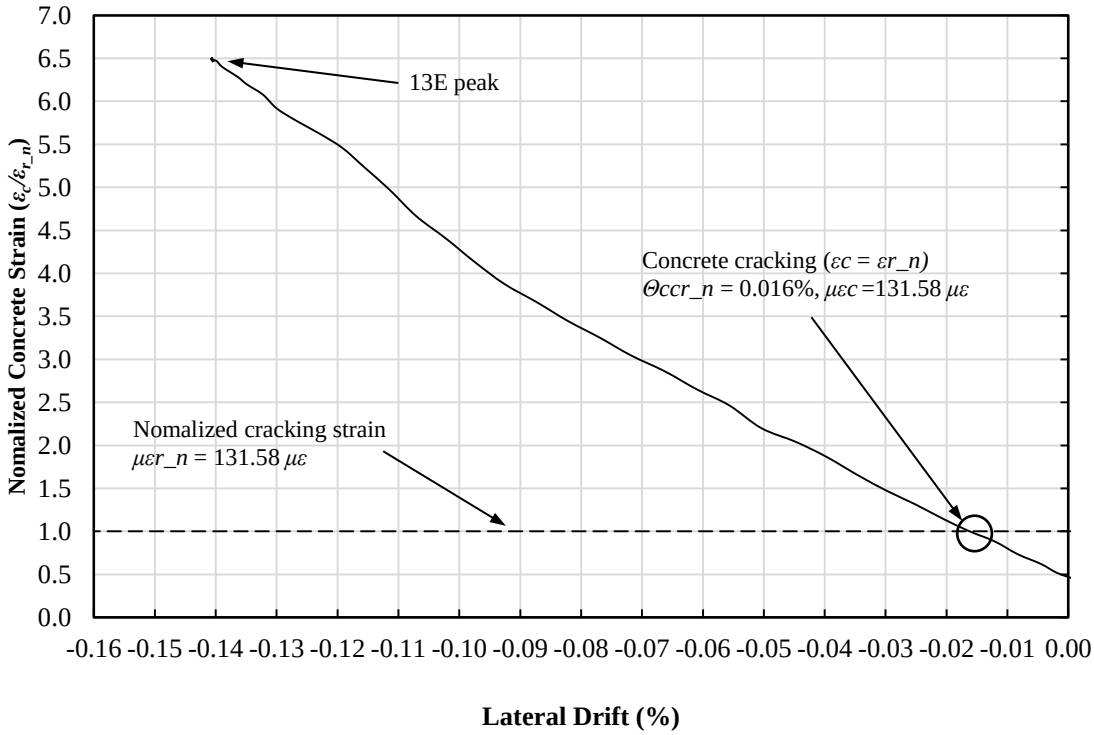

Figure 5-18 Concrete cracking strain versus lateral drift (West side)

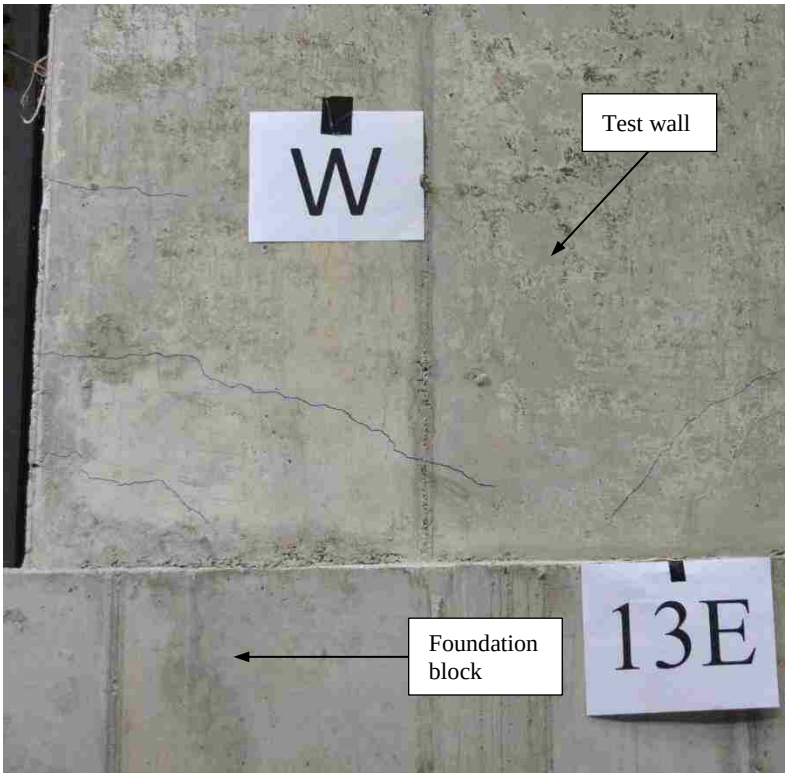

Figure 5-19 Photograph of observed initiation of concrete cracking on the West side

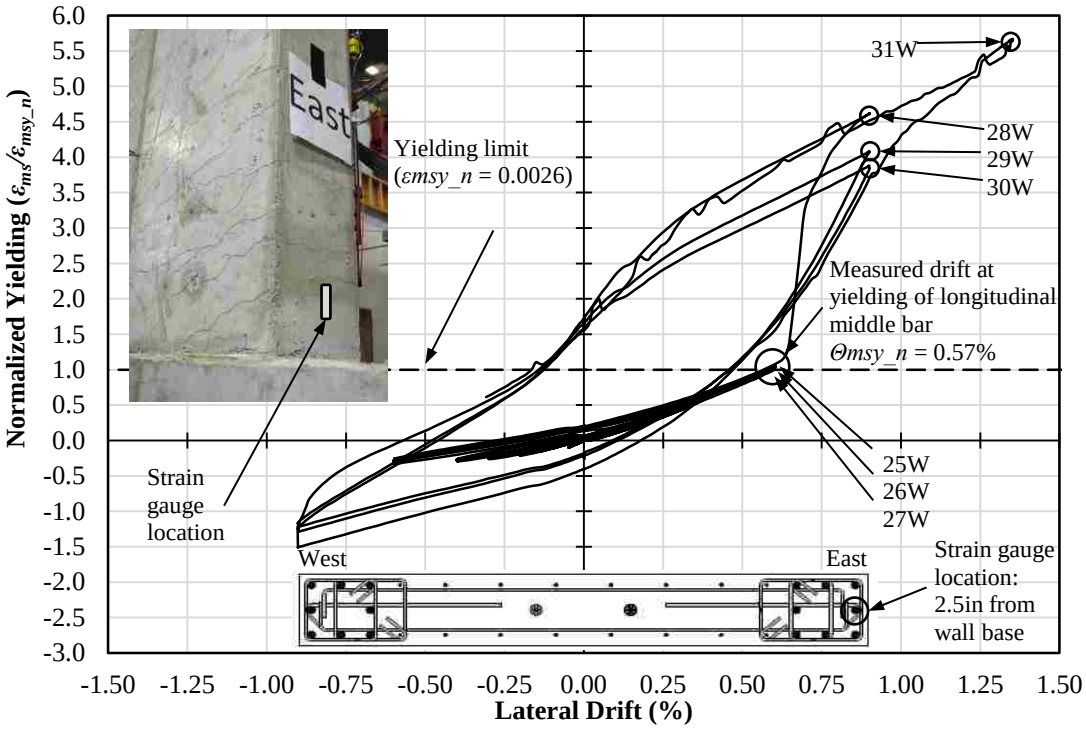

Figure 5-20 Normalized bar strain versus lateral drift

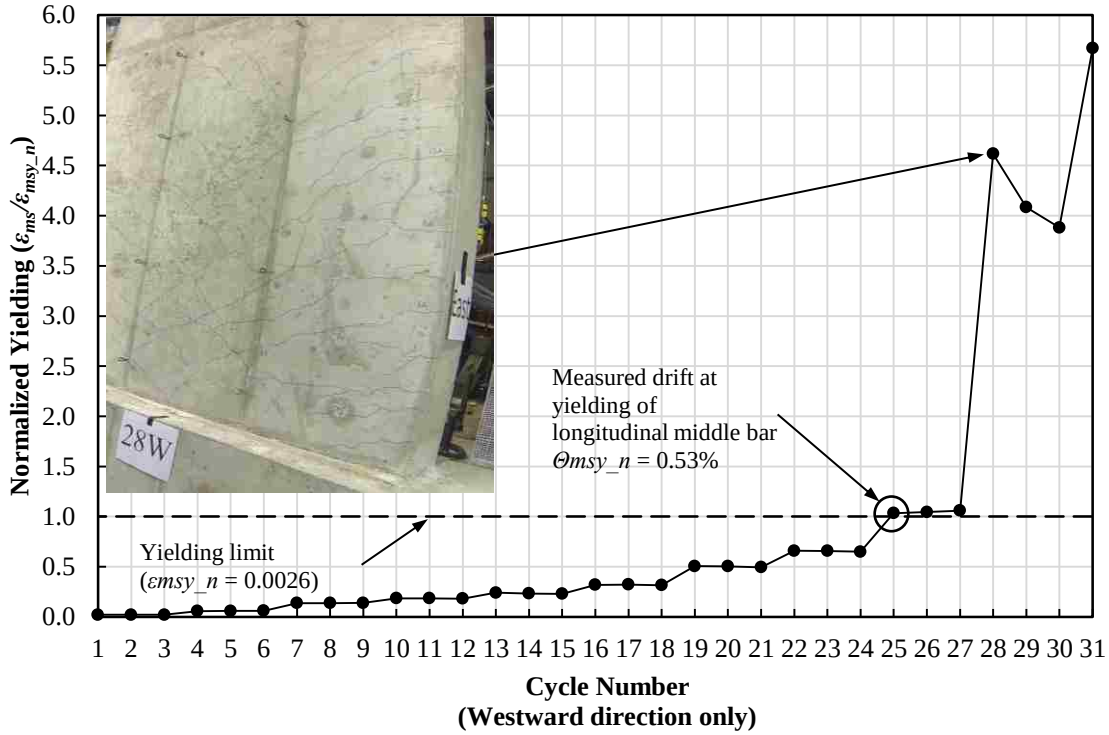

Figure 5-21 Normalized bar strain versus cycle number

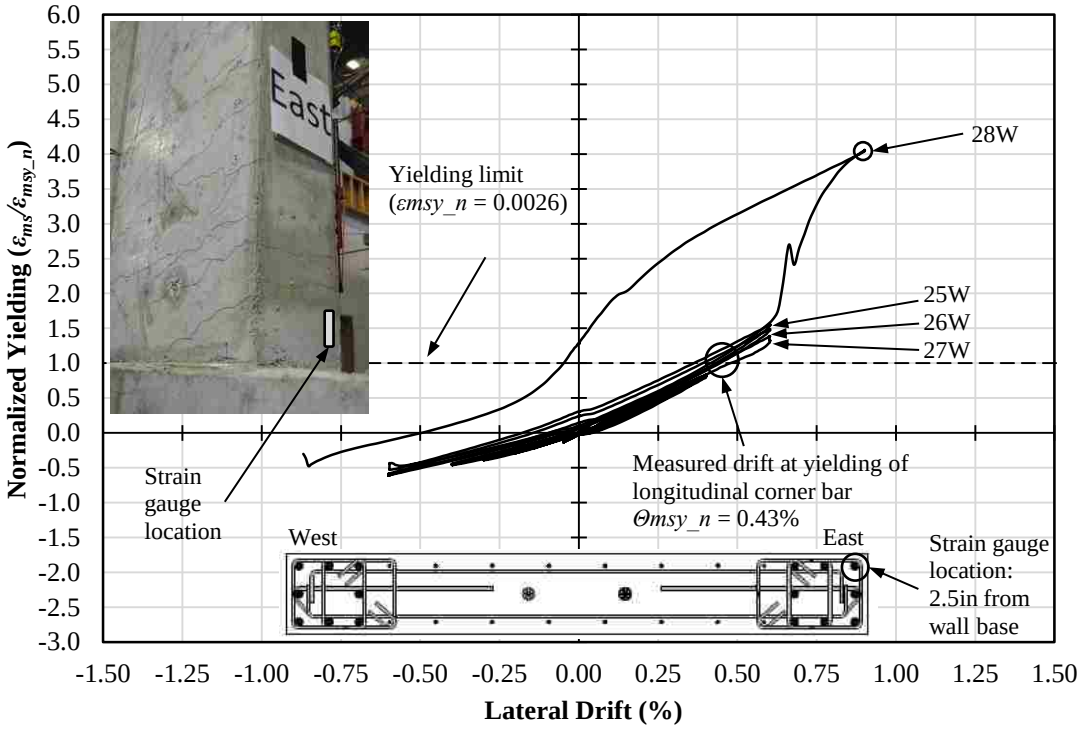

Figure 5-22 Normalized bar strain versus lateral drift

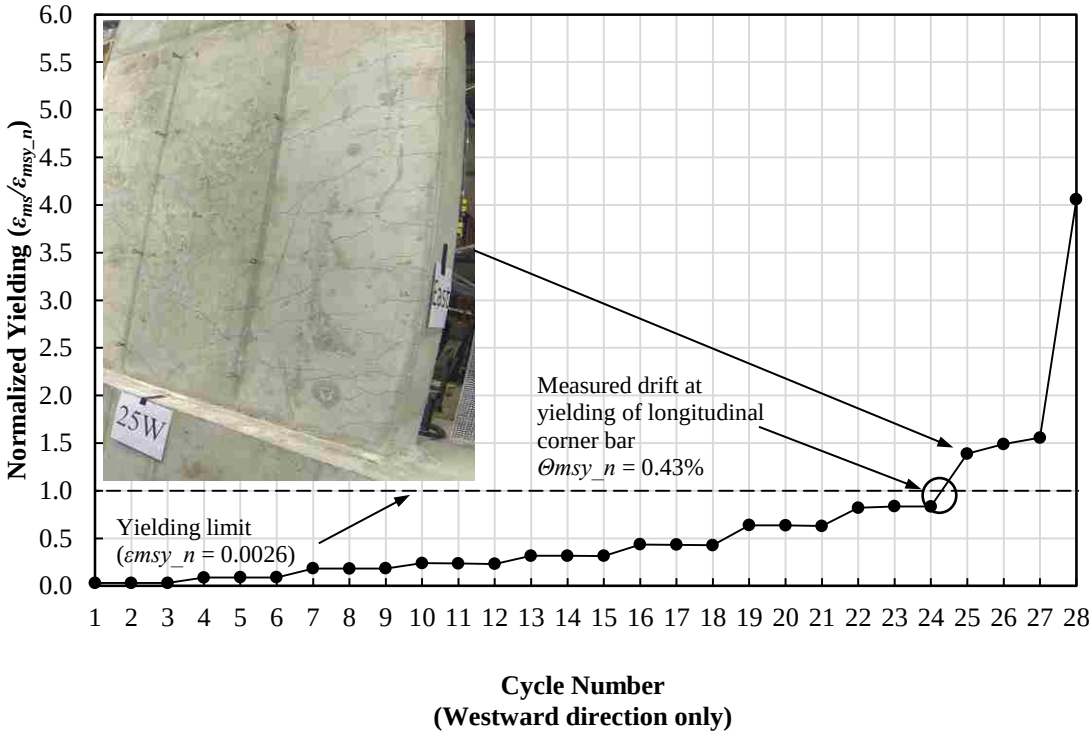

Figure 5-23 Normalized bar strain versus cycle number

Figure 5-24 Initiation of observed spalling during Loading Step 11, Cycle 31

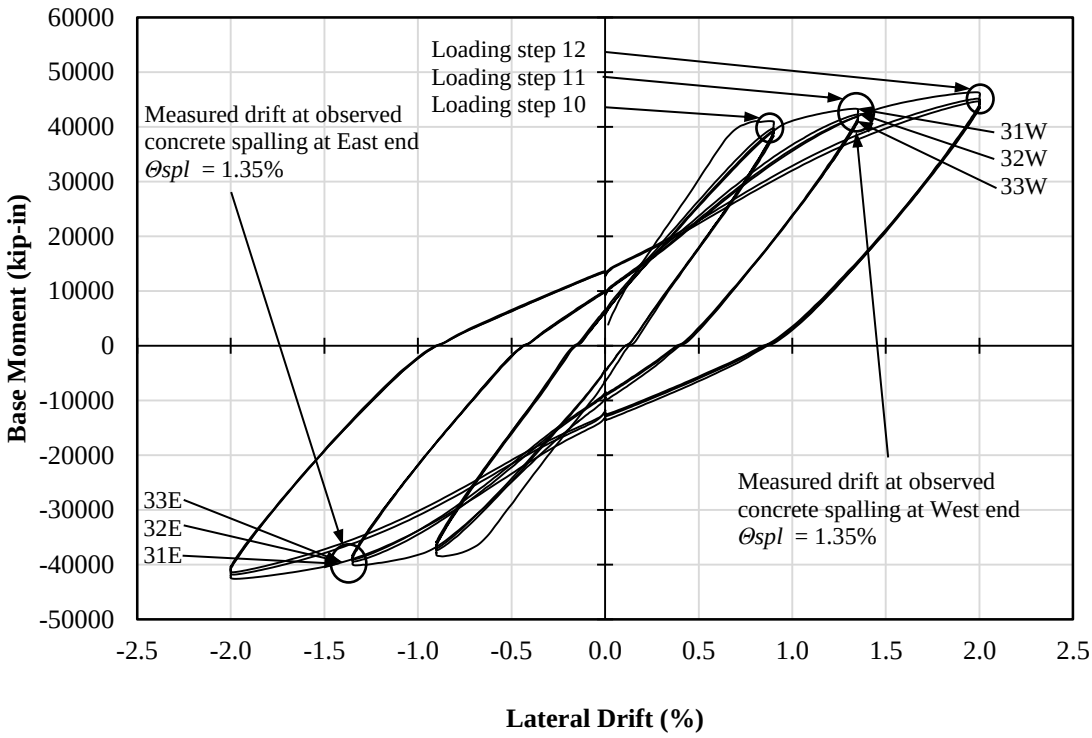

Figure 5-25 Initiation of concrete spalling during Loading Step 11, Cycle 31

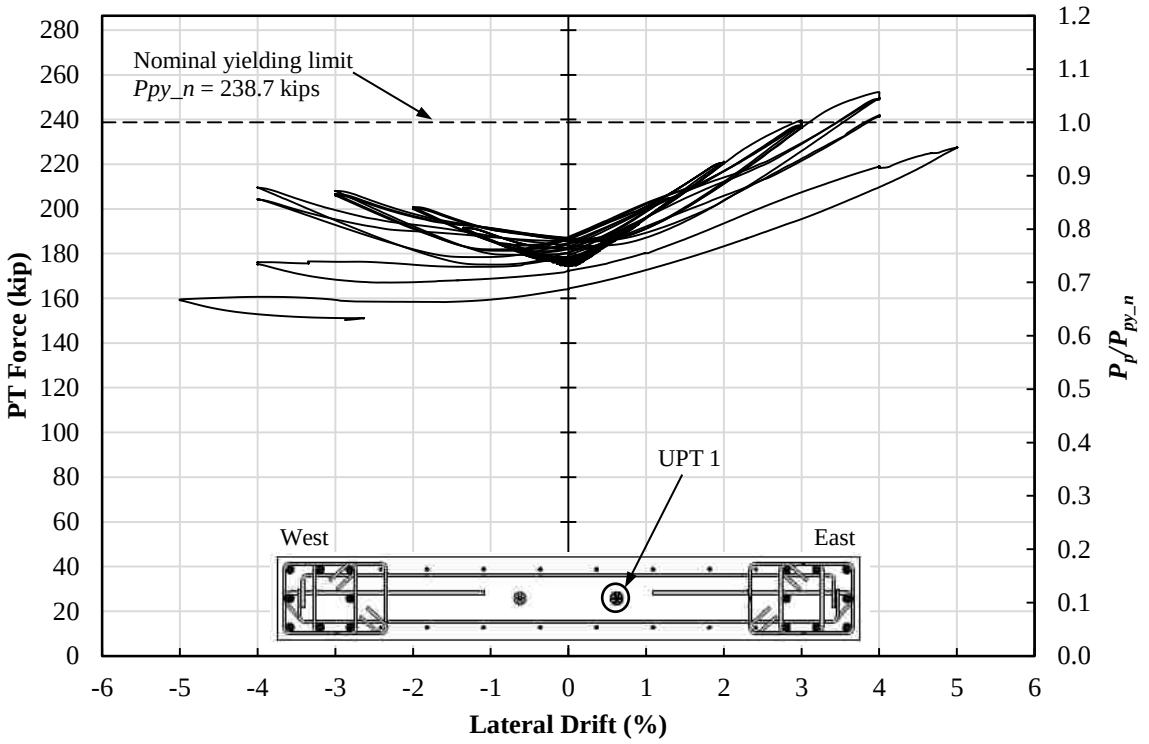

Figure 5-26 Unbonded post-tension complete response - East side

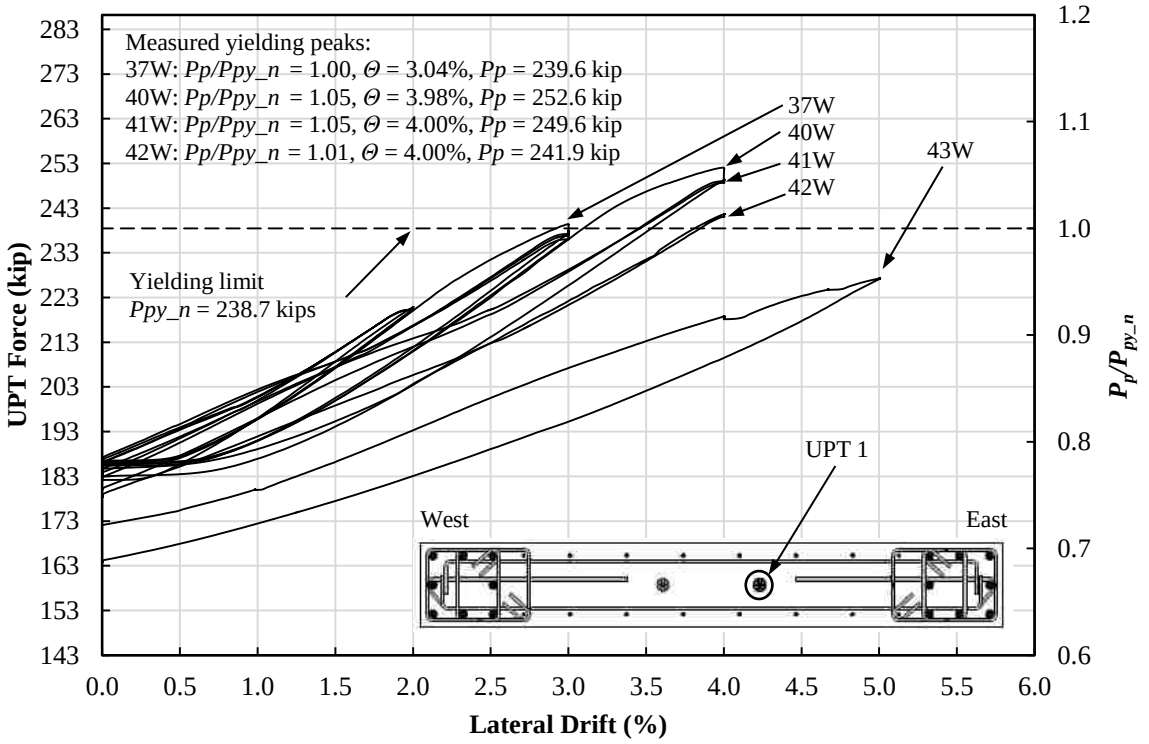

Figure 5-27 UPT yielding peaks - East side

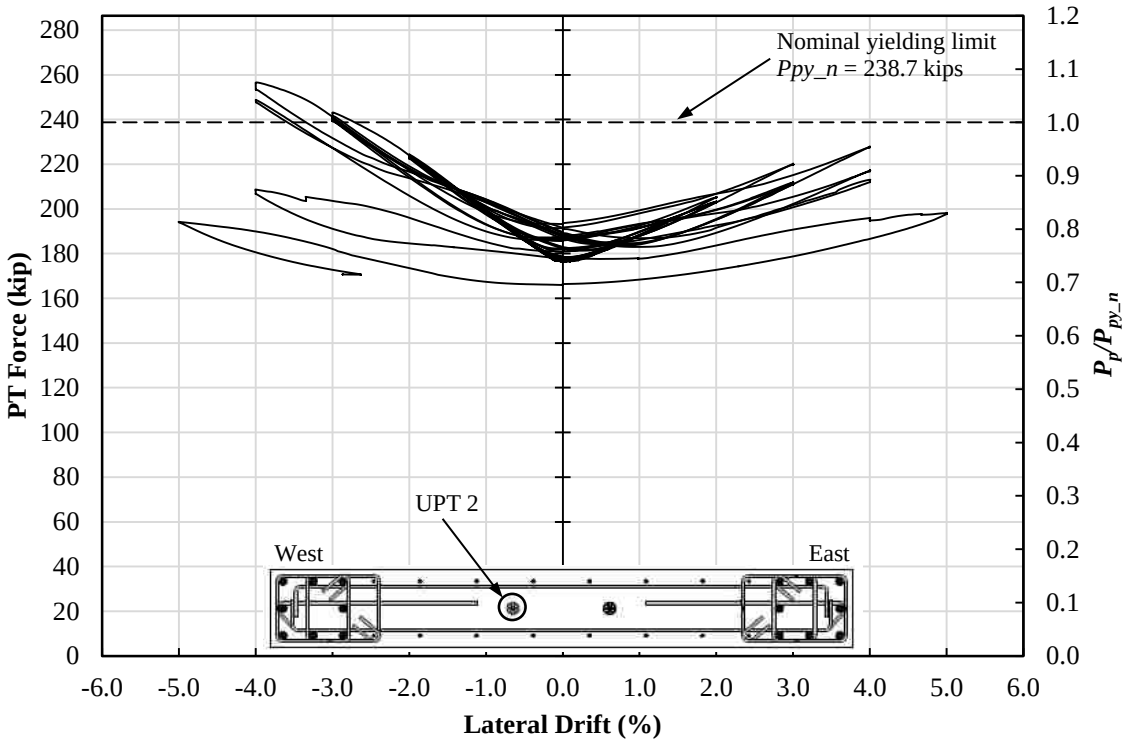

Figure 5-28 Unbonded post-tension complete response - West side

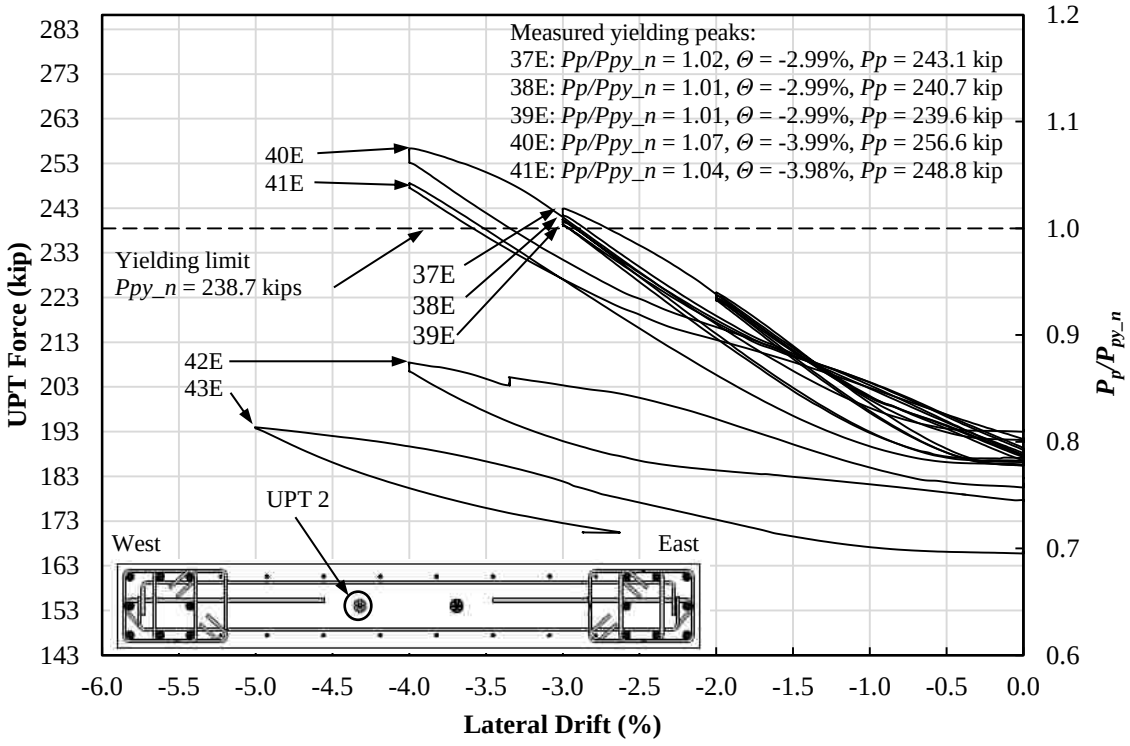

Figure 5-29 UPT yielding peaks- West side

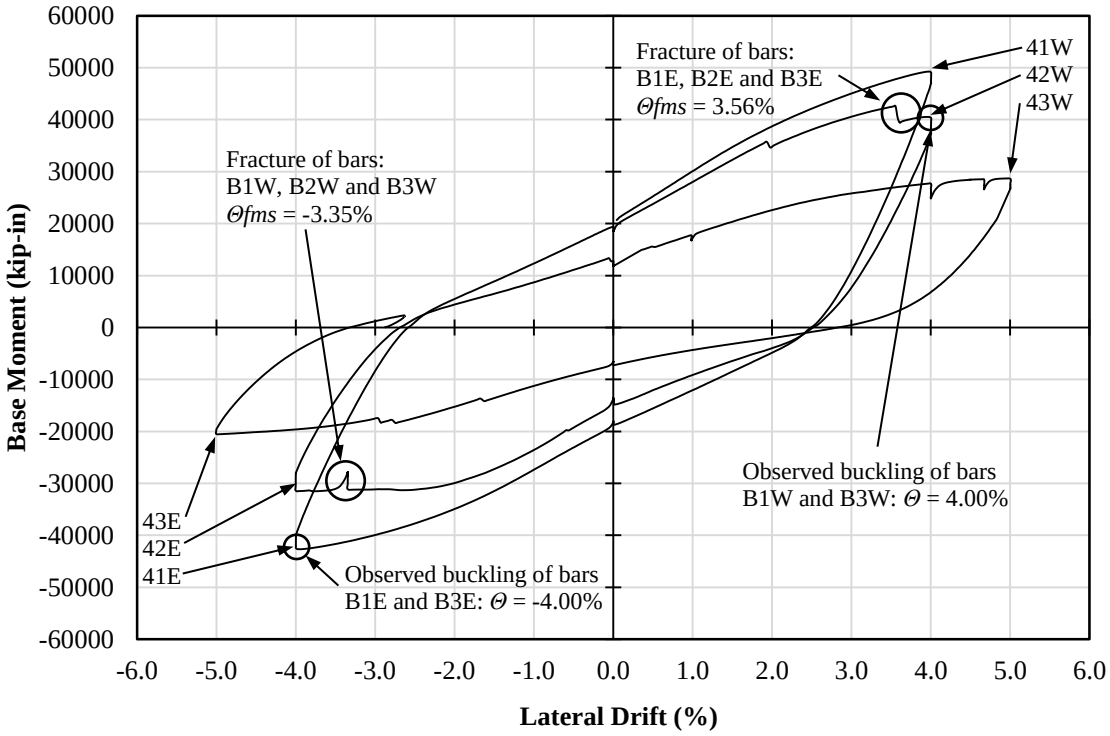

Figure 5-30 Observed fracture of longitudinal reinforcement

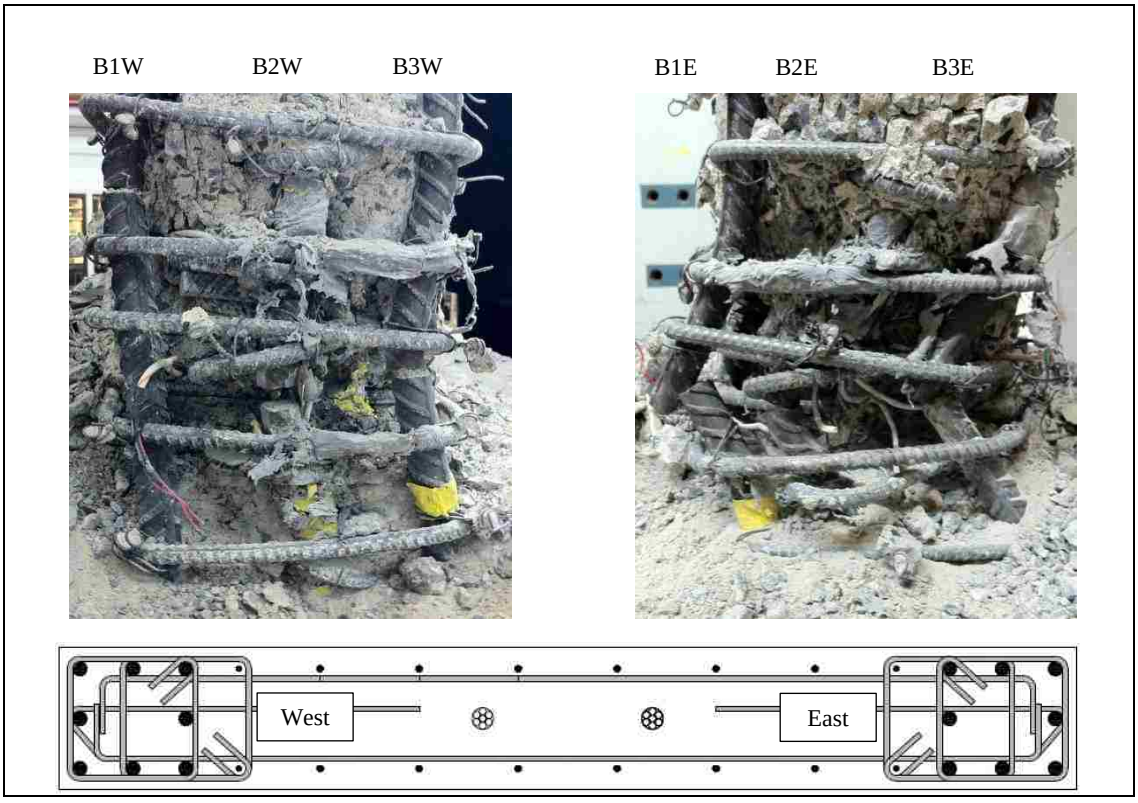

Figure 5-31 Photographs of fractured longitudinal bars on East and West side

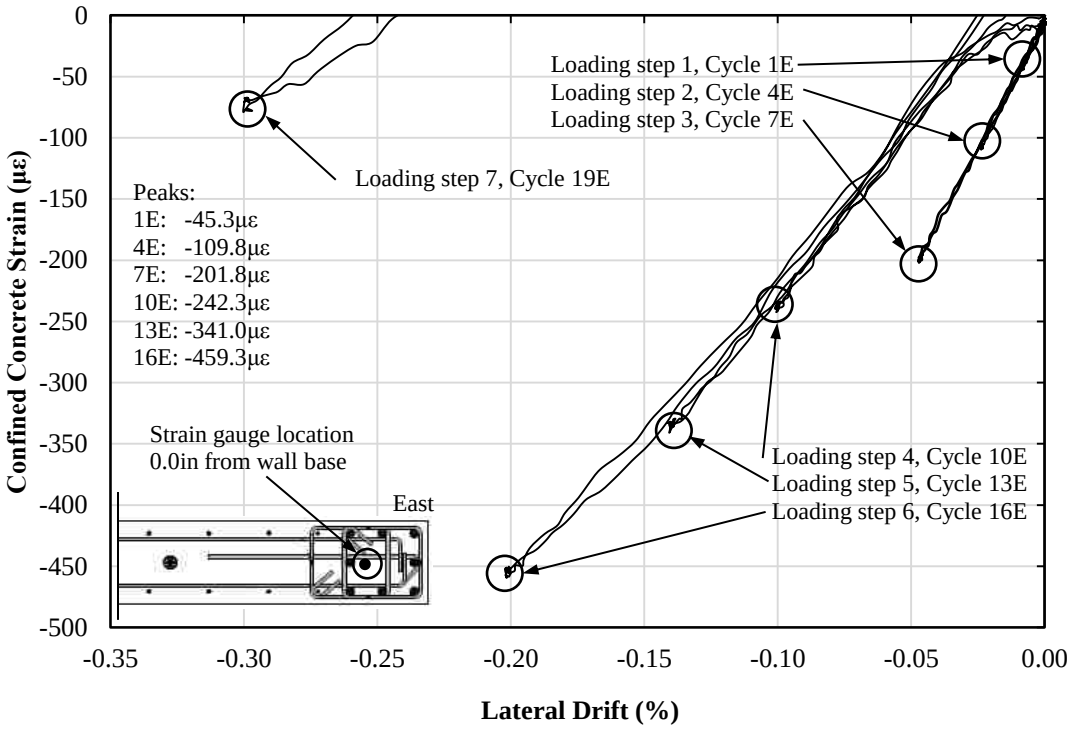

Figure 5-32 Confined concrete strain at East end of wall

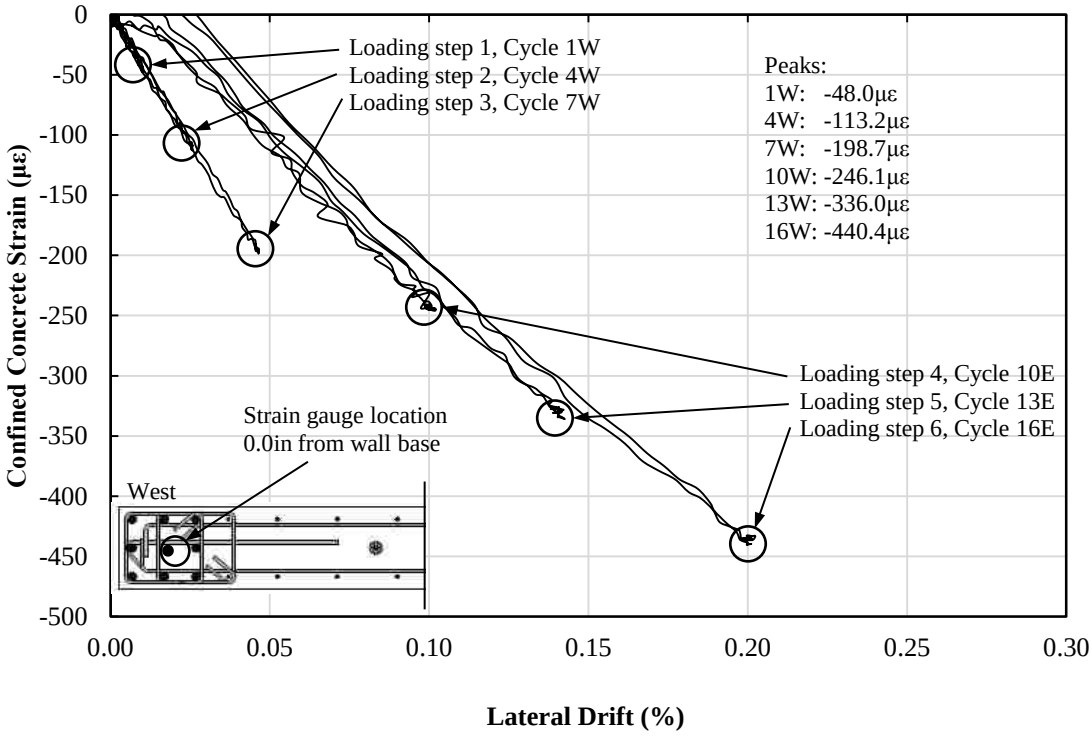

Figure 5-33 Confined concrete strain at West end of wall

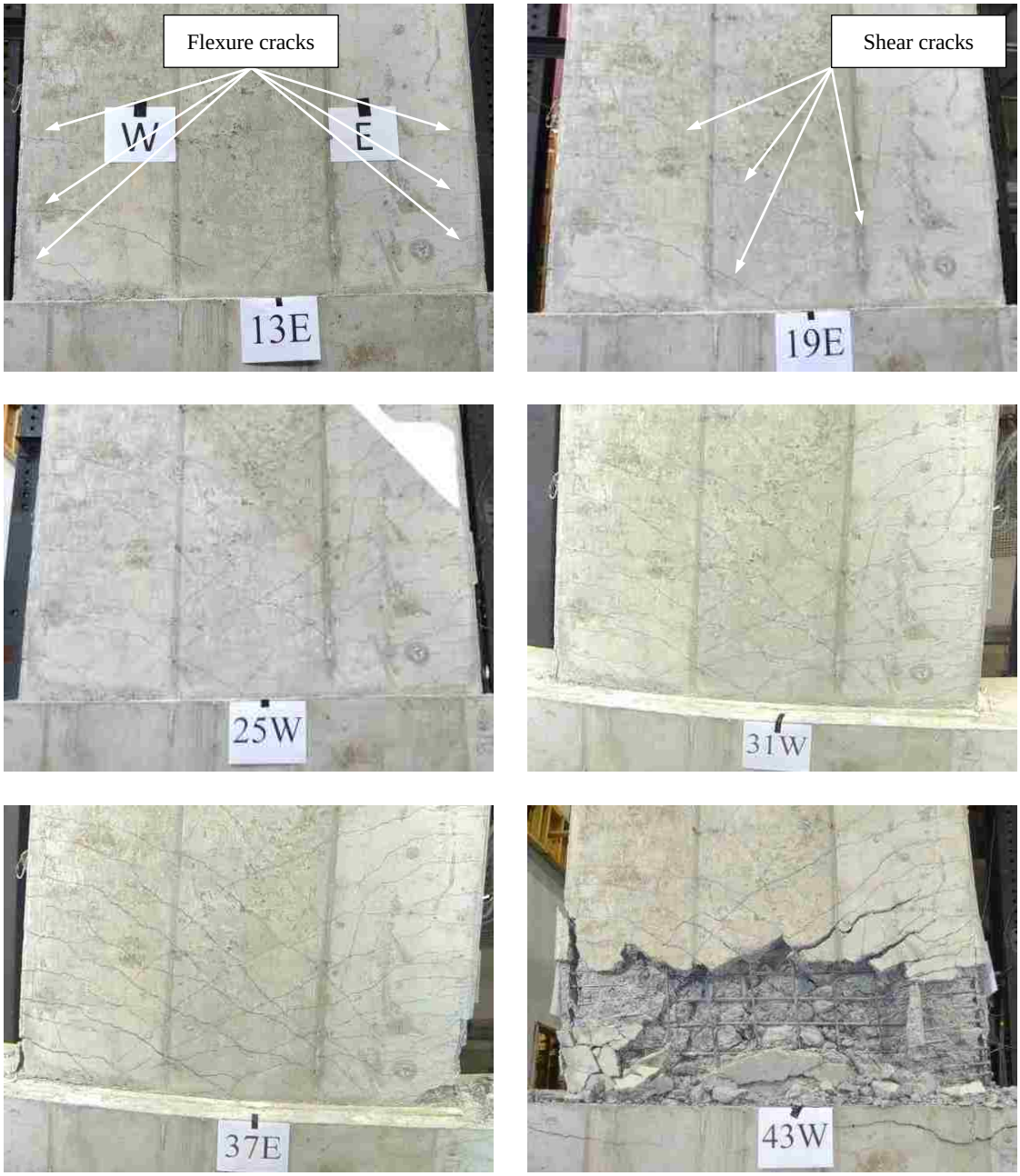

Figure 5-34 Photographs of progression of shear failure

Figure 5-35 Confined concrete in the flange portions (boundary element) of the wall

CHAPTER 6

SUMMARY AND CONCLUSIONS

This chapter presents a summary of the results and conclusions from the experimental test of Wall 1, and presents an overview of potential future work.

6.1 SUMMARY

This research investigates the lateral load response of unbonded post-tensioned cast-in-place special structural walls with bonded longitudinal mild steel reinforcement.

Chapter 2 presents a brief overview of previous work on post-tensioned structural walls. This chapter also identifies differences between cast-in-place structural walls, unbonded post-tensioned precast structural walls, and unbonded post-tensioned cast-in-place structural walls with energy dissipators. This chapter also identifies the focus of this research project, specifically, unbonded post-tensioned cast-in-place special reinforced concrete walls with longitudinal mild steel reinforcement.

Chapter 3 describes the experimental program. This chapter presents a detailed description of Wall 1. This description includes overall wall geometry, mild steel reinforcement layout, prestressing system, fabrication of test wall, loading apparatus, lateral bracing, instrumentation and data acquisition, and material properties.

Chapter 4 provides details on the analysis and design of the foundation block. This chapter describes the use of a finite element model to find the places of maximum tensile stress in the foundation block and the design of prestressing to reduce these stresses. Ultimately, the finite element model results are used to proportion the amount of steel reinforcement required to carry any remaining tension in the foundation block.

Chapter 5 describes the lateral load experimental results for Wall 1. These results include the lateral load response, concrete cracking, longitudinal bar yielding, concrete spalling, post-tensioning response, longitudinal bar fracture, confined concrete response, and failure mode.

6.2 CONCLUSIONS

The following conclusions are made from this study:

1. The limit states that characterize the lateral load response of an unbonded post-tensioned cast-in-place structural wall with longitudinal mild bonded steel reinforcement occurred as presented by Srivastava (2013).
2. Yielding of the longitudinal mild steel reinforcement was effective as an energy dissipator, resulting in wide hysteresis loops.
3. The amount of post-tensioning steel provided was not effective in reducing residual drift. Initial residual drift (Θ = 0.2%) occurred as early as the longitudinal bars started to yield (Θ = 0.57%). Therefore, self-centering capabilities were greatly diminished after the yielding of the longitudinal bars ($\Theta \approx$ 0.5%).

Ultimately, self-centering capabilities were greatly limited by the insufficiency of the restoring force provided by post-tensioning.

4. Lateral stiffness degradation occurred at all loading steps during the testing. However, significant stiffness degradation occurred early on at the time when concrete cracks were visible ($\Theta \approx 0.02\%$).
5. Strength deterioration within loading steps occurred. Deterioration ranged from 0.0% to -3.7% for the second cycle on the same loading step, and from -0.1% to -16.7% for the third cycle on the same loading step. Strength deterioration became more significant after the yielding of the longitudinal bars ($\Theta \approx 0.57\%$).
6. The test wall dissipated large amount of energy per cycle. The primary source of energy dissipation is thought to be the longitudinal mild steel reinforcement that extended from the wall into the foundation block. This energy was dissipated by yielding the longitudinal mild steel reinforcement in tension and compression.
7. The failure mode of the test wall was shear and not flexure. Shear cracks appeared as early as flexure cracks. Ultimately, shear failure dominated over flexure failure.

REFERENCES

ACI Committee 318, "Building Code Requirements for Structural Concrete", American Concrete Institute, Farmington Hills, MI, August 2011.

ACI ITG 5, "Acceptance Criteria for Special Unbonded Post-Tensioned Precast Structural Walls Based on Validation Testing and Commentary", American Concrete Institute, Farmington Hills, MI, August 2008.

Kurama, Y. C., "Seismic Analysis, Behavior, and Design of Unbonded Post-Tensioned Precast Concrete Walls", Ph.D Dissertation, Department of Civil and Environmental Engineering, Lehigh University, Bethlehem, PA, May 1997.

Kurama, Y. C., Pessiki, S., Sause, R., Lu, L. W., El-Sheikh, M., "Analytical Modeling and Lateral Load Behavior of Unbonded Post-Tensioned Precast Concrete Walls", Research Report, No. EQ-96-02, Department of Civil and Environmental Engineering, Lehigh University, Bethlehem, PA, November 1996.

Pakiding, L., Pessiki, S., Sause, R., "Analytical and Experimental Studies of Seismic Resistant Unbonded Post Tensioned (UPT) Special Reinforced Concrete (RC) Wall," Ph.D. Dissertation, Department of Civil and Environmental Engineering, Lehigh University, Bethlehem, PA, December 2014.

Perez, F. J., "Experimental and Analytical Lateral Load Response of Unbonded Post-Tensioned Precast Concrete Walls", Ph.D. Dissertation, Department of Civil and Environmental Engineering, Lehigh University, Bethlehem, PA, 2004.

Perez, F. J., Pessiki, S., Sause, R., "Experimental Lateral Load Response of Unbonded Post-Tensioned Precast Concrete Walls," ACI Structural Journal, Vol. 110, No.6, November-December 2013, pp. 1045-1055.

Perez, F. J., Sause, R., and Pessiki, S., "Analytical and Experimental Lateral Load Behavior of Unbonded Post-Tensioned Precast Concrete Walls", Journal of Structural Engineering, American Society of Civil Engineers, Vol. 133, No. 11, November 2007, pp. 1531-1540.

Srivastava, S., "Analytical Lateral Load Response of Unbonded Post-Tensioned Cast-in-Place Concrete Special Structural Walls with Bonded or Debonded Longitudinal Mild Steel Reinforcement", M.S. Thesis, Department of Civil and Environmental Engineering, Lehigh University, Bethlehem, PA, 2013

Restrepo, J. and Rahman, A., "Seismic Performance of Self-Centering Structural Walls Incorporating Energy Dissipators", Journal of Structural Engineering, American Society of Civil Engineers, Vol. 133, No. 11, November 2007, pp. 1560-1570

Smith, B. J., and Kurama, Y. C., "Design of Hybrid Precast Concrete Walls for Seismic Regions", Proceedings of 2009 Structures Congress, American Society of Civil Engineers, 2009, pp. 1-10.

Smith, B. J., Kurama, Y. C. and McGinnis, M. J., "Design and Measured Behavior of a Hybrid Precast Concrete Wall Specimen for Seismic Regions", Journal of Structural Engineering, American Society of Civil Engineers, Vol. 137, No. 10, October 2011, pp. 1052-1062.

VITA

Moises Rivera was born on November 30th, 1982 in Irapuato, Guanajuato, Mexico, son of Jose A. and Bertha L. Rivera. Mr. Rivera spent most of his childhood in Guanajuato, Mexico, and moved to the United States on August 18th, 1998. He attended Sicartsa, Justo Sierra, and Francisco Villa for elementary school, Secundaria Oficial Estatal for junior high, and Anaheim H.S. for high school. From 2008 to 2011, he attended California State Polytechnic University Pomona and graduated with a Bachelors of Science in Civil Engineering. During those years, Mr. Rivera worked as a research assistant for the Departments of Environmental and Structural Engineering, traveled to Egypt with the Department of Civil Engineering to study Transportation Engineering, and became a fellow Pratt School of Engineering REU student at Duke University. On 2011, Mr. Rivera started his graduate studies at Lehigh University in pursue of a Master's of Science in Structural Engineering. From 2013, Mr. Rivera has worked as a structural engineer at De-Simone Consulting Engineers.